Characterization of Polymeric Microspheres used in Drug Delivery via Electron Microscopy

by

Jose Carlos A. Gomez Monico
BSc. Bioengineering, University of California Riverside, 2011

A thesis submitted in partial fulfillment of the requirements for the Degree of

MASTER OF APPLIED SCIENCE

in the Department of Mechanical Engineering

Supervisory Committee

Characterization of Polymeric Microspheres used in Drug Delivery via Electron Microscopy

by

Jose Carlos A. Gomez Monico
BSc. Bioengineering, University of California Riverside, 2011

Supervisory committee
Dr. Rodney Herring, Department of Mechanical Engineering
Supervisor

Dr. Barbara Sawicki, Department of Mechanical Engineering
Department Member

Abstract

Supervisory committee
Dr. Rodney Herring, Department of Mechanical Engineering
Supervisor
Dr. Barbara Sawicki, Department of Mechanical Engineering
Department Member

Drugs can be made up of nucleic acids, sugars, small organic and inorganic compounds, peptides, and large macromolecules. Drug therapy can be optimized by controlled delivery systems that release an appropriate dose to the site of action, extend the duration of delivery, reduce administration sessions, and can target a precise site of activity. An advanced method of controlled drug delivery is through injectable polymeric biomaterial microparticles that entrap drugs within their matrix for slow release (1-6 months). Surface morphology of polymer microparticles is known to affect drug release; however, it is often reported in qualitative terms only.

In this thesis, a mastery over the controlled fabrication of biodegradable poly (ε-caprolactone) (PCL) microspheres is shown, as well as their characterization using different imaging conditions/techniques of the scanning electron microscope (SEM). Retinoic acid (RA), a morphogenic molecule, is encapsulated to create RA/PCL microspheres that are used to successfully deliver drug to human induced pluripotent stem cell aggregates. Furthermore, this works reports the creation of variable surface morphology PCL microspheres and their characterization via size analysis and stereo-microscopy. A rough morphology candidate is identified and selected for 3D SEM surface model reconstruction via a computer vision technique. Surface studies via SEM

have a lot of potential to advance the development of these particles. The 3D model first reported here serves as foundation for quantitative surface morphology measurements.

Table of Contents

Contents

List of Tables

List of Figures

Abbreviations

AFM	Atomic force microscope
BSA	Bovine serum albumin
BSE	Backscattered electron
CCD	Charged-couple device
CHT	Circle Hough transform
CLSM	Confocal laser scanning microscope
CT	Computed tomography
DAPI	4′, 6-diamidino-2-phenylindole
DCM	Dichloromethane
DSC	Differential scanning calorimetry
EB	Embryoid body
ECDF	Empirical cumulative distribution function
ECM	Extra cellular matrix
EM	Electron microscopy
ESC	Embryonic stem cells
EVA	Ethylene-vinyl acetate
HA	Hydroxyapatite
hiPSC	Human induced pluripotent stem cell
IgG	Immunoglobulin G
KDE	Kernel density estimate
mESC	Murine embryonic stem cells
Mn	Polymer molecular weight
NIM	Neural induction medium
o/w	Oil-in-water
OVA	Ovalbumin
PBS	Phosphate buffer saline
PCL	polycaprolactone
PEG	Poly (ethylene glycol)
PET	Polyethylene terephthalate
PGA	polyglycolide
PLA	polylactide
PLGA	co-polymer poly(lactide-*co*-glycolide)
PLO	Poly-L-ornithine
PVA	Polyvinyl chloride
RA	Retinoic acid
rms	Root-mean-square
SE	Secondary electron
SEM	Scanning electron microscope
SMP	Scanning probe microscope
SOX2	(Sex determining region y)-box 2
SSEA-4	Stage-specific embryonic antigen-4
SURF	Speeded up robust features
TEM	Transmission electron microscope

TUJ1	Neuron-specific class III beta tubulin
w/o/w	Water-in-oil-in-water
XRD	X-ray powder diffraction

Dedication

To my family,

Thank you for your unwavering support and love – distance, no matter how great, will never make me feel separate from all of you.

To my friends,

Thank you for listening and challenging me – **y**ou are the family I have made along my journey.

Love you all,

Jose

"However vast the darkness, we must supply our own light"
Stanley Kubrick

Chapter 1 Introduction and Motivation

1.1 Background

Medical practitioners use drugs to treat disease. Generally, drugs can be divided between chemically synthesized small molecules and biologically derived macromolecules. The delivery of each type of drug can benefit from controlled drug delivery systems that extend the duration of delivery, reduce administration sessions, and can target a precise site of activity [1, 2].

Controlled drug delivery technology can take many forms, from slow dissolving coatings on compressed pills (once-a-day) to implantable-refillable drug infusion pumps (3-6 months). A well studied biomaterial-based method of advanced controlled drug delivery is through injectable polymeric microparticles that entrap drugs within their polymer matrix for slow release (1-6 months) [3, 4]. Microparticles can range from 1 to 1000 µm in diameter and can encapsulate, protect, and release drugs *in situ* thereby acting as an injectable reservoir-based (depot) drug delivery system [5].

Biodegradable synthetic polymers, such as the aliphatic class of polyesters, are popular materials for microparticle formulations as they can breakdown into biocompatible monomers for natural resorption or excretion, thus eliminating the need of surgical removal after drug delivery is completed [3-6]. The most commonly used polyesters for this purpose include: polyglycolide (PGA), polylactide (PLA), the co-polymer poly(lactide-*co*-glycolide) (PLGA), and polycaprolactone (PCL). Small hydrophobic drugs are usually encapsulated through the oil-in-water (o/w) single emulsion/solvent evaporation technique, whereas large hydrophilic macromolecules are encapsulated

through the water-in-oil-in-water (w/o/w) double emulsion/solvent evaporation technique [7, 8]. Other formulation techniques and motifs exist, and excellent reviews can be found in the following references [9, 10].

Microparticle characterization is a critical step during (or after) fabrication to estimate how a particular formulation may perform *in vivo*. Characterization techniques for microparticles quantify and establish particle size and distribution, surface state (morphology), internal structure (porosity), drug encapsulation efficiency, residual organic solvent, and *in vitro* drug release profile [4]. Scanning electron microscopy (SEM) is perhaps the most widely used technique to report microparticle morphology, however as noted by Mao *et al.*, (2012) "some of the results generated using SEM are qualitative in nature," and this includes assessments on surface state [4].

Recently, Bile *et al.,* (2015) noted that "most publications focused on drug release [more] than morphology," and brought attention to reported links between damaged microparticle surfaces and faster drug release [11]. Bile and co-workers extensively studied how fabrication parameters affect the morphology of PCL microparticles used to deliver vitamin D_3, a hydrophobic and environmentally sensitive molecule. The researchers sorted PCL microparticles into five morphologies (smooth, rough, scarred, dumbbell-shaped, and holy) by carefully controlling the fabrication parameters of an o/w single emulsion. They demonstrated that morphology can be controlled on-demand, conducted a 10-day drug release study, and provided further evidence of surface effects on drug release. While SEM was used by the team to observe the various morphologies,

the categories were strictly qualitative, indicating an existing gap in knowledge and an opportunity for further examination.

Micrographs obtained through SEM appear to have a 3D-like effect due to a large depth of focus. However, each micrograph remains a 2D representation of a 3D specimen and a large depth of focus effectively obscures height and roughness variations in each image. This thesis presents a model for potentially measuring the surface state (roughness) of polymeric microparticles with a non-contact SEM-based technique. Stereo-SEM is a multi-view approach that uses at least two micrographs captured at different tilt angles to reconstruct a virtual 3D surface for quantitative assessment.

The goal of this work was to use SEM and other techniques to quantitatively characterize polymeric microparticles used in drug delivery. This was achieved by creating various PCL microsphere formulations, measuring drug encapsulation efficiency, drug release, particle size, surveying particle morphology, and measuring stem cell effects from drug delivery via microparticles. A qualitative survey of different surface morphology microparticles with the SEM identified a candidate for 3D surface reconstruction. Stereo-micrographs of each formulation were recorded and software was used to obtain a 3D model.

1.2 Motivation

Many academic publications have studied drug release mechanisms, suitable polymer materials, drug types, delivery routes, and novel applications in drug delivery; all with the goal of designing formulations relevant to clinical use [2]. Academically, polymeric microparticles for drug delivery are a mature technology, however only about a dozen

products are commercially available, highlighting the difficulty of bringing new technology to market and the need to maximize every resource to perfect it [2, 4, 12].

SEM is generally used to observe the surface morphology of microparticle formulations. The micrographs obtained are undeniably valuable, but descriptive assessments fail to capitalize on the potential of SEM. Indeed, recent advances on computational power and algorithms have increased the speed (and accuracy) of 3D SEM surface reconstructions [13]. Recovering the "hidden" third dimension (height) via stereo-SEM would be of considerable benefit to quantitatively assess microparticle morphology and, to the best of our knowledge, has not been performed with a non-contact versatile technique like SEM.

A quantitative assessment of microparticle surface morphology through stereo-SEM could provide new data to categorize drug delivering polymer microparticles. Furthermore, non-contact techniques such as SEM provide several advantages over existing contact surface profiling techniques, such as: 1) spatial resolution in contact profiling techniques (e.g. atomic force microscopy) is fixed, determined by a fixed probe size, whereas SEM offers variable spatial resolution, determined by a variable probe size, 2) vast regions of interest can be easily surveyed through SEM in a short period of time, to then use higher spatial resolution on selected regions of interest. For these reasons, surface studies via SEM have a lot of potential to advance the development of these particles.

1.3 Structure of the Thesis

The goals of this thesis are contained in the following three projects. 1) Present a mastery over PCL microsphere fabrication via the o/w single emulsion technique by encapsulating retinoic acid (RA), a morphogenic molecule, into PCL microspheres in a reproducible manner. 2) Characterize RA/PCL microspheres in terms of drug encapsulation efficiency, drug release, size, and morphology, and combine RA/PCL microspheres with human induced pluripotent stem cells (hiPSCs) to measure drug delivery effects in the production of neural progenitors. 3) Fabricate variable morphology PCL microspheres as reported in literature and identify a rough morphology microsphere for 3D surface reconstruction through particle analysis (e.g., size and stereo-microscopy). I use the selected microsphere to create a quantitative morphology (surface roughness) 3D model of microspheres surface. For this last project, I present the background knowledge required for an understanding of contrast (luminance) in electron microscopy and its implication for stereo-reconstruction.

The chapters of this thesis are organized as follows:

- *Chapter 2* provides background information on electron microscopy. It presents an introduction to biomaterials and drug releasing polymeric microspheres. Microscopy contributions to understand microspheres are also reviewed. State-of-the-art on the existing techniques of surface characterization is discussed.
- *Chapter 3* describes the materials and methods used in this thesis.
- *Chapter 4* presents results from the three projects. Mastering RA/PCL microsphere fabrication, RA/PCL effects on hiPSC aggregates, and variable morphology microsphere measurements obtained through stereo-SEM.
- *Chapter 5* provides discussion on the three projects and suggestions for future work.

Chapter 2 Background Information

2.1 Electron Microscopy

In this section, an attempt is made to discuss the principles of electron microscopy, development milestones, microscope types, image generation, and conditions that affect contrast in scanning electron microscopy (SEM). This thesis uses SEM to study surface detail.

2.1.1 Development of Electron Microscopes

Microscopy refers to the science of observing and measuring minute objects with the aid of microscopes [14]. Ernst Abbe (1873) demonstrated that the smallest distance at which two point-like objects could be distinguished, spatial resolution, would be theoretically limited to about half the wavelength of the light employed ($\delta \approx 0.2\mu m$ for violet light) [15]. Some years later, Lord Rayleigh (1896) mathematically defined the smallest resolvable distance as the Rayleigh Criterion, shown in Equation 1 and Figure 1, based on Sir George Airy's (1834) work on diffraction disk patterns as a function of light [14, 15]. Thus, electron microscopy (EM) was born out of a desire to "see" objects beyond the limits of optical microscopy imposed by the diffraction and wavelength of light.

$$\delta = \frac{0.61\lambda}{\eta \sin \alpha}$$

where: δ is resolvable distance
λ is the imaging wavelength
η is the refractive index between the lens and specimen
α is the semi-angle of collection of the lens

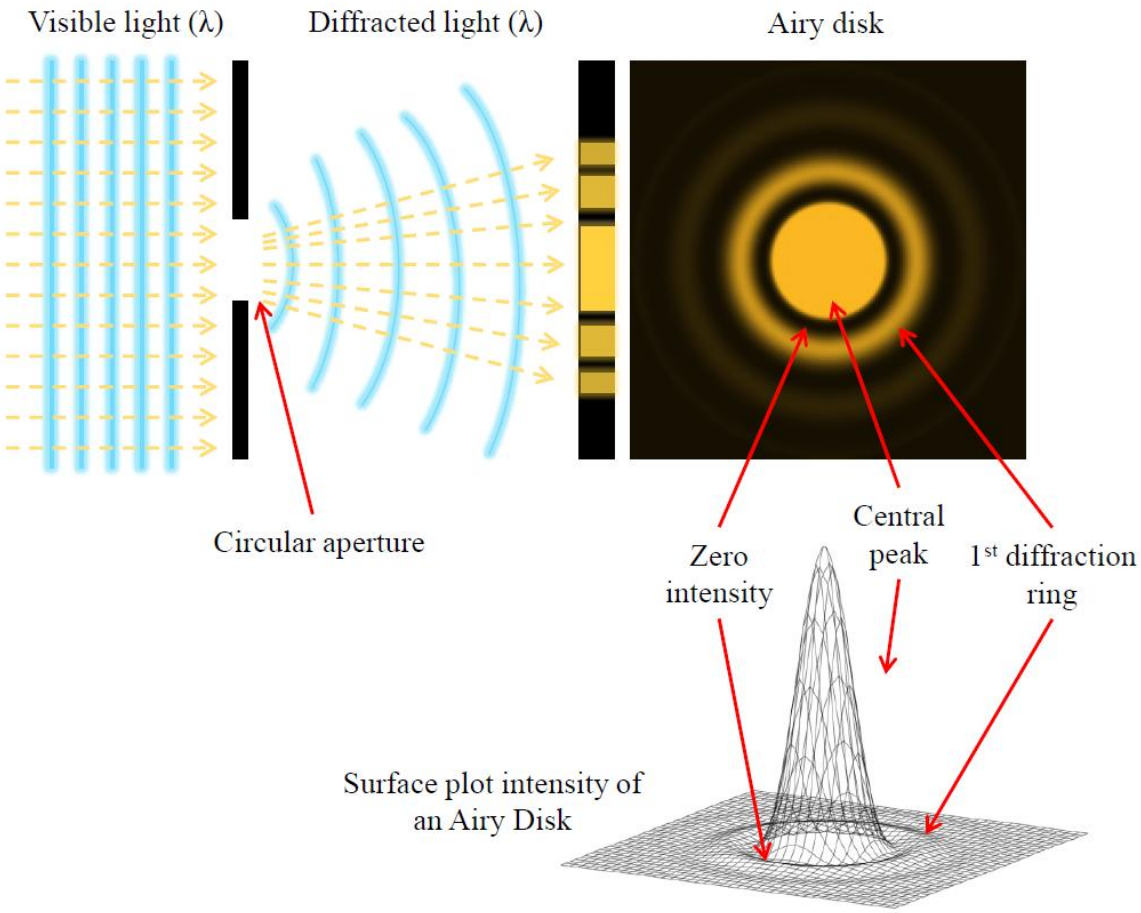

Figure 1 – Diffraction disk patterns as a function of light - Airy Disks. Light is diffracted by the circular aperture resulting in diffusive, delocalized circular pattern centered by the source of light.

Three major works enabled the development of the electron microscope. First, J.J. Thomson (1897) discovered a subatomic particle, the electron, which possessed an intrinsic mass and a negative charge that allowed its manipulation through electrostatic and magnetic fields [16]. Second, Louis de Broglie (1924) proposed that matter showed wave-like behaviour and derived the de Broglie wavelength from the Einstein-Planck energy relation [17]. Third, Max Knoll and Ernst Ruska (1932) used Hans Bush's theoretical work (1926) to build axially symmetric magnetic fields that concentrated electrons, thus creating electron "lenses" [14, 18]. Together, the ideas suggested that an

electron accelerated by an electric potential could exhibit a wavelength shorter than that of visible light, and, akin to light in classical optics, could be focused through electron lenses into a beam to “illuminate” a specimen.

In light microscopy, the light reflected or absorbed by a specimen produces image contrast, i.e., the difference in luminance (intensity) or colour that sets objects apart. However in EM, the energy signals produced by the electron beam – specimen interaction are used to create contrast. As there is no colour component in the electron beam and in the digitally recorded image, EM micrographs are traditionally shown using a gray scale. The electron beam – specimen signals and their relationship to image contrast will be explored in further detail in section 2.1.2.

Generating images from solid specimens remained the primary goal of EM throughout its development. The construction of the first electron microscopes occurred independently in Europe and North America in the 1930s, and two methods of producing images emerged at the time [14, 19]. One method, developed by Knoll and Ruska (1934), obtained high resolution images by analyzing transmitted electrons, i.e., electrons that passed through the specimen [14, 18]. Notably, two graduate students at the University of Toronto, Albert Prebus and James Hillier (1939) used transmitted electrons to design a transmission electron microscope (TEM) that remains the basis of almost all commercially available TEMs. The second method, explored by Knoll (1935), obtained images by scanning a specimen with an electron beam and analyzed emitted signals, i.e., electrons and other electromagnetic radiation emitted by the specimen [19]. Unfortunately, the development of the scanning electron microscope (SEM) was

abandoned for some time due to poor image quality and the successful commercialization TEMs.

Electron microscopists in the 1930s and early 1940s regarded the development of the SEM as “a complete waste of time” [19]. It was until 1948, when Charles Oatley of the University of Cambridge and his graduate students sought to enhance signal quality of emitted electrons, that the SEM was revisited for high resolution imaging [19]. Oatley’s students were critical for the successful commercialization of SEMs. In particular, Thomas Everhart and Richards Thornley (1960) who successfully developed an electron detector capable of collecting and enhancing emitted electrons rapidly to produce high resolution SEM images not seen before [20]. The detector bears their name (ET detector) and it is found in all modern SEMs.

A simplified design for a TEM is shown in Figure 2. A TEM consists of the following elements: 1) an electron gun (source), 2) one or more condenser lenses (to focus the electron beam), 3) a specimen, 4) an objective lens (to magnify the intermediate image), 5) one or more projector lenses (to further enhance the intermediate image), and 6) an image recording mechanism; usually a charge-coupled device (CCD) type sensor in modern TEMs.

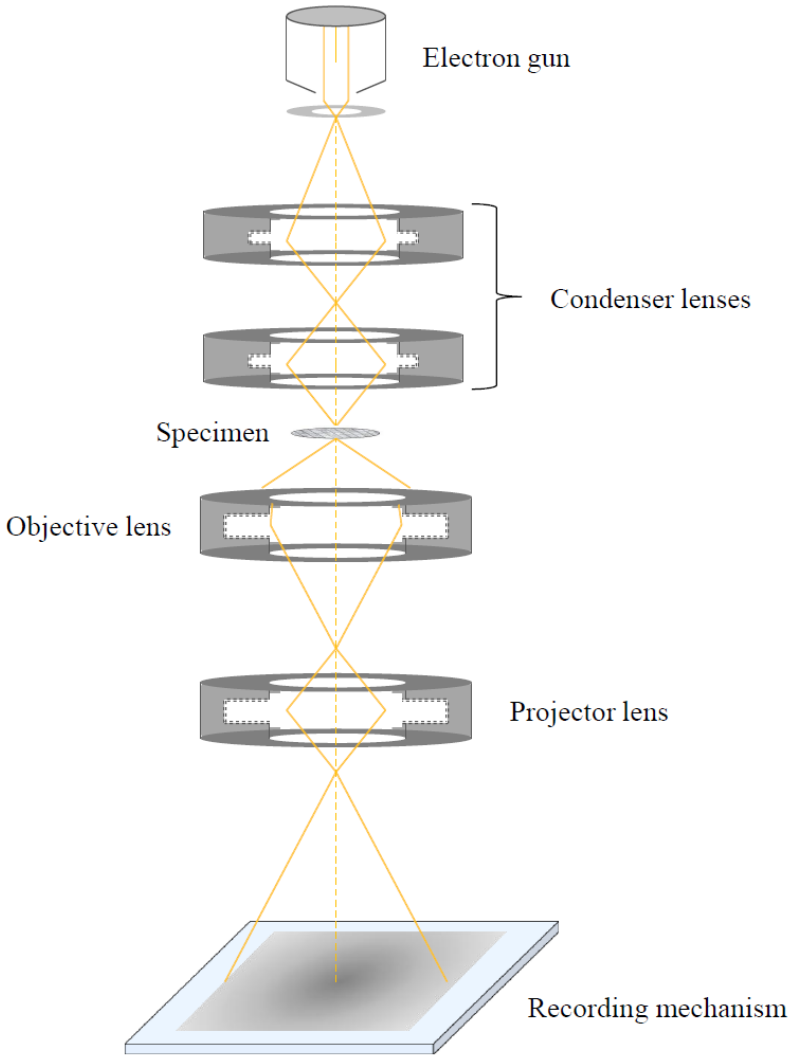

Figure 2 – Simplified transmission electron microscope (TEM) diagram

A simplified design for a SEM is shown in Figure 3. The SEM and TEM share many elements of the electron column, with the exception that all lenses serve to focus the electron beam. A SEM consists of the following elements: 1) an electron gun, 2) two or more condenser lenses, 3) a set of scanning coils (fluctuating magnetic fields to reflect the beam in a raster fashion), 4) an objective lens, and 5) an ET detector.

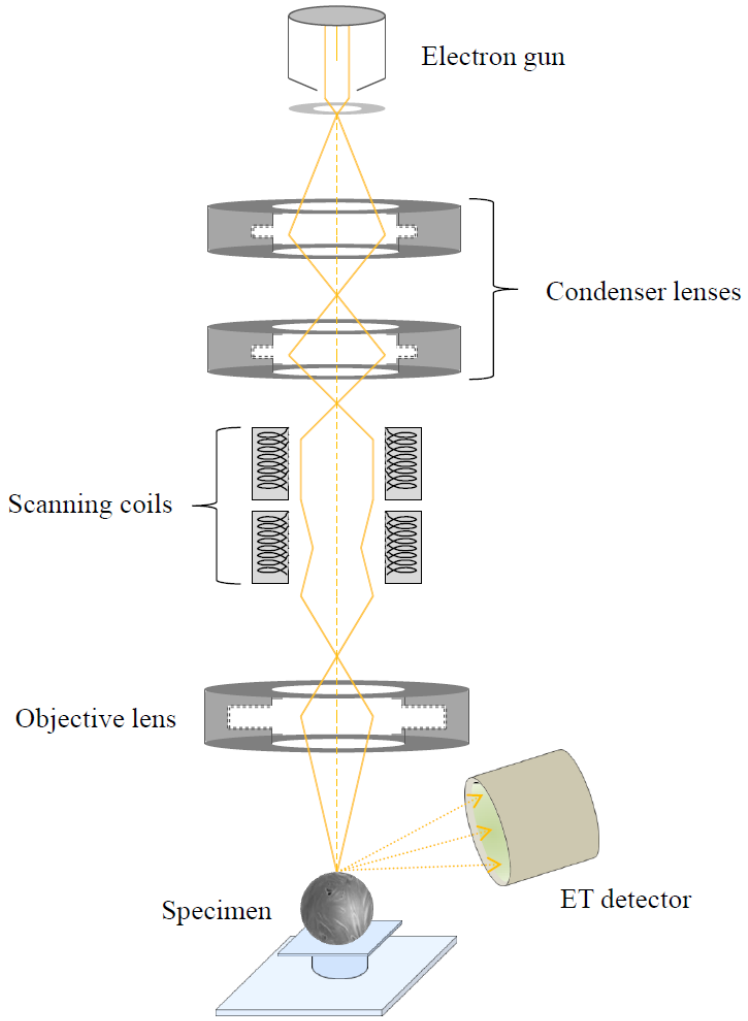

Figure 3 – Simplified scanning electron microscope (SEM) diagram

The resolving power of the TEM and SEM has been invaluable to advance our knowledge in many fields, including biology, medicine, materials science, and manufacturing. However, resolution improvements are not solely dependent on electron wavelength, and lens aberrations have prevented microscopists from achieving the limits of EM. Indeed, perfectly symmetric lenses are impossible to manufacture and they give rise to geometric errors that limit resolution beyond the effects of electron diffraction. For example, spherical aberration is one of the principal errors that limits resolution and it

can result in an unfocused, blurred image if not minimized or corrected [14, 21, 22]. While a detailed discussion on lens aberrations is beyond the scope of this section, it is important to be aware of such errors (see Appendix 1) [14, 23]. Historical accounts and state-of-the-art reviews on aberration correction can be found in the following references [24, 25].

Spherical aberration, chromatic aberration, and astigmatism outweigh the effects of other lens aberrations, and correcting or minimizing them allows for quality EM images in most circumstances. Ultra-high (atomic) resolution EM, however, requires careful consideration of the remaining lens aberrations as well as extensive planning to eliminate extrinsic sources of errors i.e., mechanical vibrations, external magnetic fields, unsteady electric currents, specimen contamination, temperature changes, etc. The following book chapters provide a thorough account on instabilities and methods for ultra-high resolution EM, as well as a suggested checklist for the interested microscopist [26, 27].

2.1.2 Electron Beam – Specimen Interactions

A focused electron beam can be imagined as a narrow cone of electrons changing after colliding with a specimen. In the TEM, electrons transmitted through the specimen are used to gather information and generate an image. A sufficiently thin specimen (~100 nm) is electron transparent and it allows a number of incident electrons to pass through the specimen with no changes in energy or direction. Part of the incident electrons however, are scattered with some changes in energy, direction, or both. Elastically scattered electrons are deflected at large angles with no loss of energy. Inelastically scattered electrons lose energy but are deflected at small angles. The scattering gives rise

to a common TEM imaging method used in biology, bright-field “mass-thickness” amplitude contrast, where heavier atoms deflect electrons at larger angles and appear as dark areas. Other TEM contrast methods exits such as dark-field “mass-thickness” amplitude contrast, where electrons scattered at a large angle are selected to pass to the objective lens and carry information of their strong interaction with the specimen. Phase contrast is another form of TEM imaging based on phase changes of incident electron waves after interacting with a specimen, particularly useful for studying crystalline specimens with defined patterns [28].

In the SEM, the electron beam acts as a probe that releases electrons and electromagnetic radiation upon colliding with the specimen. In general, specimens are much larger in the SEM than in the TEM; ranging from nanometers to centimeters. Due to the increased thickness of the specimen, incident electrons are not transmitted through the sample. Incident electrons interact with matter, some are elastically scattered from the vicinity of the contact point and reflect at a large angle without losing energy. Other incident electrons are inelastically scattered, travel deeper into the specimen, lose energy, and reflect at a small angle. A portion of the incident electrons travel in a direction opposite to the beam, these electrons include secondary electrons (SEs) and backscattered electrons (BSEs), which provide compositional information from the specimen through BSE detectors or by releasing secondary electrons as they spring out from the specimen.

Electromagnetic radiation is also emitted, including X-rays, Bremsstrahlung, and visible light, which can be used to analyze composition and observe the specimen. In particular characteristic X-rays occur when an incident electron knocks out a bound

electron from the inner shell of an atom (e.g., K shell), thereby exciting the atom. If the electron vacancy is filled by another bound electron from a higher shell (e.g., L, M, etc), then an X-ray photon is emitted equal in energy to the difference between initial and final states [29]. The X-rays can be measured by their wavelength or energy and form the basis of elemental quantification/mapping in a SEM. This technique is known as energy dispersive X-ray spectroscopy (EDX) or electron probe micro-analysis (EPMA), and is used in conjunction with most modern SEMs.

The primary form of contrast in the SEM however, is through secondary electrons (SEs) emitted from the surface of a specimen. A coulombic interaction between incident or scattered electrons and bound specimen electrons can eject the latter from a narrow area (within 10 nm) close to the surface. A widely accepted value for SE energies is less than 50 eV and only those SEs with enough kinetic energy can escape the bulk material (~ 3 – 6 eV) [29]. The emission yield (ε) of SEs is dependent on the type of material; however the emission energy does not carry information that is characteristic of the specimen. Since SEs are only emitted from the narrow area upon which the focused electron beam is colliding, the strength of the signal collected is proportional to the local topographical features [21]. In theory, for a SEM, the spatial resolution depends only on the diameter of the focused electron probe; image quality is a result of reflected or secondary electron emission [14]. A cartoon of the electron beam – specimen interactions is shown in Figure 4. The arrows do not track actual trajectories; rather they serve to illustrate radiation used in various measurement modes.

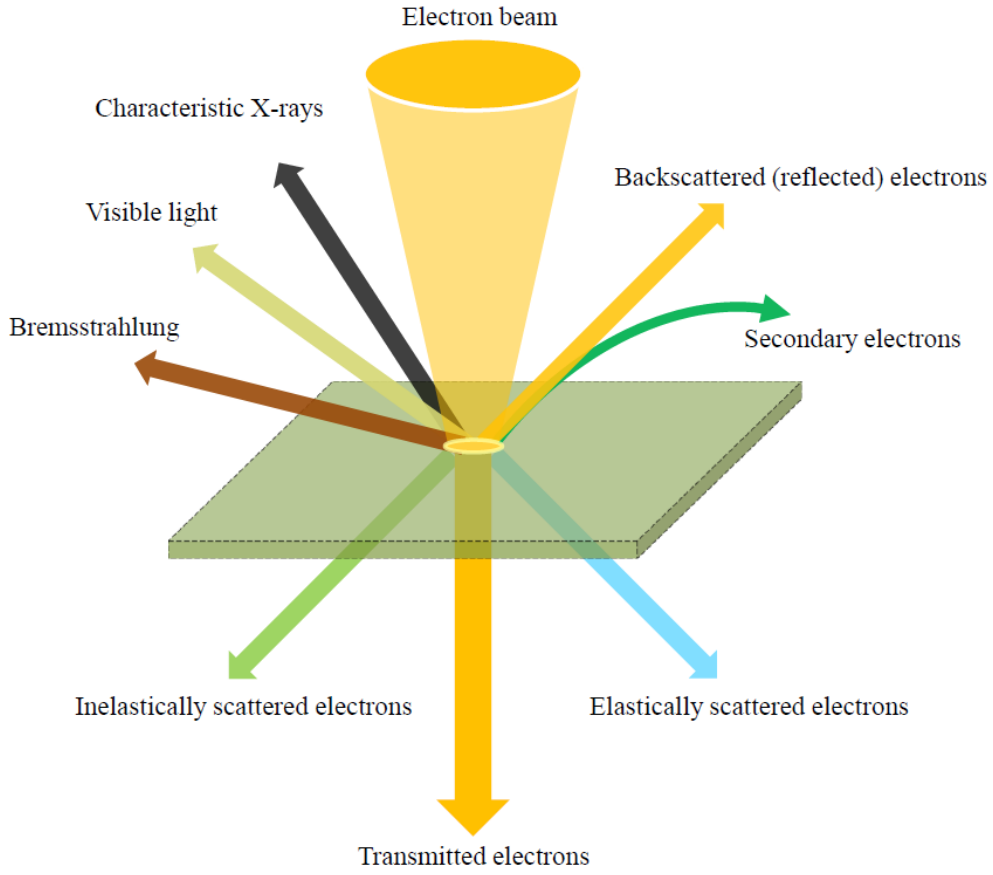

Figure 4 – Electron beam - specimen interaction summary illustration

2.1.3 SEM Imaging – Edge Effect

SE emission is responsible for topographical detail obtained with the SEM [14, 29]. First observed by Louis W. Austin and H. Starke (1902) while studying metals surfaces, SEs are widely recognized to change emission yield (ε) rate with changes on material and incident angle [30-32]. Preceding the development of the SEM, Hajo Bruining (1936) questioned how surface features affect SE emission by comparing smooth to rough carbon targets and varying the angle and energy of incident electrons [30]. Bruining's results showed that a smooth target SE emission was more susceptible to changes in angle of incident electrons than a rough target. It was reasoned that rough surfaces

produce similar SE emissions, nearly independent of incident angle, because an irregular surface did not favor an orientation from which to emit secondaries. At the time of Brunning's experiment image generation through SE emission was limited; however the effect of incident angle electrons on SE emission reported would later become an important phenomenon in SEM imaging known as the "edge effect."

Contrast in the SEM is proportional to the quantity of SEs emitted at a given spot. Therefore, higher SE emission as a result of a wider, more favorable, emission area can obscure surface detail. Figure 5 illustrates this event. Suppose an incident electron beam collided with a specimen containing fine details. As the beam is rastered, moved back and forth, topographical changes along the specimen will enhance or reduce SE emission by widening or narrowing the emission area. Edges will enhance the amount of SEs emitted whereas pits will reduce emission. Furthermore, the location of the SE ET detector within the specimen chamber plays a role, as areas facing away from the detector are unfavoured in terms of SE collection. The edge effect can be mitigated by lowering the energy of the incident electrons. Conversely, the edge effect can be exploited to locate features (edges) at low magnification. Because of the edge effect, microscopists using a SEM are recommended to tilt specimens to face the ET detector in an effort to maximize the quantity of SEs collected.

In this thesis, SEM is used to reconstruct a 3D model for surface morphology of polymeric microparticles. Thus, it is critical to be conscious of the edge effect, how it may impact a SE image, how it may be exploited, and any possible effects in multi-view surface reconstruction techniques when specimen tilting and rotation is required.

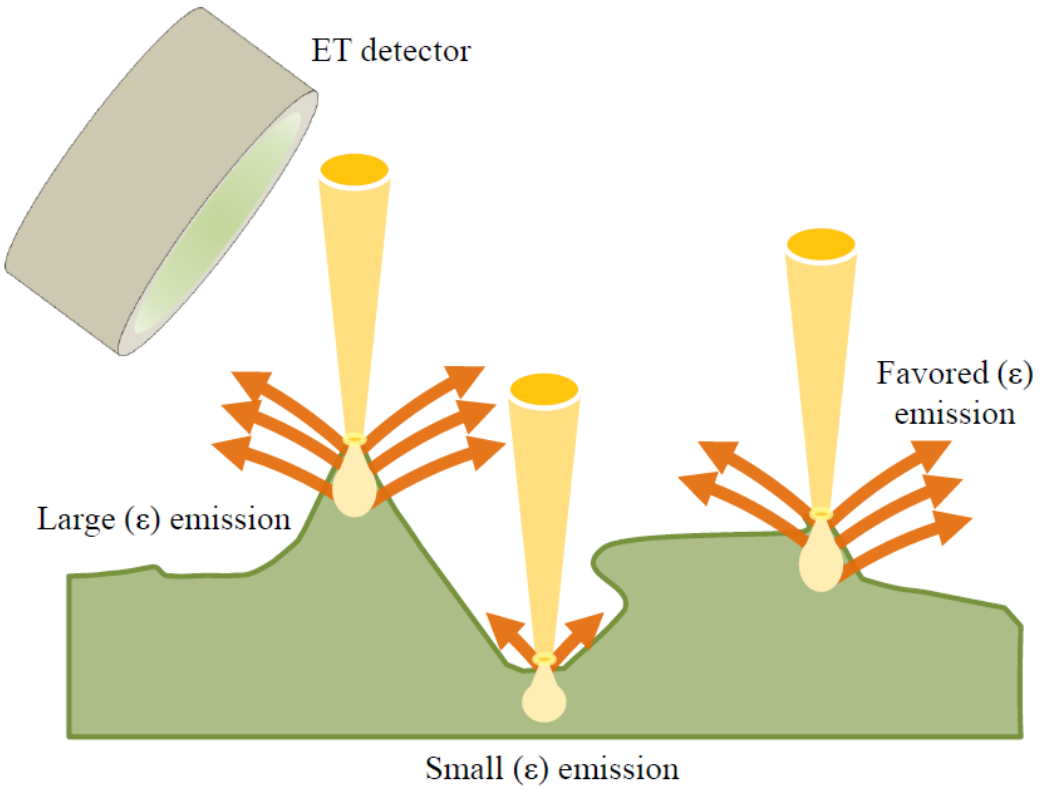

Figure 5 – Edge effect in various topographical configurations

2.2 Biomaterials and Drug Delivery

In this section, an attempt will be made to introduce and define biomaterials. This section also provides a brief introduction to the concept of controlled drug delivery, the contributions of pioneer Robert Langer to the field of controlled release, and the progression to tissue engineering. Biodegradable polymer microspheres are emphasized as delivery vehicles in drug therapy and tissue engineering. The research outlined in this thesis applies microsphere technology to human stem cells and attempts to quantitatively characterize their surface morphology via electron microscopy. Therefore, the concepts introduced in this section are relevant to understand microsphere fabrication/applications.

2.2.1 Biomaterial Definitions

The cross between materials and biology traces back to antiquity. Artifacts from ancient Egypt support the theory that early prostheses were meant not only to aesthetically replace lost body parts, but were also motivated by a desire to recover function [33]. Indeed as medical knowledge improved, specifically the nature of infection, materials began to transition from simple prostheses towards medical devices/implants [34]. World War II provided a leap forward, as the war effort created an abundance of new substances which were later made available for medical experimentation [34-36]. Materials science and medicine merged out of necessity in a period known as the “doctor/surgeon hero” era following World War II. This period was marked by a lack of regulatory oversight and willingness by surgeons to use any material to preserve life [36]. To achieve this goal, surgeons and doctors selected materials that showed minimal, or no host immune response.

As a result of the doctor/surgeon hero era, the scientific community attempted to define a biomaterial as *"a substance that has been engineered to take a form which, alone or as part of a complex system, is used to direct, by control of interactions with components of living systems, the course of any therapeutic or diagnostic procedure, in human or veterinary medicine''* [37]. Biomaterials can fall into three main types of substances; these are metals, ceramics, and polymers [35, 38]. Each biomaterial can be further classified by its interaction with living systems as biocompatible, bioactive or inert, and biodegradable or non-biodegradable [35, 38].

Biocompatibility is defined as *"the ability of a material to perform with an appropriate host response in a specific situation"* [35]. Biologically active materials are substances that can form interfacial bonds with the host tissue and trigger a desired response [35]. In contrast, inert materials are substances that show minimal or no host immune response while providing a desired outcome. Vert *et al.* (1992) has defined biodegradable in the context of polyesters as *"polymeric devices which break down to macromolecule degradation with dispersion in an animal model,"* where the prefix "bio" refers to contact with living tissues, cells or fluids [39]. By extension, non-biodegradable biomaterials are those that maintain their molecular structure despite contact with a biological system.

Bioactivity is perhaps best exemplified by the mineral material hydroxyapatite (HA), a naturally occurring calcium phosphate with a similar composition to human bone, often used for its ability to promote new bone growth without inflammation or foreign body response [35, 36]. HA can be processed into ceramics through wet, dry, and high temperature methods for different degrees of crystallinity/purity and it is currently one of

the major components that enables engineering of artificial bone [35, 36, 40, 41]. Similarly, stainless steel is perhaps the most prominent metal alloy classified as biocompatible, inert, and non-biodegradable. Originally developed in a pursuit of non-rusting steel to prolong the life of gun barrels, stainless steel is widely used in orthopaedic devices such as screws, plates, and nails [42]. Stainless steel was among the first generation of bioinert materials and it continues to be a prominent material used in many medical devices due to its low cost, corrosion resistance, and mechanical properties [42-44]. Although ceramics, metals, and alloys are important biomaterials widely used in clinical applications, further discussion into their properties is beyond the scope of this section as we narrow our focus towards biocompatible polymers.

Polymers are characterized by repeating subunits. Biomaterial polymers can be divided into natural or synthetic types. For example, collagen, a structural protein abundant in bone, skin, cartilage, tendons, and ligaments, is one of the most popular natural polymers for its ability to be processed into meshes, hydrogels, membranes, and sponges [35, 38]. Natural polymers, which monomer units consist of proteins, sugars, or nucleic acids, are generally considered to be more biocompatible than synthetic polymers. Usually derived from animal sources, natural polymers must be carefully sterilized without destroying the material to avoid introducing contaminants or an immune reaction before any clinical application [45].

Synthetic polymers are generally derived from petroleum sources and are widely used in medical applications because they can be mass produced and sterilized, posses a diversity of physical and mechanical properties, and can be modified to fit specifics needs

[6, 45]. Aliphatic (non-ringed structured) polyesters belong to a family of synthetic polymers that do not share structural features in common with natural polymers [39]. Commercially found in sutures, aliphatic polyesters break down via hydrolysis into biocompatible monomers. For example polyglycolic acid (PGA) was first obtained by ring-opening polymerization of glycolide, a molecule related to the metabolite glycolic acid found in mitochondria, peroxisomes, and bodily fluids [39, 46]. Although it remains the subject of academic research, aliphatic polyesters have shown bioresorption, i.e., complete removal through metabolization or filtration of degradation by-products [39, 47]. Synthetic biomaterial polymers that exhibit biodegradation and bioresorption, in the case of some aliphatic polyesters, have gathered interest for temporary clinical applications in medicine or drug delivery. Biodegradable polyesters and their use in microspheres for controlled drug delivery are discussed in further detail throughout this section.

2.2.2 Controlled Drug Delivery

The goal of drug therapy is to improve quality of life by curing illness or reducing symptoms while avoiding harmful side effects. The drugs can be made up of nucleic acids, sugars, small organic and inorganic compounds, peptides, and large macromolecules [48-51]. These molecules possess a large diversity of structures, modes of action, manufacturing techniques, and degrees of suitability for conventional drug administration (e.g., oral delivery via pills or parenteral delivery via injections) [12, 52]. Small molecules (< 900 Da) make up a majority (90%) of drugs in the pharmaceutical industry and owe their widespread use to an ease of manufacture and administration [52, 53]. In contrast, biologics are macromolecules (1 > kDa) with complex structures based

on proteins, sugars, nucleic acids, or combinations obtained from biological sources that owe their therapeutic effect to improved specificity and potency relative to small molecules [12, 52, 53]. Drug therapy stands to benefit from controlled delivery systems by effectively releasing drugs at an appropriate dose to the site of action.

A therapeutic effect is achieved by maintaining drug concentration bellow a toxic level and above an effective minimum, in a range referred to as the therapeutic window [1, 3]. To illustrate this concept, suppose a bolus injection of insulin is administered subcutaneously to treat diabetes. After injection, blood insulin concentration can be roughly modeled as a spike followed by decay as shown in Figure 6A. Insulin above a therapeutic level can prove fatal by severely depleting glucose levels, whereas insulin below this level will prove ineffective in treating diabetes. Therefore, optimizing the therapeutic effect by lowering the “peak,” extending the “valley,” and controlling when a drug is released, as shown in Figure 6B, is desirable in drug therapy and the motivation behind controlled drug delivery [2].

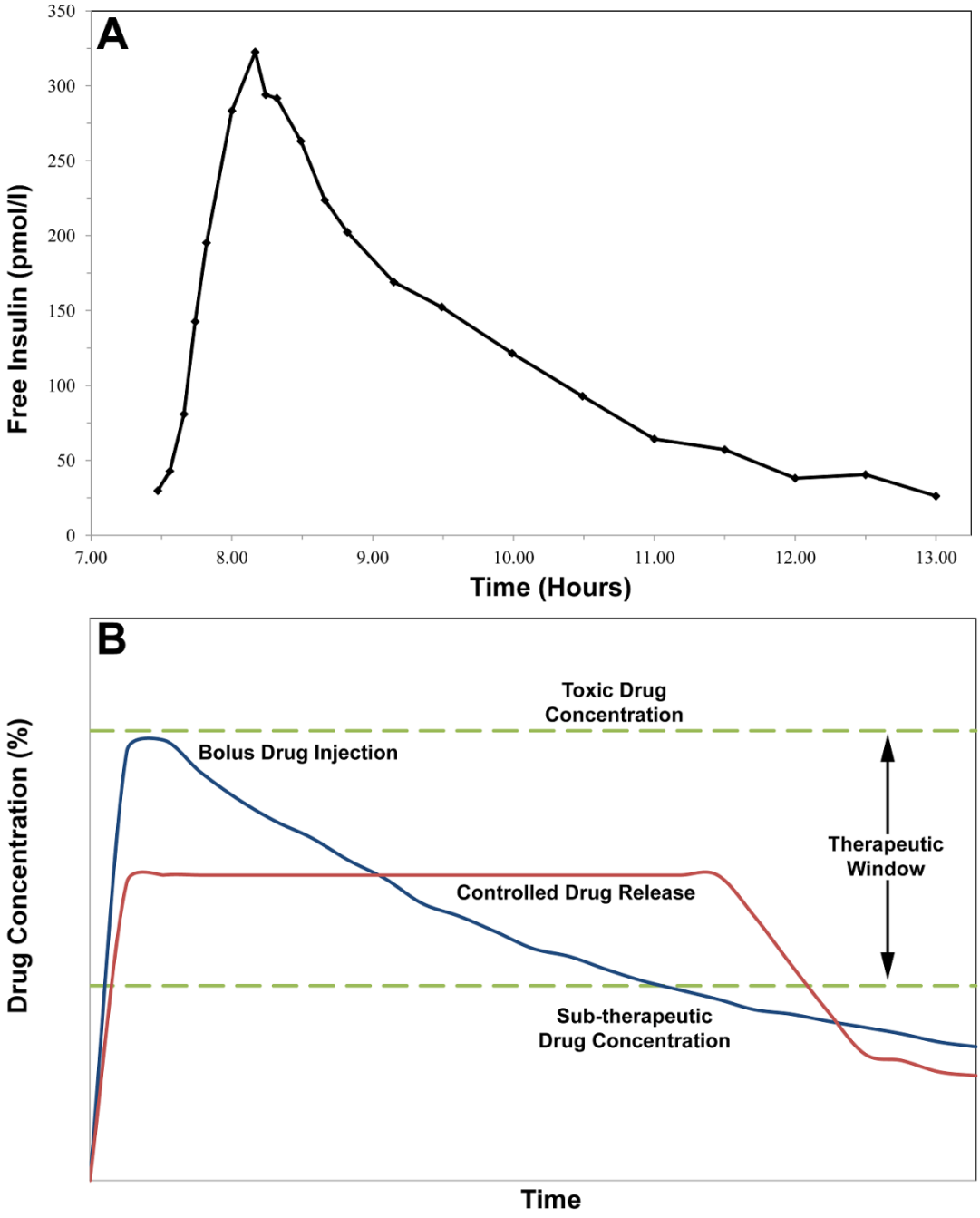

Figure 6 – Drug concentration over time. A) Plasma concentration of insulin analog after a subcutaneous injection; adapted from [54]. B) Idealized controlled drug release maintains concentration at therapeutic range to maximize effectiveness; adapted from [2, 3]

Drug therapy can be divided in two parts, the drug itself and the delivery system [55]. Early drug therapy (pre-20th century) focused on drug administration via the digestive tract due to its convenience and safety [55]. These formulations coated pills and tablets with sugar and gum, and more popularly with gelatin (derived from collagen), to improve taste and protect drugs from the environment [55]. This 0th generation of drug delivery systems delayed disintegration or dissolution of compressed pills and tablets for multiple daily doses [55]. Although a detailed discussion on the history of controlled drug delivery systems is beyond the scope of this section, three notable contributions from the following references are discussed to highlight the evolution of controlled drug delivery systems, divide the technology into generations, and introduce microspheres [2, 55-59].

The first notable contribution is the earliest example of controlled drug release, the Dexedrine Spansule®, introduced in 1952 by Smith Kline & French Laboratories (a predecessor to the pharmaceutical giant GlaxoSmithKline) [2, 55]. The "span" capsule was notable for two reasons: 1) it achieved an unprecedented 12 hour (twice-a-day or once-a-day) delivery of dextroamphetamine, and 2) it combined uncoated drug pellets (for an immediate dose) with several hundred drug pellets of differing coating thicknesses (1 or 2 mm diameter pellets for controlled, time-dependant doses) in a single oral formulation [55]. The complexity of the Dexdrine Spansule® inspired numerous pharmaceutical products and it is described by Kinam Park as marking the 1st generation of controlled drug release systems [2].

The second notable contribution focused on a different drug release mechanism, diffusion rather than dissolution, and enabled the rapid coating of micro-meter sized

particles. Patented by Dale E. Wurster (1953), wurster-based fluid bed microencapsulation is a method of uniformly coating air suspended drug tablets with a synthetic biomaterial polymer [36, 55, 60-62]. The novelty of this approach corresponds to the use of a biomaterial polymer film to coat particles with micro-meter precision [60, 62]. This form of microencapsulation enables solution to permeate the coating, "wet" the drug pellet, and creates a high concentration of drug in an enclosed membrane. To exit the delivery system, the drug must diffuse through the polymer membrane at a rate determined by thickness and properties of the polymer. This contribution is an example of drug delivery systems that progressed knowledge on diffusion based release and microtechnology.

The third notable contribution is the development of biomaterial microparticulates to deliver small molecules and macromolecules. The controlled and sustained release of macromolecules was regarded as impossible until Robert Langer (1976) used synthetic polymers in the form of "pellets" to encapsulate and release drug for a corneal assay [2, 59, 63]. Briefly, the goal of Langer's experiment was to isolate angiogenesis inhibitors relevant to cancer research, and solving this problem required a non-inflammatory implantable drug delivery system capable of releasing biologically active macromolecules in the order of days. The "pellets" were made by dissolving ethylene-vinyl acetate (EVA), a non-biodegradable and inert polymer, in volatile organic liquid, such as methylene chloride (dichloromethane; DCM), and introducing drug with an aqueous solution of polyvinyl alcohol (PVA). The mixture was then molded and as DCM evaporated the macromolecule would become trapped within the polymer matrix. The success of this novel drug delivery system was met with great skepticism; candid

accounts by Langer reveal that the scientific community did not believe that large molecules could diffuse through polymers and function as drug carriers [64, 65].

For small molecules, Beck *et al.,* (1979) used the biomaterial poly(lactic acid) (PLA) to create "microcapsules" containing norethisterone or progesterone in effort to create new contraceptive technology. The team sought to achieve this by dissolving drug and a biodegradable polymer in DCM, or chloroform and acetone, and combined the solution with an aqueous liquid like PVA, which serves as a stabilizing agent, to create an immiscible mixture of drug-polymer-solvent and aqueous solution. External forces, such as mechanical stirring, combine the immiscible liquids and create microscopic droplets of drug/polymer that shrink as the volatile organic solvent evaporates, and polymer precipitates, thereby entrapping drug. Beck *et al.,* (1979) tested microcapsule injection effects in the menstrual cycle of rat and baboon animal models; achieving success in extending target drug concentration and affecting the test animals ovarian cycle [57, 58].

To the best of my knowledge, the Langer "pellets" were the first microsphere-like device for sustained release of macromolecules via polymer molding, and the Beck "microcapsules" were the first for small molecules. Variations of Beck methodology are referenced as the oil-in-water (o/w) emulsion/solvent-evaporation technique and Langer "pellets" can now be achieved via water-oil-in-water (w/o/w) double emulsion/solvent evaporation. The novelty of these drug delivery system spawned the 2nd generation of controlled drug delivery technology referred to by Park as "smart" delivery systems [2]. Perhaps the most popular commercialization of this technology is Lupron Depot, an injectable month-long poly(lactic-co-glycolic acid) (PLGA) microsphere system

releasing leuprolide acetate (a hormone analog) developed from Langer's research, used to treat prostate cancer [8, 66].

Today, controlled drug delivery technology is an important part of drug therapy through 1st generation pills/tablets or 2nd generation smart systems. Beyond drug therapy, however, controlled drug delivery has been harnessed to introduce biomolecules into non-native environments and elicit a response. In principle a drug delivery system can be applied to protect a biomolecule from degradation (e.g., protein denaturation, chemical isomerization, oxidation, photodegradation), control release, and influence a biological system [67-69].

The idea of combining drug delivery technology with stem cells was quickly recognized by Langer, when he proposed using biomaterial drug delivery systems as scaffolding to support stem cell growth. In a popular 1993 paper titled *Tissue Engineering*, Langer proposed *"an interdisciplinary field that applies the principles of engineering and the life sciences toward the development of biological substitutes that restore, maintain, or improve tissue function"* [70, 71]. For example, in neural tissue engineering, scaffolds can be constructed out of biomaterial polymers to support stem cells in potential peripheral and central nerve regeneration [72]. Electrospun biodegradable polymer materials can create nanofiber scaffolds that mimic the extra cellular matrix (ECM) of cells and act as temporary support while the cells construct their own ECM [73]. The ideal properties of a polymeric scaffold for nerve regeneration have been outlined by Subramanian *et al.,* (2009) as biocompatibility, controlled biodegradability with non-toxic byproducts, minimal inflammation response, porosity for

vascularization and cell migration, the ability to form 3D matrices with appropriate mechanical properties to mimic the ECM, potential as a delivery vehicle of cells for transplantation, and the ability to promote re-growth via **drug delivery** of neurotrophic factors or small molecules [72]. Similar properties are applicable to other types of tissue engineering and readers interested in these areas are referred to a recent summary by Robert Langer [70].

It is accepted that advances in controlled drug delivery technology enabled tissue engineering by releasing drugs onto stem cells through biomaterials in a spatio-temporal manner. An example of the cross-over includes biodegradable polyester microspheres used in both drug therapy and tissue engineering to release macromolecules or small molecule drugs. As of 2014, there are almost a dozen PLGA microsphere-based pharmaceutical products in the market [12]. Furthermore, some researchers have successfully combined microsphere to direct stem cell differentiation in tissue engineering [74, 75].

2.2.3 Biodegradable Microspheres

Microspheres are a subtype of microparticle delivery systems capable of encapsulating small and large molecules for sustained release. Unlike Wurster-coated microparticles however, microspheres engulf drug throughout a polymer matrix; polymer properties and drug physicochemical properties such as hydrophilicity and lipophilicity determine if the drug is dispersed throughout the polymer, or if it separates into phases to form distinct regions/pockets. Microsphere drug release is affected by the amount of drug loaded, microsphere particle size, porosity and morphology, drug size and solubility, and polymer

concentration [9, 76]. Microsphere-based controlled drug delivery can protect and release various types of drugs in a localized and time-dependant manner. Additionally, microspheres are relatively easy to manufacture with biocompatible polyesters, making them simple and accessible drug carriers for applications in drug therapy or tissue engineering.

Drug therapy with large and small molecules is improved with controlled drug delivery via microspheres by the following reasons: 1) Sustained release; microspheres have been shown to release small or large molecules at a relatively steady rate for month-long periods. This effect reduces the number of drug administration sessions as drug concentration can predictably remain in a desired therapeutic range. 2) Protection; drugs released from microspheres have been shown to remain biologically active after encapsulation and release i.e., retain therapeutic potential. This feature is particularly useful for biologics, whose therapeutic potential is derived from molecular structure and do not lend themselves to delivery via oral formulation; where the digestive process breaks down molecular structure. 3) Targeting; microspheres can be injected in close proximity to diseased tissue, e.g., Lupron Depot injections to a cancerous prostrate. This can reduce side effects by effectively delivering a drug payload away from healthy cells.

Tissue engineering exploits the drug therapy benefits of microspheres in a novel way. In stem cell research, small molecule morphogens such as retinoic acid (RA) can be used to direct stem cell differentiation [77, 78]. Stem cells intended for applications in tissue engineering are often cultured as 3D aggregates known as embryoid bodies (EBs) to produce large number of cells and test pluripotency, i.e., the stem cell ability to become

any specialized cell-type, as EBs spontaneously rearrange into three germ layers mimicking gastrulation [79]. Cell culture techniques introduce RA to EBs in a 4-/4+ protocol (i.e., 4 days with RA in solution, 4 days without) to primarily promote neural progenitors [80]. Such protocols require a time-dependant dosage and careful monitoring to maintain the desired drug concentration.

Introducing morphogenic molecules into solution can restrict EBs into one germ layer to produce homogeneous differentiation. However, due to the 3D spherical nature of an EB, morphogen concentration varies across the spheroid volume and causes some stem cells to receive an uneven dose. A mass transfer model by Van Winkle *et al.,* (2012) showed that atomic molecules, such as oxygen, vary concentration across EB volume due to the size of the aggregate, number of cells, and cellular uptake [81]. To address this challenge, stem cell researchers introduced morphogen-loaded microspheres directly into the EB microenvironment to achieve homogenous morphogen distribution and gain additional control over stem cell differentiation [74]. Carpenedo *et al.,* (2009) reported the novel use of drug delivery technology by combining mouse embryonic stem cells with RA/PLGA microspheres and the technique continues to gain traction [74, 82].

Microspheres are often manufactured with polyesters, which have the ability to break down in situ thereby eliminating the need of surgical removal. Uhrich *et al.*, (1999) has described polyesters as the most well-studied biodegradable polymer systems with extensive use in drug delivery [3]. In general, the ester bonds that hold biodegradable polyesters have poor hydrolytic stability, in contrast to the well-known non-biodegradable polyester polyethylene terephthalate (PET) used in clothing or containers

[83]. As biodegradable polyesters hydrolyze, the resulting monomers or oligomers are themselves biocompatible and can be resorbed or excreted via natural pathways [3, 6]. For example, it is theorized that poly (ε-caprolactone) (PCL) breaks down into smaller molecular weight sections via hydrolytic cleavage until low molecular weight (< 3000) PCL can be absorbed by cells and break down via enzymatic reactions [84]. It is widely accepted that biodegradable polyesters can undergo bulk degradation or surface erosion; with surface erosion being preferred over bulk erosion due to its predictable effect on drug release [3, 84].

Biodegradable microparticles can be manufactured in various ways. Wischke *et al.,* (2008) published a comprehensive review covering various drug properties that affect microencapsulation, such as drug solubility in aqueous and organic media and drug-polymer interactions [9]. Furthermore, the review includes the most popular methods for fabricating polyester microparticles to deliver hydrophobic drugs, such as the various microsphere emulsions (e.g., solid-in-oil-in-water (s/o/w), o/o, o/w, and w/o/w), in-situ forming microparticles, salting out/phase separation, polymer melting, and spray-drying techniques among others [9]. The classic oil-in-water (o/w) single emulsion/solvent evaporation technique, first described by Beck *et al.,* (1979), has been extensively used to encapsulate small molecule hydrophobic drugs and it remains one of the most accessible methods for microsphere fabrication [57, 58]. For instance, the o/w single emulsion technique was used to encapsulate RA for the novel application of microspheres in tissue engineering, and industrial versions of the technique are used in the commercially available pharmaceutical product Vivitrol®, used to encapsulate the small molecule drug naltrexone to treat alcohol dependence [74, 85, 86].

As 3rd generation drug delivery systems are being developed, the need for long-term controlled drug release (6 months - 1 year) has been identified and microspheres are well positioned to breach this gap by using long-term biodegradable polyesters. Achieving long-term drug release will require exhaustive examination of microsphere properties. There is a known link between microsphere surface morphology and drug release rate. However, most academic papers focus on drug release kinetics to evaluate microsphere drug carrier potential, often describing surface morphology in qualitative terms. In this thesis, I use PCL as it has received renewed interest for its long-term biodegradation, biocompatibility, low cost, and lack of local acidity increase upon degradation. Additionally, I employ the o/w single emulsion/solvent evaporation technique due to its simplicity, and potential to fabricate large quantities of microspheres with distinct surface morphologies as reported by Bile *et al.,* (2015) [11].

2.3 State of the art – Microsphere Characterization

In this section, an attempt is made to review a few publications that primarily sought to characterize microsphere properties; as most publications focus on drug release or pharmacological effects. I begin by introducing early publications and note the family of techniques used to characterize microsphere structure/physical properties. I end by reviewing 2000s publications that explored quantitative assessment on microsphere morphology via microscopy.

2.3.1 Microscopic Detail

The Langer studies were the first to achieve sustained release of macromolecules but the researchers focused on the pharmacological effects of their invention; microscopy

results were not included and physical properties of the drug delivery device were not reported [59, 63]. The Beck studies however, confirm particle "completeness" via SEM as well as characterized pharmacological effects of drug delivering "microcapsules" in-vitro and with animal models. The reported micrographs were used to discern if particles were spherical (or irregular) in nature and to estimate if precipitated drug could be located on the particle surface [57, 58]. Comments on sample preparation for electron microscopy were not included in either Beck study. These early microsphere micrographs were valuable to reveal the drug delivery device surface and shape, but did not provide quantitative analysis. Indeed in one of the studies, the authors admit to performing a "visual inspection of the microcapsules [to] reveal extremely symmetric spheres [and] relatively smooth surface[s]," and focused on characterizing the "microcapsules" via drug release and biological effects, thus providing the template for most microsphere studies [58].

Benita *et al.,* (1984) not only recognized the pharmacological significance of the Beck microcapsules but also noted that "little [had] been reported about the physical properties of such microspheres" [7]. Benita *et al.,* encapsulated progesterone or lomustine in PLA in process similar to Beck *et al.,* to explore the effects of emulsifying agent (stabilizer) type and concentration, amount and type of drug dissolved, duration and mixing speed, and continuous vs. interrupted organic solvent evaporation [57]. The study shed light on fabrication conditions that minimize the formation of free drug crystals and reported associated morphology changes via optical and scanning electron microscopy. Although qualitative in nature, the researchers were able to determine via SEM that microsphere surface morphology ranged between "very smooth surfaces" when free drug crystals did

not form and “rippled and rough” surfaces when free crystals were present. While no comments are included about sample preparation for microscopy, four micrographs (three SEM and one optical) confirmed a range of surface morphology. The other results provided evidence of a relationship between higher stirring rates and smaller mean particles size, as well as storage conditions that preserve drug-loaded microsphere shelf-life. Interestingly, drug loadings are reported for various microsphere batches but no drug release studies were included. Therefore, it can be concluded that Benita *et al.,* performed this study to explore microspheres as a function of fabrication parameters, thereby establishing a new way of analyzing the drug delivering devices; primarily based on morphology and supported with drug release or biological effects.

Another example of a morphology-oriented study was published by Rosilio *et al.,* (1991), who suggested that microsphere morphology could vary substantially as a function of fabrication parameters, drug loading, and thermal history [87]. To test their hypothesis, Rosilio *et al.,* used an o/w emulsion process to encapsulate progesterone in PLGA with various theoretical drug loadings, different agitation rates, and surfactant (aqueous) types. The physico-chemical nature of the study pushed the researchers towards analytical techniques like SEM, differential scanning calorimetry (DSC) and x-ray powder diffraction (XRD) to study microsphere formulations. XRD was used to determine x-ray patterns of progesterone polymorphs likely to be formed during fabrication and present in the microspheres or their surface. SEM micrographs (300X magnification) were used to confirm that microsphere morphology changed with drug loading; becoming more textured and with defects as the drug loading is increased (10 wt%; uniform and smooth, 28 wt% uniform but textured with irregular polymer particles

attached). Furthermore, higher magnification SEM micrographs (2000X magnification) revealed a dimple microsphere surface with the highest drug loading (50 wt% progesterone) covered in excess polymer structures. DSC scans formed the bulk of the quantitative data obtained in the study; revealing up to four thermal events believed to be associated with residual DCM within the microspheres, melting or crystallization of drug within or on the microspheres, and glass transition temperature of PLGA. DSC scans provided evidence of residual DCM which led the authors to conclude that the solvent's presence played a role in introducing drug polymorphs observed via XRD. Born out the same research team, a similar analysis by Courteille *et al.,* (1994) used drug-loaded polystyrene, a non-biodegradable inert polymer not approved for drug delivery, microspheres to further explore the structure and behaviour of polymer microspheres [88]. Notably, Courteille *et al.,* reported coating polystyrene microspheres with a layer of gold/palladium to aid their surface morphology study via SEM, a practice used to increase contrast and sample conductivity. As a result of the works of Benita, Rosilio, and Courteille *et al.*, it can be suggested that a combination of microscopy, spectroscopy (e.g., XRD), and thermal analysis (e.g., DSC) form the basis of publications that characterize microsphere physical properties to date.

Contrast and resolving power often made it difficult to distinguish polymer from drug via microscopy and thus, the data obtained was commonly limited to qualitative analysis. Early studies relegated micrographs to support data from other techniques; primarily using them to estimate microsphere particle size and shape via descriptors (such as aspect ratio and circularity) and to support comments on surface morphology. However, as new

microscopy techniques became available and computers streamlined digitization of micrographs, groups started to reveal (and quantify) microsphere details not seen before.

2.3.2 Quantifying Microsphere Morphology

Particle morphology can refer to particle size, shape, internal structure, and surface properties [89]. Microsphere studies have successfully used microscopy to report sizes and shapes, however, internal structure and surface properties have been more challenging to report. One of the first studies to quantify the internal morphology of microspheres included Lamprecht *et al.,* (2000), who used a confocal laser scanning microscope (CLSM) to study the internal structure of w/o/w double-emulsion PCL microspheres by encapsulating fluorescent molecules and bovine serum albumin (BSA) [90]. The micrographs reported by Lamprecht *et al.,* confirmed discrete regions of polymer and model drug. More importantly, their work showed how a CLSM could be used to study planar sections of an intact microsphere.

The idea of enhancing contrast to study the internal structure of double-emulsion microspheres via microscopy was further exploited by Zhao and Rodgers (2006) [91]. Careful staining of ovalbumin (OVA) loaded PLGA double-emulsion microspheres with osmium, and post-staining with uranyl acetate and lead citrate, allowed the researchers to detect protein content via bright-field TEM. Imaging several 80 nm cross sections allowed the researchers to create a 3D computer model of protein distribution and visualize the details of the internal morphology of a selected particle. While the researchers admit that the staining process was time consuming, and a disadvantage of the technique, the creative use of microscopy revealed quantitative data from

microspheres not seen before, enabling a direct measurement of drug content. Indeed, a drug release study of the microspheres was combined with their staining method, and pixels representing protein content were counted to estimate how much drug remained at different time points in a selected microsphere. The authors showed that independent TEM data analyzed by pixel counting had good agreement with experimental data obtained in the protein release study, but more importantly, it enabled them to "see" how the protein was being depleted throughout a selected microsphere in a transient manner [91].

A culmination on quantifying internal morphology for the purpose of studying a correlation between drug distribution and burst release can be found in the recent work of Huang *et al.,* (2015); where a combination of SEM, CLSM, and nano-computed-tomography (nano-CT) were used to image cross sections and the internal pore network. Pixel analysis was used with nano-CT data to create 3D models of intact BSA-loaded PLGA microspheres [92]. It is critical to note that Lamprecht *et al.*, Zhao and Rodgers, and Huang *et al.*, exploited the presence of macromolecules by enhancing contrast through staining with heavy atoms or fluorescence to reveal internal morphology and structural details. A similar labeling approach would prove more difficult in the case of single emulsion microspheres encapsulating small molecule drugs. However, the combined results showed how microscopy-based efforts could contribute new data on these drug delivery devices by creative use of high-resolutions microscopes and contrast enhancing techniques to measure internal morphology.

The previous works inspired the following question: what has been done to measure the external morphology of these delivery devices? Bile *et al.*, (2015) highlighted that "researches concerning the microparticle surface [morphology] are scarce," and set out to investigate how fabrication parameters can be controlled to promote specific morphologies. [11]. An o/w single emulsion technique was used to create PCL microspheres with various morphologies; microspheres were qualitatively categorized via SEM as smooth, rough, holy, and dumbbell-shaped [11]. The authors encapsulated vitamin D3 as a model drug and provided further evidence in support of a link between rough surface morphologies and faster drug release. While the parameters reported by Bile *et al.*, are valuable to reproduce similar morphologies, the team relied on qualitative assessments to categorize particles. Particle *smoothness* or *roughness* was not fully assessed in the Bile study suggesting further work is needed to measure the external morphology of microspheres or that such measurement is not readily obtainable.

Literature searches point towards scanning probe microscopy (SMP) as the primary family of techniques used to measure roughness (topography) and obtain images (and other properties) at the micro or nano-scale by physically interacting with a sample's surface. Briefly, these types of microscopes used a physical probe tip to raster across a surface and record a 1-dimensional profile of the z-movement of the probe in the path traveled, the probe is then moved to parallel location in an x-y plane and the process is repeated thereby generating 3D information [93].

To the best of my knowledge, atomic force microscopy (AFM), a subset of SPMs, was first used by Montanari *et al.*, (2003) on polymer microparticle drug delivery systems to

compare β or γ-irradiation effects of sterilization [94]. A spray drying technique was used to create PLGA microspheres loaded with bupivacaine, a small molecule drug, and irradiated by a nuclear source (Cobalt-60) or electron beam for γ or β-rays respectively. Their analysis showed that both forms of sterilization degraded surface morphology by reporting an increase in surface roughness. In particular, the researchers claimed statistically significant changes in roughness, measured as the root-mean-square (rms) data or the standard deviation over all height values within an area – $1\mu m^2$ in this case, after both types of radiation, with γ-rays always producing higher values.

Dorati *et al.*, (2006) continued to characterize microsphere surface via AFM and SEM to test if the presence of poly (ethylene glycol), (PEG) a protective excipient, could reduce damage incurred through irradiation [95]. A double emulsion w/o/w technique was used to create OVA-PLGA microspheres with varying amounts of PEG. Sodium chloride (NaCl) was also included at 10% w/v to reduce protein leakage. SEM analysis revealed that microspheres treated with NaCl exhibited a dense and compact structure, counteracting the porous effect obtained by adding PEG. Error signal AFM images showed that OVA/PLGA/PEG/NaCl and OVA/PLGA/NaC l microspheres were the smoothest through rms data before γ-ray irradiation [95]. Formulations that contained PEG did not significantly change rms values after γ-ray irradiation, regardless of the amount of PEG present, quantitatively confirming a protective effect. The AFM scans reported by Dorati *et al.*, covered an area of 25 μm^2 and were obtained through a series of six images from each microsphere formulation. Although microspheres are reported to have a maximum size of 50 μm, no detailed particle size analysis is included. Together, the maximum particle size, AFM scan coverage, and number of images used to calculate

rms values, suggests that despite power of AFM to obtain and report surface roughness, some limitations exists.

Perhaps the most recent use AFM to study microparticles for drug delivery can be found in the work of Lungan *et al.*, (2015), where various formulations of highly porous polysaccharide/methacrylic microparticles were carefully analyzed [96]. Briefly, a suspension polymerization technique that crosslinked glycidyl methacrylate and xanthan gum allowed them to create complex surface morphologies that appeared similar under low resolution SEM [96, 97]. High magnification SEM revealed distinct morphologies and AFM scans covering 10 μm^2 confirmed different roughness values for each formulation [96]. Unfortunately, Montanari *et al.*, Dorati *et al.*, and Lungan *et al.*, are among the scarce works that employ AFM, despite the valuable quantitative information it can provide in regards to the external surface morphology of drug delivering microparticles. It can be suggested that physical size of the probe limits the area covered by an AFM, perhaps making it deterrent to wider application in the study of microspheres. Therefore we ask: could a variable size probe microscope (e.g., SEM) be used to obtain comparable data?

SEM is excellent at capturing information from a specific spot through secondary electron emission, and other forms of radiation, generated by electron beam – specimen interaction. A high depth of field (3D effect) is achieved from a 3D object as information collected throughout a scan is simultaneously displayed in a final 2D image. Although it can be argued that this “3D-feel” is aesthetically pleasing, it unfortunately obscures focal differences that could be used to measure depth. Recovering depth from 2D images has

long been accomplished via stereoscopic vision, with examples originating alongside the development of photography. Although stereomicroscopy is not a new technology, the use of computer algorithms to match stereo-SEM micrographs pairs only began appearing within the last 30 years [98]. Since then, advances in computer vision algorithms and software tools have opened 3D analysis possibilities with older workhorse SEMs. 3D surface reconstructions are now possible based on stereomicroscopy principles and are quickly becoming an area of research within microscopy, highlighted by number of recent publications [99-102]. To the best of my knowledge, a computer stereo-vision approach has not been so far applied to the study of microsphere surface morphology.

2.3.3 Chapter Summary and Proposed Work

This chapter acknowledges that microspheres are not a novel technology, with its roots dating back to conventional drug delivery and Beck's and Langer's experiments. Furthermore, I cite some of the existing pharmaceutical products based on this technology, e.g., Lupron Depot and Vivitrol®, and reference future goals of further development e.g., long-term (1 year +) applications. Additionally, I recognize that microsphere technology has recently been explored as way to control differentiation of stem cell aggregates by the McDevitt group, starting with Capernedo's experiments successfully combining RA/PLGA microspheres with murine embryonic stem cells for added control over their differentiation. Ultimately, I highlight that microspheres have been studied through their pharmacological effects and/or physical properties, the latter including spectroscopy, thermal analysis, and beginning with basic microscopy observations but currently seeking to quantify every aspect of microsphere particle morphology; with success through advanced CLSM, TEM, nano-CT, AFM, and pixel

analysis of the imaging data. Therefore, the work submitted in this thesis includes three sections involving polyester microsphere drug delivery technology: 1) mastery over microsphere fabrication and characterization techniques, 2) the use of RA/PCL microspheres to deliver morphogenic drugs to human induced pluripotent stem cells, and 3) modern computer stereo-vision techniques applied to SEM to reconstruct a microsphere surface morphology model.

Chapter 3 Materials and Methods

3.1 Microsphere Fabrication

3.1.1 Retinoic Acid Microspheres[1]

PCL microspheres were fabricated by an oil-in-water single emulsion technique as previously described [103]. The trial microspheres had a RA encapsulation target of 3 µg/mg RA/PCL inspired by the concentration first studied by Carpenedo *et al.,* (2009) to deliver drug to mouse embryonic stem cell aggregates [74]. The experimental microspheres had RA encapsulation targets of 4 or 30 µg/mg RA/PCL to test different effects of RA release on human induced pluripotent stem cells. Briefly, 500 mg of PCL (Mn ~45,000) (Sigma) were dissolved in 3 ml of dichloromethane (DMC) (VWR International) and mixed in a hotplate (Corning-PC420) to create the oil phase. 1.5, 2, or 15mg of retinoic acid (RA) (Sigma) were added to the oil phase to create 3, 4 or 30 µg/mg (w/w) RA/PCL concentrations respectively. 3 ml of 100% ethanol were also added to the oil phase while mixing. Drug-free microspheres followed the same protocol

[1] The following section contains excerpts from: **Incorporation of Retinoic Acid Releasing Microspheres into Pluripotent Stem Cell Aggregates for Inducing Neuronal Differentiation.** Gomez, J.C., Edgar, J.M., Agbay, A.M., Bibault, E., Montgomery, A., Mohtaram N.K., Willerth, S.M. Published by the Journal of Cellular and Molecular Bioengineering in June 2015.

without RA. For the trial microspheres, 2 ml of 2% (w/v) poly(vinyl alcohol) (PVA) (Mw 13,000-23,000, 87-89% hydrolyzed) (Sigma) were carefully added for a total volume of 8 ml. In the experimental microspheres, I revised the water phase to 3 ml of 2% (w/v) PVA for a total volume of 9 ml. 2% PVA was carefully added to the oil phase so as to not disrupt the ensuing boundary layer (e.g., Figure 7).

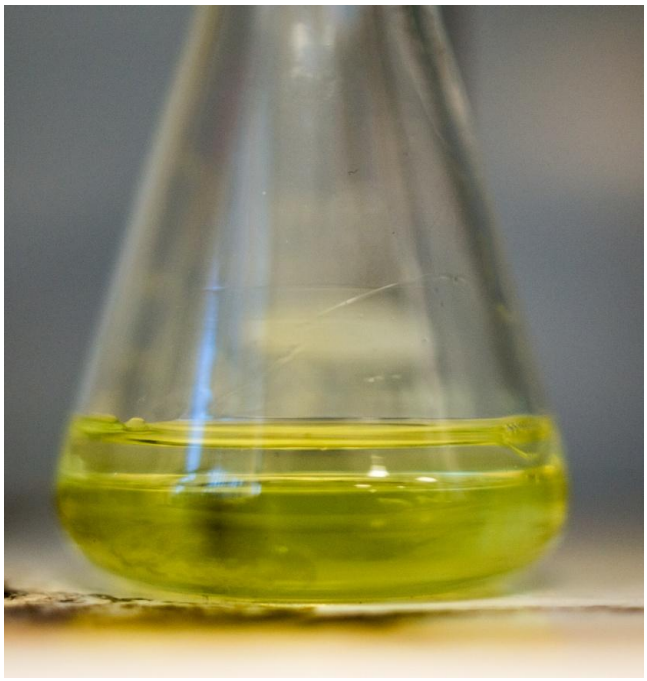

Figure 7 – An image of the oil and water phases separated before the emulsion process. RA solution has a yellow color and it is composed of equal parts ethanol and DMC. PVA solution is transparent.

For the trial microspheres, an undisturbed mixture was emulsified with a vortex mixer (Fisher Scientific) at 10 speed for 10 seconds and transferred via syringe to a 100 ml 0.3% (w/v) PVA stabilizing solution at 35°C, 400 rpm for 4 hours. The trial microspheres were collected via vacuum filtration. In the experimental microspheres, the oil-water solution was emulsified with a vortex mixer for 12 seconds and transferred via glass pipette to a stabilizing water solution of 100ml 0.3% (w/v) PVA at 35°C. The emulsion

was stirred for 4 hours at 500 rpm while DCM evaporated. Drug-free, 4, and 30µg/mg microspheres were collected by centrifugation at 4000 rpm (Eppendorf 5810R) and washed with dH_2O to remove PVA traces. Stabilized microspheres were frozen and lyophilized for 24-26 hours. Powdered microspheres were stored at -20°C until use and sterilized via air-plasma (Harrick PDC-32G) on low power for 30s before stem cell work.

3.1.2 Variable Morphology Microspheres

Microspheres were fabricates using identical settings but with changes to polymer concentration (w/w) and polymer molecular weight (Mn) to create different surface morphologies. All variable surface morphology microspheres are drug-free. Briefly, a $PCL_{45,000}$ to DCM ratio was calculated (see Table 4.7) to obtain 3, 5, and 10% w/w concentrations. The process was repeated with $PCL_{80,000}$. 2% PVA was carefully added to not disrupt the boundary layer at a 3:1 PVA/DCM ratio. The corresponding oil phase was vortexed at 2000 rpm for 3 minutes. The resulting emulsion was then transferred by careful pouring to dH_2O solution to create a stabilizing 1% PVA bath. The stabilizing batch was stirred at 600 rpm (Corning PC-220) and room temperature for 4 hours. Weight measurements before and after confirmed the evaporation of DCM. The resulting microspheres were collected by centrifugation and lyophilized as previously described in this thesis.

3.2 Microsphere Characterization

3.2.1 Retinoic Acid Microspheres[1]

A Hitachi FE-SEM 4800 field emission scanning electron microscope (SEM) was used to observe surface morphology and estimate particle size. Small volume suspensions (1 –

1.2 ml) of microspheres in 100% ethanol were used to disperse particles over SEM stubs. Following ethanol evaporation, prepared stubs were sputter coated with gold-palladium using an Anatech Hummer VI sputter coater. The quartz-PCI Image Management Systems® software was used to estimate microsphere diameter. Data was transferred to .CSV files and loaded into the R software environment for plotting and analysis. Diameter histograms were plotted with bin sizes equal to 1 μm; starting from the smallest observed diameter to the largest in each microsphere formulation. Polynomial regression was used estimate a density function for each microsphere population. Expected microsphere diameter corresponded to the first moment of the calculated density function, and variance corresponded to the second central moment of the density function.

RA loading was estimated via spectrophotometry by dissolving 10 mg of 3, 4 or 30 μg/mg RA/PCL microspheres in DCM and measuring the amount of RA recovered. PCL was removed from solution by introducing 100% ethanol and precipitated through centrifugation. The ensuing supernatant was removed and light absorbance was measured at 354nm with an Infinite M200 Pro plate reader. RA concentrations were estimated via standard curve. Drug encapsulation efficiency was defined as: recovered RA (dissolved microspheres) over total RA (amount used in each formulation).

$$\left[\frac{Recovered\ RA\ (\mu g)}{Total\ RA\ (\mu g)}\right] \times 100\%$$

RA release studies measured the amount of RA remaining in microspheres at selected time points within 28 days. Briefly, 10 mg of 3, 4 and 30 μg/mg microspheres were

measured into multiple conical vials and suspended with 1 ml of phosphate buffer saline (PBS) (Life Technologies). Sample vials were placed on a microplate shaker (VWR Microplate shaker) and incubated at 37°C to retain particle suspension and replicate cell culture temperature. Sample vials were centrifuged every 2 days to replace the PBS wash. Vials pre-labeled for retrieval were removed at this stage; i.e., day 2, 4, 8, 12, 16, 20, 24, and 28. Retrieved sample vials were prepared by washing the microspheres with dH_2O three times, lyophilized, and weighed to compare with initial mass. Trial microspheres were also prepared for SEM imaging at day 1, 4, 8, 12, 16, 20 as previously described. RA in concentration was determined as previously described. The quantity of RA released was calculated by subtracting the RA remaining in the microspheres from the RA present in day 0 microspheres.

3.2.2 Variable Morphology Microspheres

Sample preparation for SEM imaging of drug-free variable morphology microspheres followed two different methods. 1) Automated particle diameter and qualitative survey. 2) Stereo-microscopy of surface morphology and 3D reconstruction. Method one: a SEM aluminum stub was coated with a layer of PELCO® isopropanol based collodial graphite paint (Ted Pella Inc.). After drying, the coat was grinded with a paper towel on a flat surface in a unidirectional pattern. Small volume suspensions (1 – 1.2 ml) of microspheres in dH_2O were dispersed over prepared SEM stubs. Filter paper pieces were used to remove water via capillary action. An optical microscope (10X magnification) was used to aid in droplet removal. Prepared samples were stored overnight to allow for complete dH_2O evaporation. Samples were imaged at identical conditions. Micrographs were loaded into ImageJ 1.48v for image processing; removing scale bar, finding edges,

and image thresholding. Processed micrographs were then loaded into the MATLAB® programming environment and a Circle Hough Transform (CHT) was applied at appropriate radius (in pixels) guess. Detected circles were double-checked for false positive. Detected radii were converted to micrometer diameters, transferred to .CSV files, and loaded to the R software environment for plotting and analysis. Method two: small volume suspensions (1 – 1.2 ml) of microspheres in 100% ethanol were used to disperse particles over regular SEM aluminum stubs. Following ethanol evaporation, prepared stubs were sputter coated with gold-palladium using an Anatech Hummer VI sputter coater for high magnification imaging. Stereo-micrographs pairs were obtained at identical conditions with 8° tilt angle separation. Stereo-micrographs were created using Anaglyph Maker V1.08. 37 micrographs were collected at identical conditions as described in Figure 4.28 for a 3D model. Model reconstruction was obtained from Autodesk ReMake. Autodesk NetFabb was used to digitally slice the model, measure, and scale.

3.3 RA/PCL effects on hiPSC aggregates[1]

3.3.1 Pluripotent Stem Cell Culture

Human induced pluripotent stem cells (hiPSCs) (iPS(Foreskin)-1, Lot 1-DL-01, WiCell) were maintained on Vitronectin XF™ (STEMCELL, Technologies) coated 6 well plates and cultured with TeSR™-E8™ media (STEMCELL, Technologies) as previously described [104]. Briefly, stem cell aggregates were formed by dissociating cells with ReLeSR™ (STEMCELL Technologies) and inoculating 2ml of neural induction medium (NIM) (STEMCELL Technologies) with a single cell suspension of $1x10^6$ cells into

AggreWell™ 800 inserts (STEMCELL Technologies). 0.5mg of RA-PCL microspheres were suspended in a small volume (< 100µl) of NIM and combined with experimental stem cell groups. A loaded AggreWell™ plate was centrifuged at 100 x g for 5 minutes to force cells and microspheres into aggregates. hiPSC and hiPSC-microsphere aggregates remained in the AggreWell™ plate with 2ml of NIM for 5 days with daily media changes. After 5 days, aggregates were carefully removed via pipetting and transferred to poly-L-ornithine (PLO)/laminin (Sigma) coated 24 well plates. Aggregates without microspheres were selected to receive 500nM of RA in media or left untreated as a positive control group and negative control respectively.

3.3.2 Characterization of hiPSC Differentiation

Flow cytometry and immunocytochemistry techniques were used to assess hiPSC differentiation as previously described [105]. On day 5, cell density and viability was measured with Guava ViaCount reagent (Millipore). SSEA-4 and SOX2 expression was measured with a Human/Mouse Pluripotent Stem Cell Multi-Color Flow Cytometry Kit (R&D Systems). Briefly, test aggregates were removed from suspension and rinsed twice with PBS before enzymatic dissociation with 0.05% trypsin-EDTA (Life Technologies) for 20 minutes at 37°C. For viability and cell density, single cell suspensions were diluted to 1:10 concentration in ViaCount reagent, protected from light, and incubated for 5 minutes at room temperature. For SSEA-4 expression, single cells suspensions were diluted to $1x10^6$ cells per 1ml of fixation buffer and incubated for 20 minutes at room temperature. Cells were forced into a pellet by centrifugation and re-suspended in permeabilization buffer. A single SSEA-4 marker or isotype control was added at this stage. Cells were then incubated for 1 hour at 4°C, rinsed and suspended in 1x assay

buffer. A similar protocol was followed for SOX2. A Guava EasyCyte HT (Millipore) flow cytometer was used to study prepared samples.

Immunocytochemistry was performed on day 12 of differentiation for TUJ1 as previously described [105]. Briefly, test aggregates were fixed with 10% formalin (Sigma) for 1 hour at room temperature, permeabilized using 0.1% Triton-X100 (Sigma) in PBS for 45 minutes at 4°C, and blocked using 5% normal goat serum for 2 hours at 4°C. The samples were incubated overnight with 1:500 dilution of TUJ1 primary antibody (anti-III-β-tubulin) (Millipore) and followed by three rinses of PBS and a 1:200 dilution of immunoglobulin G (IgG) (H+L) secondary antibody (Alexa Fluor 488 goat anti-mouse) (Life Technologies) for 4 hours at room temperature in the absence of light. Samples were rinsed three times to remove unconjugated secondary antibody and counterstained with DAPI (Invitrogen). Imaged were collected with a Leica DMI3000B inverted microscope, Lumen Dynamics X-Cite® 120Q LED fluorescent light source, and QImaging camera and software.

3.4 Statistical Results[1]

RA encapsulation efficiencies are reported as mean ± standard deviation (n=2, n=6 in revised experiments). RA release studies are reported as mean ± standard error (n=2, n=3 in revised experiments). Flow cytometry results are reported as mean ± standard deviation (n=3). Statistical significance was determined through various statistical test as appropriate (highlighted in parenthesis) using the R statistical programming language. * indicates $p < 0.05$.

Chapter 4 Results

For this section, I would like to thank John Edgar for performing the drug release study of the trial microspheres. John provided recommendations to improve protocols and insight after combining the trial microspheres with mouse embryonic stem cell aggregates.

4.1 RA/PCL Microspheres

A primary objective of my thesis is to combine RA/PCL microspheres with human induced pluripotent stem cells (hiPSCs) aggregates. To achieve this, it was necessary to practice RA encapsulation and characterization techniques of PCL microspheres. Particle size distributions and surface morphologies were observed via SEM to assess fabrication results. Particle diameters are estimated manually via the Quartz-PCI software and comments on surface morphology are **qualitative**. Microspheres formulations are divided into two groups: trial microspheres and experimental microspheres. The trial microspheres were primarily used to test reproducibility and make initial observations on collection, RA encapsulation efficiency, particle size, and RA release measurement techniques. Table 1 summarizes the trial microsphere groups in this part of the study.

Table 1 – Trial microsphere fabrication conditions

Sample	Yield	PCL Concentration	Collection Technique
3 µg/mg (Batch A)	25.05%	45,000 Mn	Vacuum Filtration
3 µg/mg (Batch B)	40.81%	45,000 Mn	Vacuum Filtration
3 µg/mg (New)	84.22%	45,000 Mn	Freeze-Dry

4.1.1 Microsphere Reproducibility

Trial microspheres were fabricated in two batches following similar conditions to test reproducibility. The vacuum filtration technique recovered 125/499 mg (25.05%) of PCL for batch A and 212.2/520 mg (40.81%) for batch B. The low yields show that between 60-75% of the initial PCL mass was not recovered with this technique. RA encapsulation efficiency for batch A and B is shown in Table 2. The average RA encapsulation efficiencies are close to 100%, which deviate from analog formulations involving the polyester PLGA and RA (~48-59%) [103]. However, the reported averages are within standard deviation and are not statistically different from each other, suggesting some consistency with the RA measured (two-sample Wilcoxon test $p > 0.05$).

Table 2 – Trial microsphere encapsulation efficiency

Sample	Encapsulation Efficiency (%)
Batch A	98.6 ± 21.4
Batch B	98.5 ± 25.9

(n = 2, mean ± standard deviation (SD))

SEM micrographs of batch A and B reveal similar spherical particles clustered together with irregularly-shaped excess particles present on some surfaces (Figure 8). Microsphere surfaces of both batches appear to contain small ridges throughout, with slight dimples and holes/scars present in some particles. Panel A shows an example of fiber-like material connecting particles. Panel B shows sheet-like material connecting several particles into a cluster. Qualitatively, both batches appear to be similar, showing further consistency in particle fabrication. To aid the comparison, both SEM micrographs were recorded at identical settings.

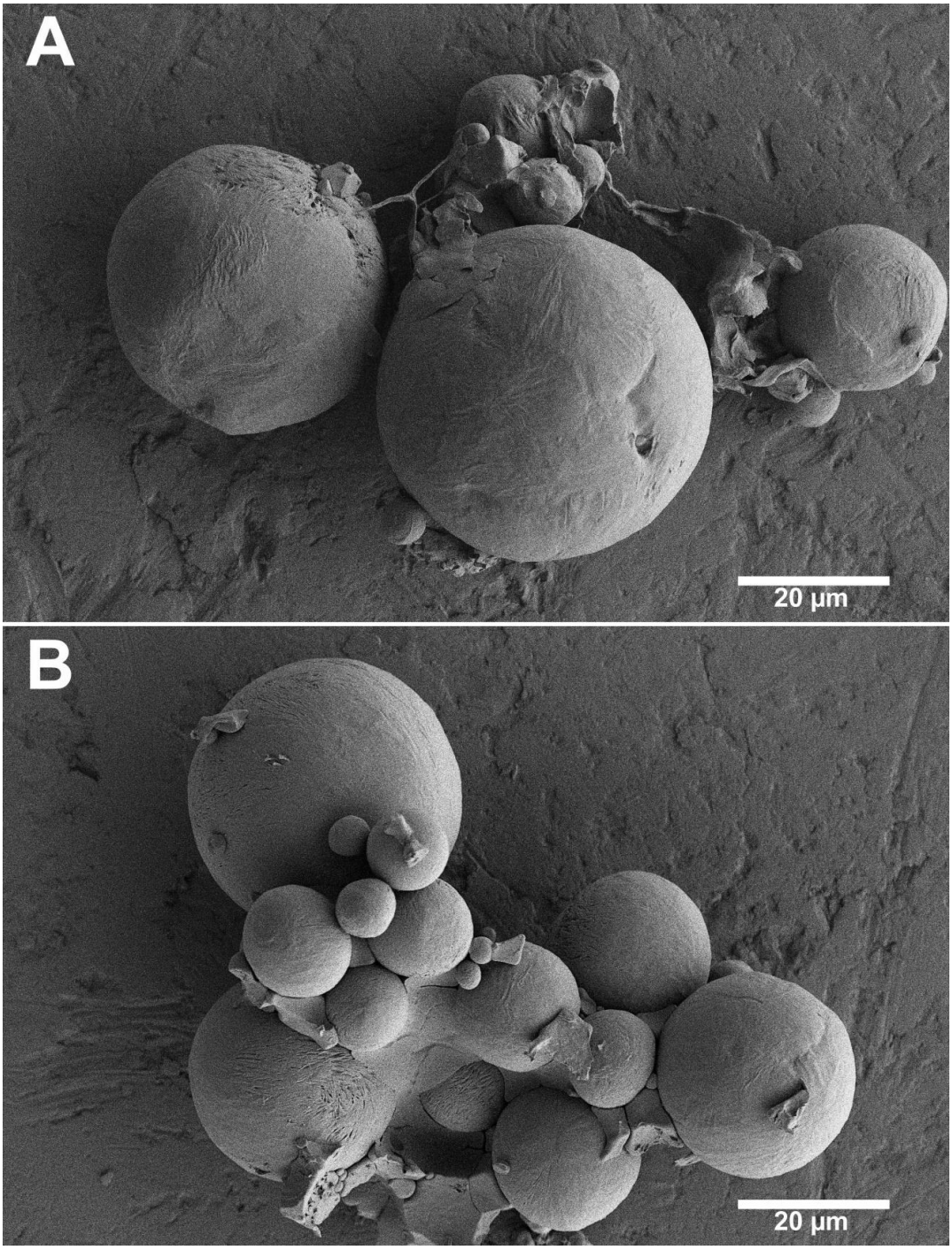

Figure 8 - Trial 3 µg/mg RA/PCL microspheres show rough surface features and are larger than desired. (A) 3 µg/mg Batch A. (B) 3 µg/mg Batch B. Hitachi FE-SEM 4800, WD = 9.4mm, Mag = 1000X, Vacc = 1kV, Current = 10µA, SlowScan(80).

A total of 100 particles of batch A and B were manually measured via SEM to estimate size and to determine if average microsphere diameters are similar for both populations. An arithmetic sample mean and standard deviation for batch A and B are 18.1 ± 12.4 μm and 17.7 ± 11.9 μm respectively, revealing similar statistics, and suggesting that the fabrication conditions yield comparable particles. However, further analysis via histograms shows distinct, right skewing, non-normal populations (Figure 9A and 9B), where both datasets fail normality tests (Shapiro-Wilk test, $p < 0.05$). Indeed, comparing a normal density distribution (blue line) to kernel density estimate (KDE) (red line) shows that both microsphere populations are more accurately described by a density estimate, where differences between populations are reflected by the shape of their respective KDE function, and raises the possibility of a different particle size.

The KDE function for each microsphere population can be used to calculate an expected value, variance, and standard deviation. The results are near identical to those obtained assuming a normal distribution; 18.1 ± 12.9 μm and 17.7 ± 12.6 μm for batch A and B respectively. Plotting empirical cumulative distribution functions (ECDF) for both datasets shows the similarity between microsphere diameters (Figure 9C), suggesting that despite the different shape of KDE functions, both samples are not different (Kolmogorov-Smirnov test, $p > 0.05$). Further testing suggests the average particle diameter of batch A and batch B are not statistically different (Welch two-sample t-test[2], $p > 0.05$). Collectively, the results show that microsphere fabrication is reproducible in terms of particle size.

[2] A technical paper from researchers at Minitab suggests that a Welch two-sample t-test can be applied if $n \geq 15$, despite non-normality.

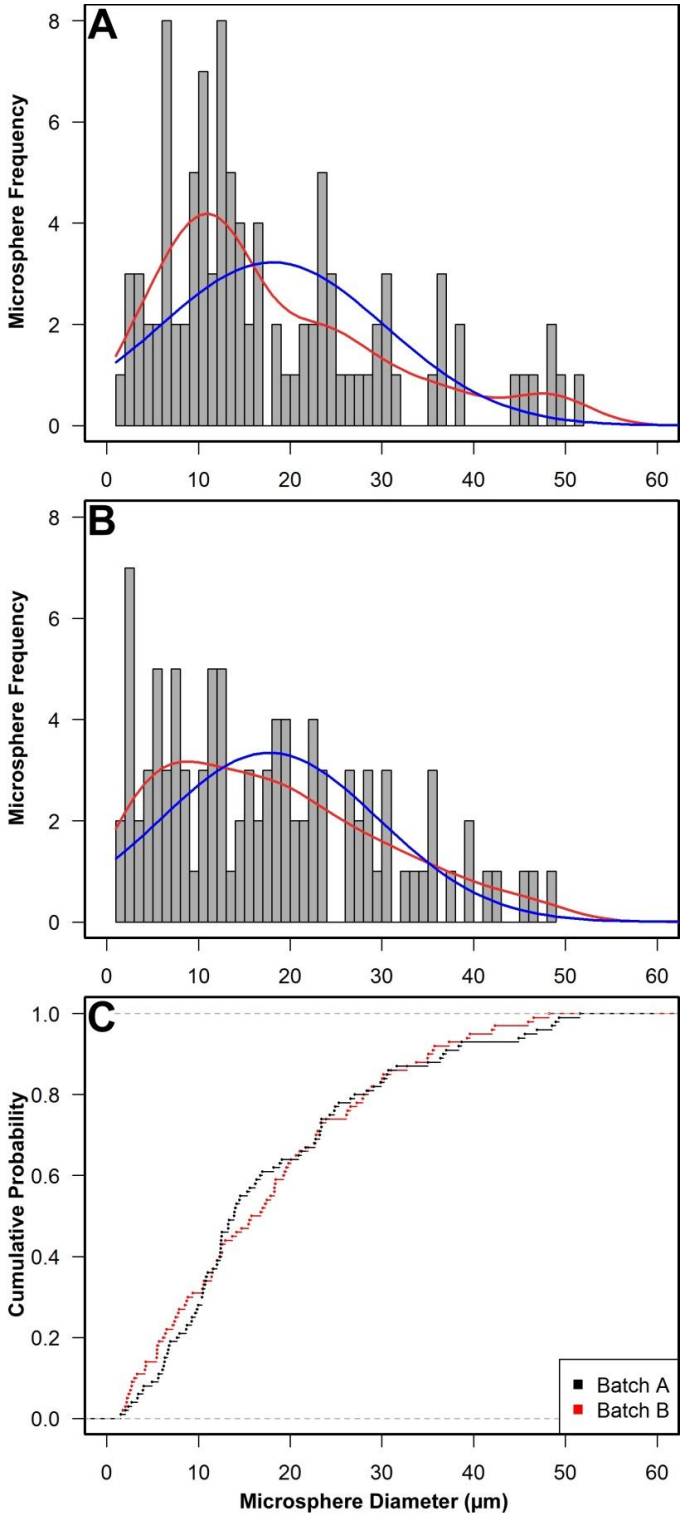

Figure 9 – Microsphere diameter comparison via histogram and distribution functions. (A) 3 µg/mg Batch A. (B) 3 µg/mg Batch B. (C) Empirical cumulative distribution (ECDF) comparison**.**

A RA drug release study from batch A and B was performed in duplicate for 28 days (Figure 10). An analysis between batch A and B shows that cumulative release does not differ across the experimental window (two-sample Wilcoxon test, $p > 0.05$). Indeed, release curves from both batches appear to follow a similar trend. By Day 28, batch A had a cumulative release of 52 ± 1.8% and batch B a cumulative release of 64 ± 0.4%, suggesting that over about half the amount of drug loaded had been released.

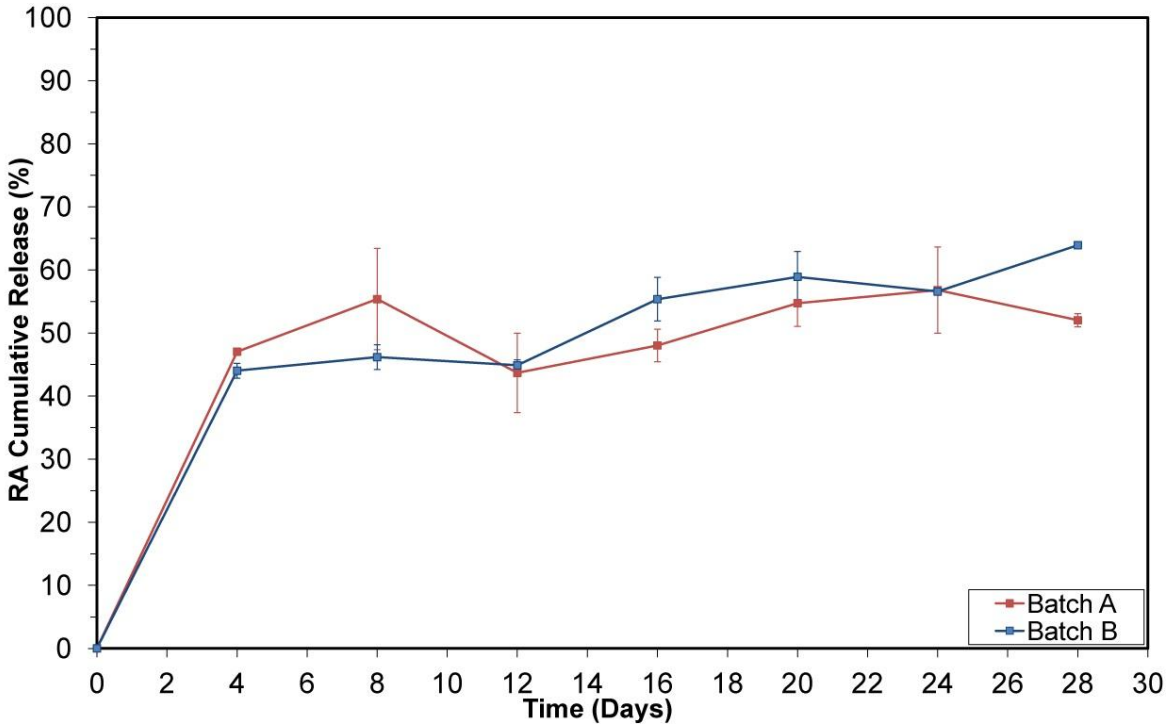

Figure 10 – RA drug release study for trial microspheres over 28 days. Batch A and B produce statistically similar release profiles (n = 2).

In summary, the low microsphere yields reported in the reproducibility experiment indicate that vacuum filtration is inadequate to collect microspheres in this study. The high standard deviation reported with the encapsulation efficiency could signify issues with the measurement technique; therefore the protocol is revised for further experiments. The surface morphology of the microspheres appears identical, with similar features

found in both batches. Quantitative analyses of microsphere diameter and drug release trends show no significant differences between batches. Taken together, the combined parameters of surface morphology, encapsulation efficiency, average particle size, and drug release show I can fabricate reproducible microspheres.

4.1.2 Microsphere Size and Morphology in a Drug Release Assay

As part of the drug release study, various sample microspheres of Batch A were collected and prepared for SEM to investigate possible particle size or morphology changes. I collected microspheres at Day 1, 4, 8, 12, 16 and 20. SEM micrographs were recorded at identical settings, with minor variations in magnification.

SEM micrographs reveal that surface morphology remains similar throughout the study (Figure 11). Qualitatively, surface features such as ridges, dimples, and holes that are present in particles at Day 1 (Figure 11A) are also visible in particles collected in the rest of the study (Figure 11B-F). Microspheres remain spherical by Day 20 and no major changes in surface morphology are recorded. A high-resolution SEM micrograph composite of day 12 microspheres (Figure 12) shows the presence of the discussed surface features in all visible microspheres, consistent with those observed in day 0 microspheres.

For further analysis, I performed a quantitative study of microsphere diameter by measuring 100 particles from each test day. A pairwise Welch two-sample t-tests and box plots are used to compare and visualize data. Table 3 summarizes measured diameters and standard deviations from each test day. Summary data suggest the overall particle diameter is close to 18 μm with a range of ~ 9 to 15 μm.

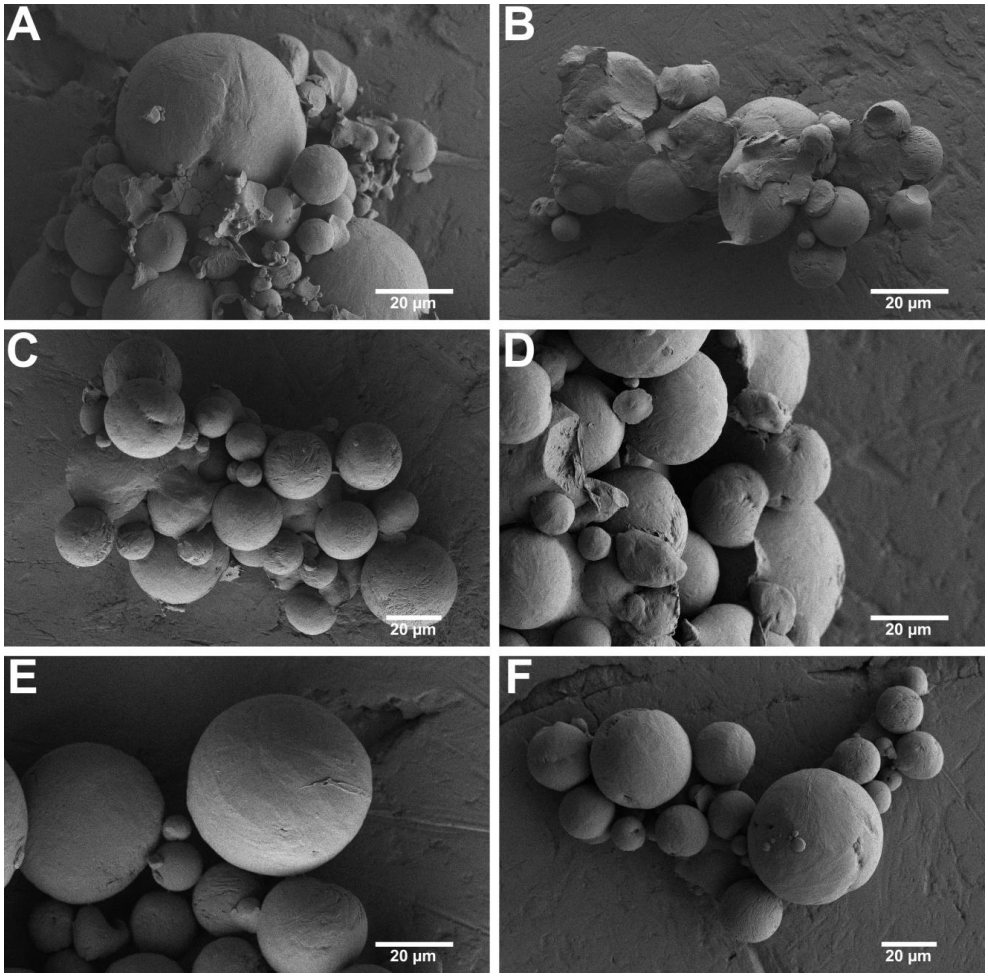

Figure 11 – Batch A microsphere surface morphology in a drug release study. Qualitatively, microsphere surface appears identical after undergoing release for 20 days. (A) Day 1. (B) Day 4. (C) Day 8. (D) Day 12. (E) Day 16. (F) Day 20. Hitachi FE-SEM 4800, WD = 9.1-9.2mm, Mag = 700X or 1000X, Vacc = 1kV, Current = 10µA, SlowScan(80)

Table 3 – Measured microspheres diameter across release study

Batch A Size (Release Study)	Expected Diameter ± SD (µm)
Day 0	18.1 ± 12.9
Day 1	14.5 ± 9.3
Day 4	15.4 ± 13.4
Day 8	18 ± 9.3
Day 12	21.2 ± 14.8
Day 16	19.7 ± 12.9
Day 20	18.7 ± 9.9

(n = 100, mean ± SD)

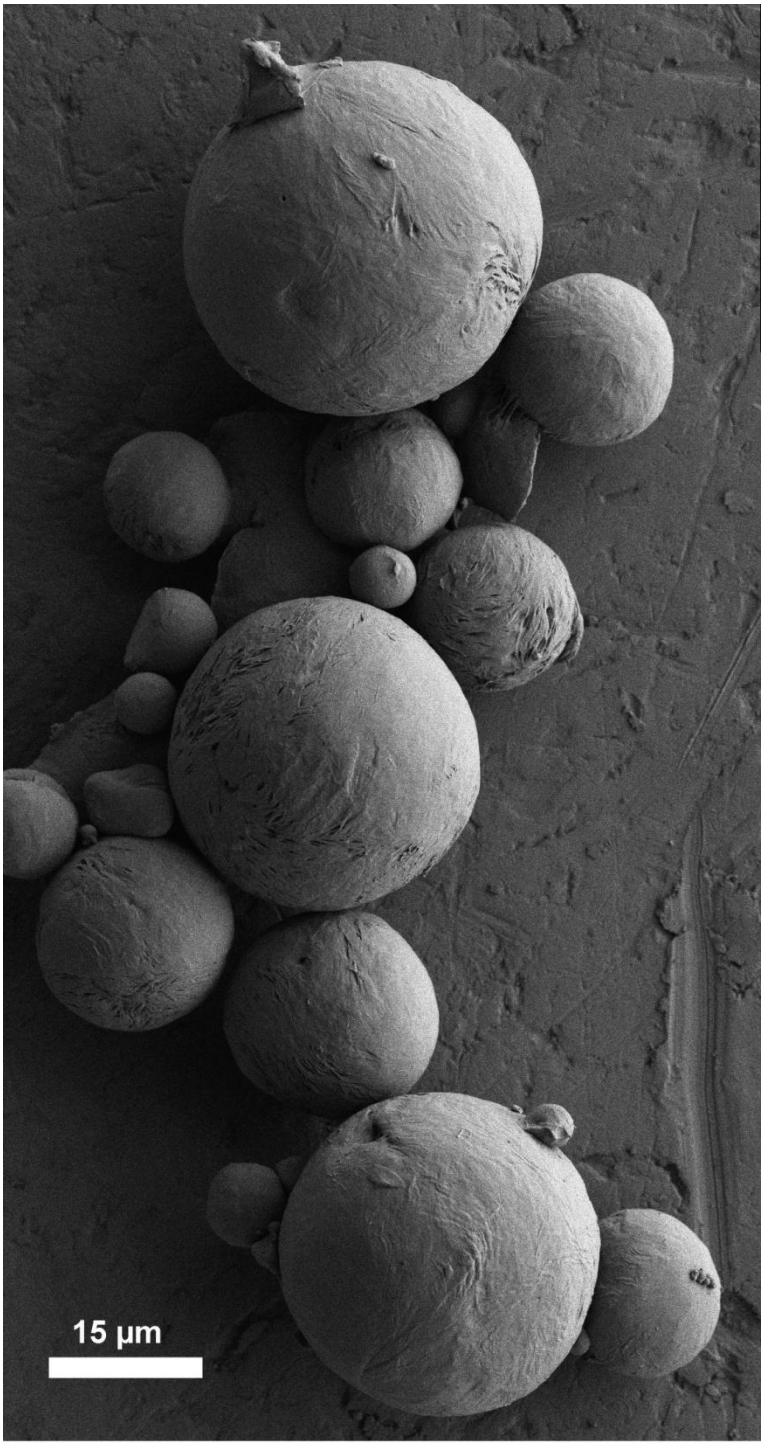

Figure 12 – High-resolution three image composite of day 12 microspheres shows qualitatively that ridges, holes, and dimples observed in day 0 remain present in all visible microspheres. Hitachi FE-SEM 4800, WD = 9.2mm, Mag = 1500X, Vacc = 1kV, Current = 10.5µA, SlowScan(80).

Figure 13 shows a visual comparison of all measurements, where day 0 is used as a control and its average diameter is shown as a dashed line. Outliers are shown as dots above their corresponding test day and highlight deviations from normal distributions that were present in all test groups (Shapiro-Wilk test, $p < 0.05$). Day 1 and 4 report average microsphere populations of 14.5 and 15.4 µm respectively, in an apparent reduction of microsphere diameter, the remaining test groups reported average diameters between 18 and 21.2 µm, closer to the control diameter. However, statistical testing reveled that the average measured diameters from all test groups are not different when compared to day 0 (pairwise Welch two-sample t-test[2], $p > 0.05$).

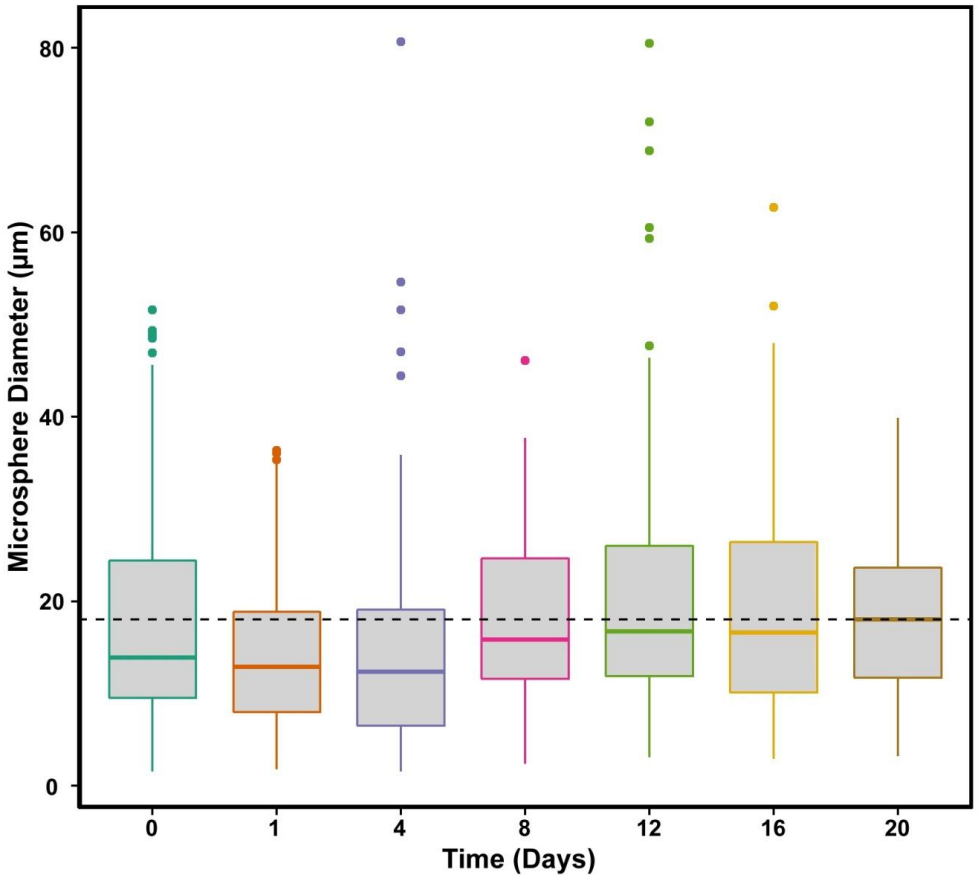

Figure 13 – Microsphere diameter across release study shows no statistically significant change in diameter (n=100)

The morphology observations and diameter data obtained during the drug release experiment show that microspheres did not visibly change in 20 days. Biodegradable polymers like PCL are expected to lose mass as polymer chains are cleaved; however, it is possible that micrographs do not capture this change at the current resolution. Alternatively, 20 day submersion in a water-based solution (PBS) may not be long enough to cause visible degradation of PCL. Polymer loss could also cause changes in spherical shape and overall microsphere diameter. However, the data showed no significant change to microsphere diameter during the release study. Collectively the data from this experiment showed that my microspheres remain with the same surface morphology and size after drug release and submersion in PBS for 20 days.

4.1.3 Refined Protocol Results

The objective of the RA/PCL microspheres is to deliver drug to human induced pluripotent stem cells (hiPSCs). The previous experiments succeeded in showing I learned to fabricate reproducible microspheres, learned to measure drug content/release, and observed no changes to microsphere morphology or diameter over a release assay. However, a few drawbacks were identified: 1) recovery of microspheres is too low (60-75% loss), 2) average microsphere diameter is too large (~18 μm) for successful incorporation with stem cell aggregates, 3) release curves should be performed in triplicate, and 4) absorbance measurements for drug content should be performed with different equipment. The following experiments compare pooled data from batch A and B against a new batch of 3 μg/mg RA/PCL microspheres to test effectiveness of improved fabrications conditions and measurement techniques.

Table 1 showed that freeze-drying recovers 420.1/498.8 mg (84.22%) of PCL for the new 3 µg/mg RA/PCL batch. This recovery rate doubles the best yields obtained via vacuum filtration, suggesting more microspheres are collected by freeze-drying. Previous drug measurements were performed via absorbance spectroscopy with a standard quartz cuvette. Briefly, test microspheres were dissolved and diluted for sample preparation. Cuvettes were loaded with solution, carefully sealed, and horizontally placed into a plate reader for measurements. The revised protocol switched to a 96-well quartz plate. The new equipment enabled me to load multiple samples and perform several readings per run. The higher microsphere yields and revised equipment allowed me to sacrifice six replicates to obtain more accurate encapsulation efficiencies. The new encapsulation efficiency is shown in Table 4 and it appears consistent with previous results [103].

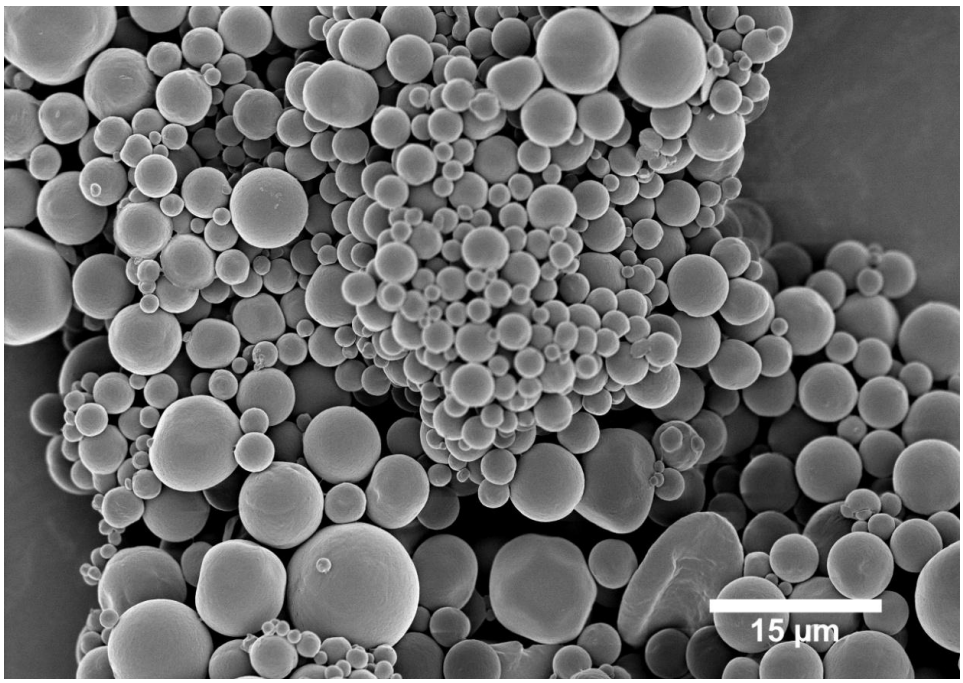

Figure 14 – New 3 µg/mg RA/PCL microspheres are smaller and with smooth surfaces. Hitachi FE-SEM 4800, WD = 7.9mm, Mag = 1500X, Vacc = 1kV, Current = 10µA, SlowScan(80).

Table 4 – Encapsulation efficiency with revised protocols

Sample	Encapsulation Efficiency (%)
3 µg/mg (Pooled)	98.5 ± 19.4
3 µg/mg (New)	69.19 ± 2.24*

(*n = 6, mean ± SD)

The diameters reported with the trial microspheres made them unsuitable for incorporation of with hiPSC aggregates [75]. To address this, I increased vortexing time to 30 seconds and stabilizing PVA bath speed to 500 rpm for new batches; longer mixing can create smaller initial particles and faster bath speed can prevent particle coalescence. SEM micrographs of the new 3 µg/mg RA/PCL batch showed multiple particles clustered together with smooth surfaces and spherical shape (Figure 14). Some charge up is visible and possibly the result of uneven Au/Pd coating of clustered particles. Overall, the micrographs show the revised protocols produce microspheres that are smaller than 18 µm. Quantitative size analysis shows that both datasets deviate from normality with some outliers (Shapiro-Wilk test, $p < 0.05$) (Figure 15). The new 3 µg/mg RA/PCL microspheres are significantly smaller than the pooled results, with an average diameter of 4.2 ± 1.9 µm versus 17.9 ± 12 µm (Welch two-sample t-test[2], $p < 0.05$).

A 28 day drug release study for the new 3 µg/mg RA/PCL microspheres was performed in triplicate with the revised drug measurement protocol. The new results are compared to pooled drug release data (Figure 16). The cumulative release shows the new batch is releasing drug at a lower rate, with the exception of Day 12 (Welch two-sample t-test[2], $p < 0.05$). Additional release data at Day 2 shows that an initial burst release

remains present. After 28 days, the new batch had a lower cumulative release of 39.4 ± 3.2%, compared to 58.0 ± 7.0% for the pooled results.

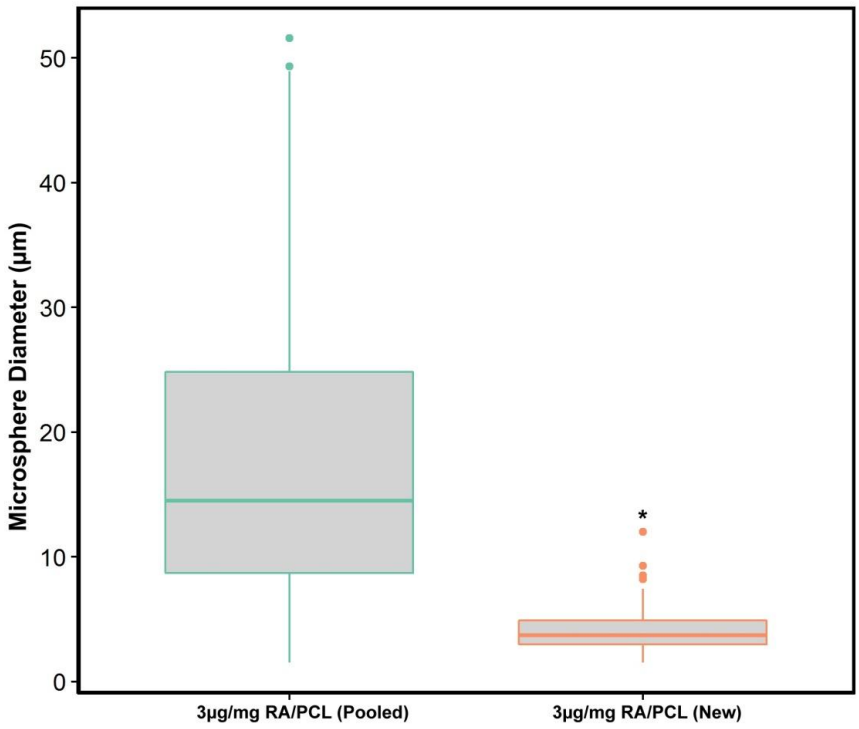

Figure 15 – Microsphere diameter analysis shows a significant reduction in size with the new microspheres (n = 100).

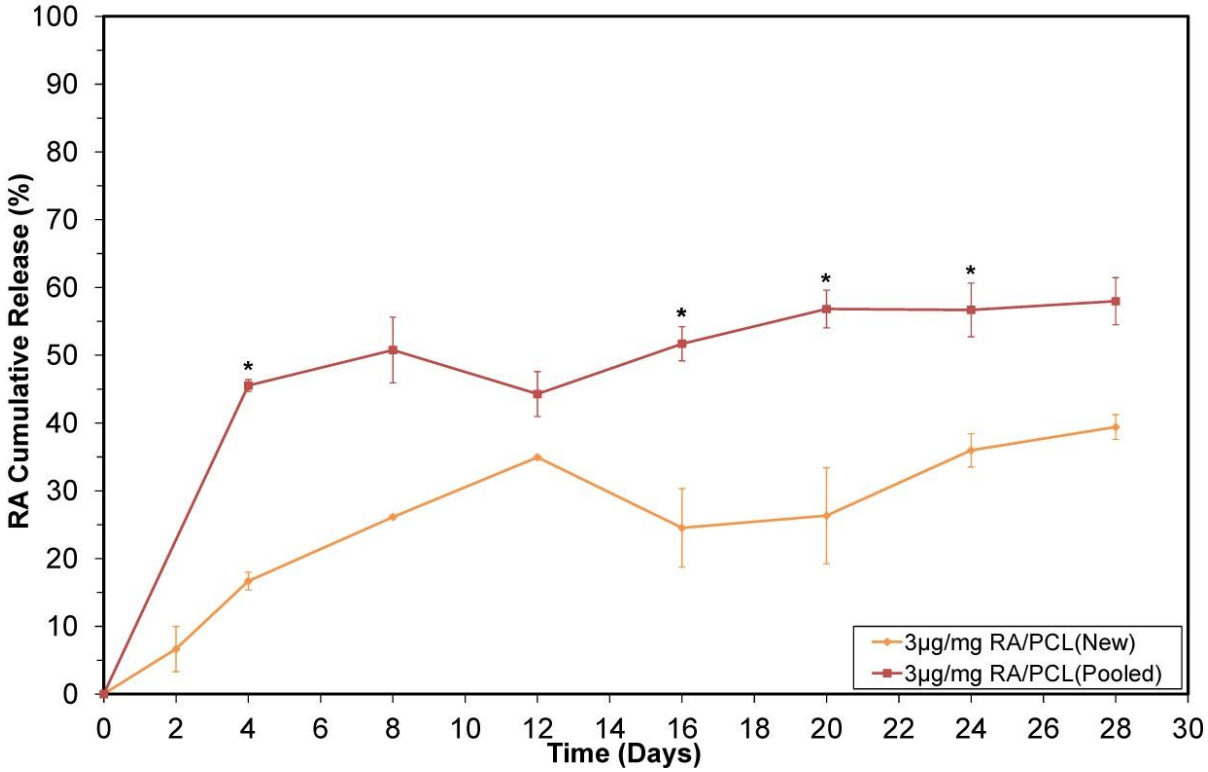

Figure 16 – Drug release comparison between new 3 µg/mg microspheres and pooled 3 µg/mg results. Drug release occurs at a lower rate with the smaller batch (n = 3)

The refined protocols show improvements to the new 3 µg/mg RA/PCL microspheres. Freeze-drying increases microsphere yield, which enables me to perform multiple replicates to measure drug content. Furthermore, new drug measurements have relatively small standard deviations and are consistent to those found in literature, suggesting the new techniques are producing reliable results. Additionally, microsphere diameter is significantly smaller than the trial microspheres, thereby bringing the particles to a suggested range for incorporation with hiPSC aggregates. Although drug release kinetics have changed, compared to the trial microspheres, this change is expected as particle size and drug loading are known to affect release trends. Collectively, the results of the refined protocols experiments show I can fabricate microspheres with the desired properties for drug delivery to hiPSC aggregates.

4.2 RA/PCL effects on hiPSC Aggregates[1]

Pluripotent stem cells have the potential to differentiate into any specialized cell found in the body. Induced pluripotent stem cells are somatic cells that have been genetically reprogrammed back to a stem cell-like state. First produced in 2007, human induced pluripotent stem cells (hiPSCs) are relatively new and combination with tissue engineering technology offers an excellent tool for developing personalized tissues in regenerative medicine. In this section, I encapsulate different concentrations of RA with the insight gained from the trial microspheres, size/morphology drug release assay, and refined protocols experiments to deliver drug to hiPSC aggregates.

Unloaded (drug-free) PCL microspheres are used as a control and two different RA concentration microspheres are used to test RA/PCL effects on stem cell experiments. The following experiments manually characterized particle diameter, qualitatively assessed surface morphology via SEM, and performed drug release kinetics over 28 days. Next, I recorded incorporation of PCL microspheres to hiPSC aggregates and measured percent cell viability and pluripotency markers SSEA-4 and SOX2 after 5 days of cell culture. By Day 12, microscopy was used to record changes to the experimental hiPSC groups. Table 5 shows the experimental microsphere groups in this part of the thesis.

Table 5 – Experimental microsphere summary

Sample	Yield	PCL Concentration	Collection Technique
4 µg/mg	75.25%	45,000 Mn	Freeze-Dry
30 µg/mg	77.31%	45,000 Mn	Freeze-Dry
Unloaded	N/A	45,000 Mn	Freeze-Dry

4.2.1 Experimental Microsphere Characterization

SEM micrographs of unloaded, 4, and 30 µg/mg microspheres showed a smooth, round surface with some clustering (Figure 17). Some irregular particles and excess polymer can be observed in the unloaded microspheres (Figure 17A), however the majority of fit the smooth and round description. The drug loaded 4 and 30 µg/mg microspheres are statistically similar in size with a diameter of 3.52 ± 2.44 and 3.41 ± 1.62 µm respectively. Unloaded microspheres are statistically smaller with a diameter of 2.52 ± 1.26 µm (Figure 18) (pairwise Welch two-sample t-test[2], $p < 0.05$).

Table 6 shows the encapsulation efficiency for the different RA loadings. Both microspheres reported a similar encapsulation efficiency (~60%), consistent with those reported in literature using an o/w single emulsion/solvent technique with the PLGA polyester [103]. Statistical analysis revealed no differences between the encapsulation efficiencies of 4 and 30 µg/mg microspheres ($n = 6$) (Welch two-sample t-test[2], $p > 0.05$).

I performed a RA drug release studies in triplicate and analyzed it over 28 days (Figure 19). Unloaded microspheres do not participate in this experiment as there is no RA to measure over 28 days. 4 µg/mg microspheres showed an initial burst released followed by a period of gradual release. In contrast, 30 µg/mg microspheres maintained a higher rater of release throughout the experimental window. After 28 days, the 4 µg/mg microspheres had a cumulative release of 28 ± 10%, whereas the 30 µg/mg microspheres had a cumulative release of 53 ± 2%, suggesting the release rates are influenced by the amount of RA loaded. The cumulative release percent between the two groups remained statistically similar until day 24 (Welch two-sample t-test2, $p < 0.05$)

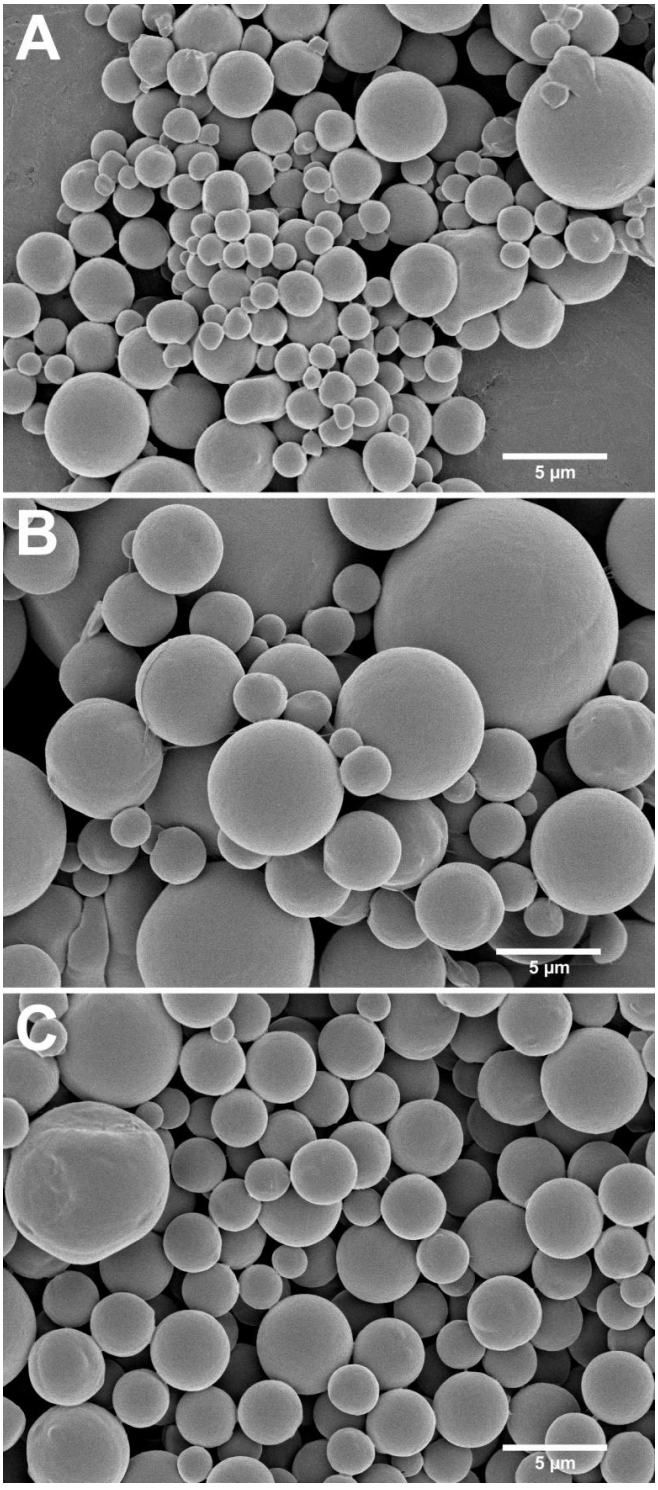

Figure 17 – Experimental RA/PCL microspheres surface morphology are shown to be smooth and spherical. (A) Unloaded. (B) 4 µg/mg RA/PCL. (C) 30 µg/mg RA/PCL. Hitachi FE-SEM 4800, WD = 8.0mm, Mag = 4000X, Vacc = 1kV, Current = 10µA, SlowScan(40).

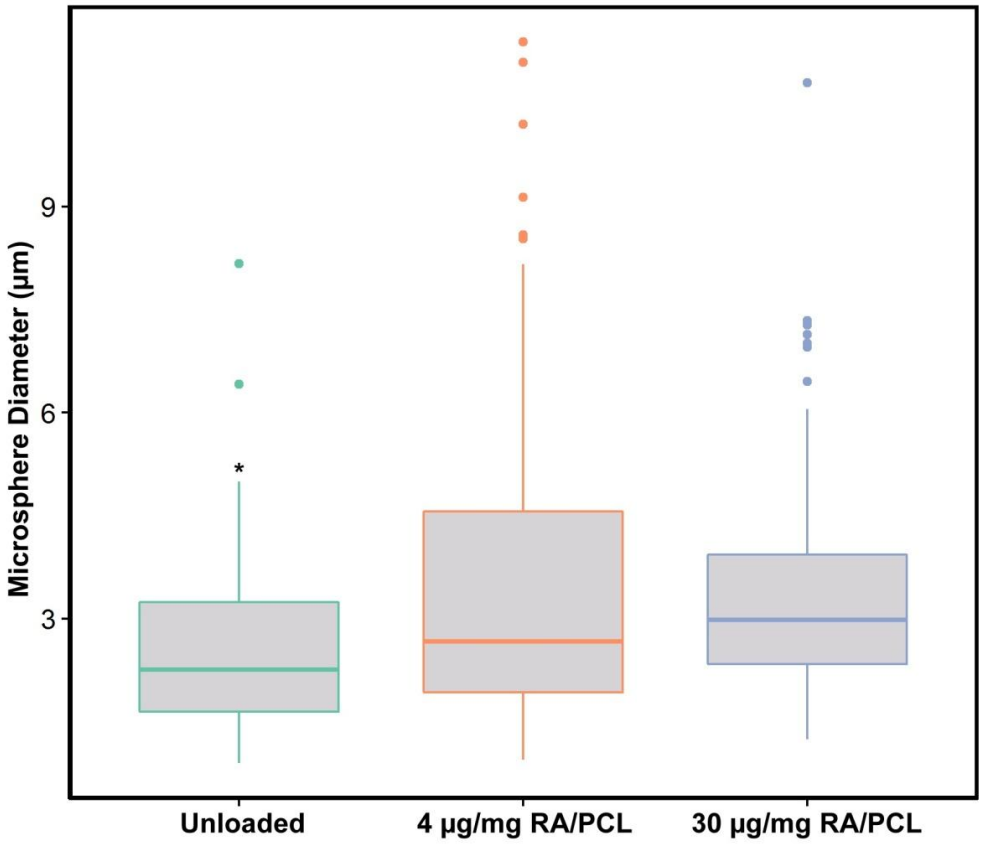

Figure 18 – Experimental microsphere diameter analysis shows drug loaded groups are similar in size, whereas unloaded microspheres are smaller (n = 100).

Table 6 – Encapsulation efficiencies for drug loaded microspheres

Sample	Encapsulation Efficiency (%)
4 µg/mg	60.9 ± 1.9
30 µg/mg	58.4 ± 3.3

(n = 6, mean ± SD)

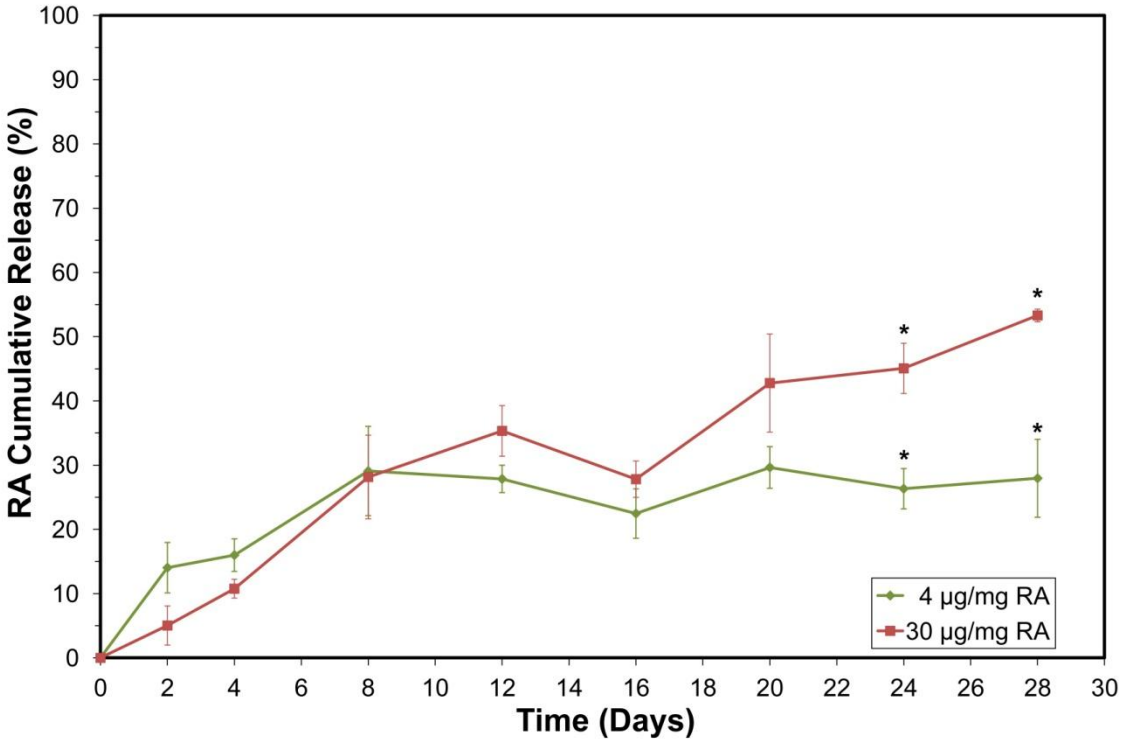

Figure 19 – Drug release study of experimental microspheres over 28 days. Cumulative drug release is increased by day 24 with higher drug loading (n = 3).

The characterization experiments show that the experimental particles are ready for combination with hiPSC aggregates. For instance, microscopy observations reveal a few excess amorphous polymer structures on some particles, but all experimental groups are indeed spherical. Furthermore, microscopy shows particle morphology is smooth across all experimental groups with a few examples of dimples and creases present in the larger microspheres. Quantitative diameter analysis shows that although all three samples contain small standard deviations, large microspheres (> 5µm) are present among the measured particles from all three groups. These particles are possibly the result of uneven mixing speed in the container during fabrication. However, all microspheres groups are in the desired size range. Drug measurements reveal both drug-loaded groups are consistent with published expectations in terms of encapsulation efficiency and drug-release trends.

4.2.2 hiPSC incorporation

0.5 mg of microspheres were combined with hiPSCs to form microsphere/stem cell aggregates following John Edgar's suggestion. The experimental groups consist of control hiPSC aggregates without microspheres (Untreated), control hiPSC aggregates with PCL microspheres (Unloaded), and hiPSC aggregates with PCL microspheres loaded with two RA concentrations (4 vs. 30 μg/mg). Microscopy techniques are used to observe microsphere incorporation and morphology changes to stem cells. Flow cytometry is employed to detect biomarkers for cell viability and pluripotency.

Living cells are transparent and phase contrast microscopy uses phase shifts to increase brightness in sample regions, thereby creating contrast. Therefore, untreated stem cells appear as a cluster of transparent objects at Day 0 and can be observed forming a distinctly spherical aggregate after 24 hours of culture in microwells (Figure 20A, B). Microspheres can be observed as circular objects with a well-defined edge; however, the large number of particles scatters too much light that microspheres appear as a dark amorphous object. hiPSCs groups containing microspheres appear to be covered by dark clusters at Day 0 (Figure 20C, E, G). After 24 hours, microsphere/hiPSC aggregates are formed, although some excess microspheres can be observed outside the aggregates. Microspheres are engulfed by hiPSCs in all experimental groups and form tight aggregates (Figure 20D, F, H).

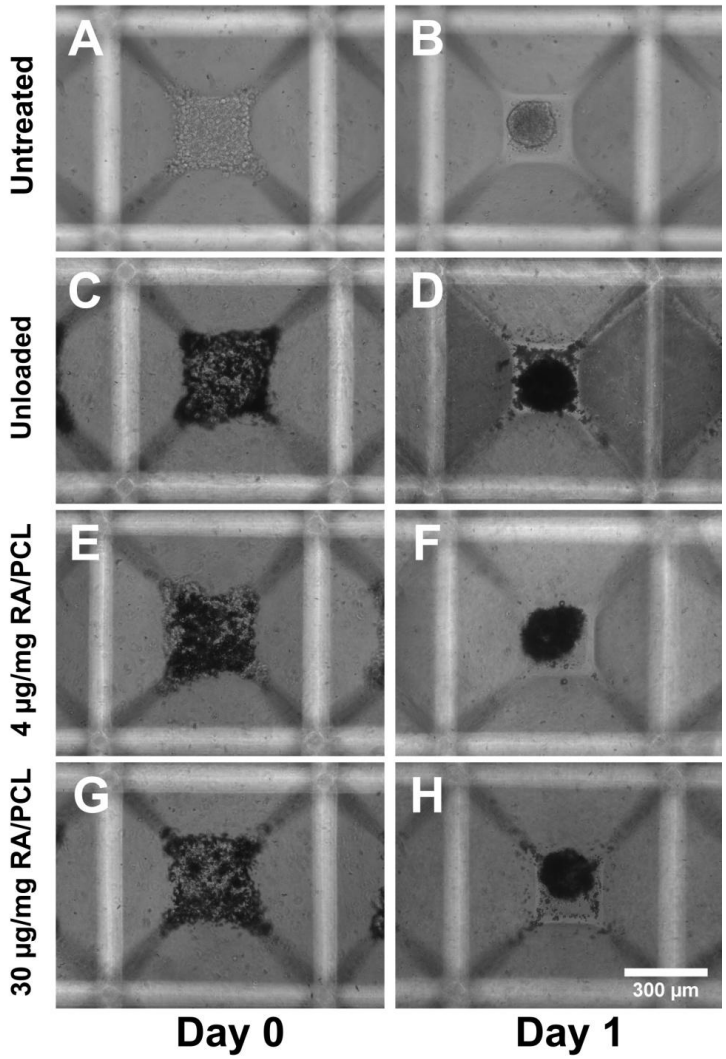

Figure 20 – 24 hour human induced pluripotent stem cell aggregate formation without microspheres (A, B) and with microsphere groups (C – H). Leica DMI3000 B equipped with Qimaging Retiga-2000R camera, Mag = 10X.

Flow cytometry of hiPSC aggregates was performed on Day 5 of cell culture to assess cell viability and determine if the controlled release of RA from microspheres had any effect on cell differentiation. After 5 days, the percent viability of hiPSC and hiPSC-microsphere aggregates remained similar to Day 0 undifferentiated cells (Figure 21) (one way ANOVA, $p > 0.05$). The viability studies showed that hiPSC aggregates were not

negatively affected by sterilized PCL microspheres, suggesting PCL is not leading to cell death.

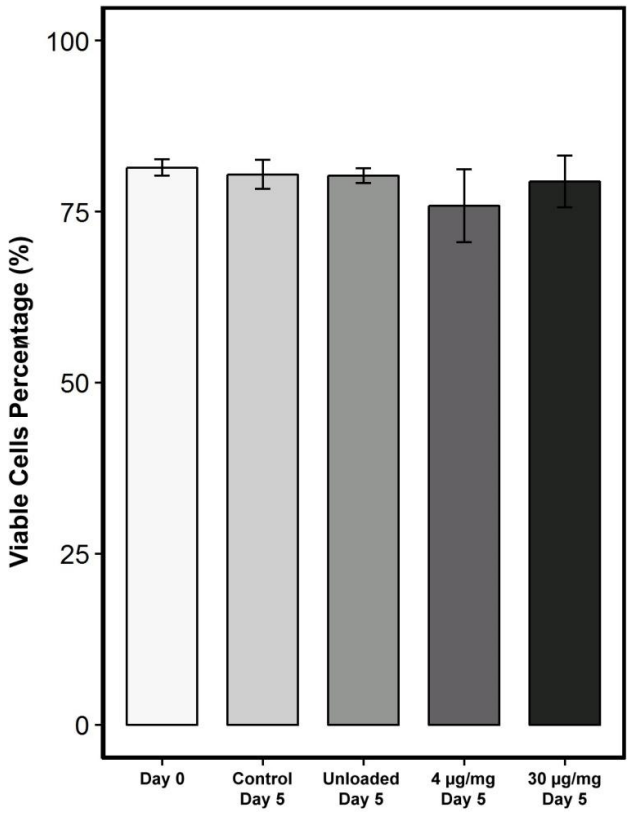

Figure 21 – Percentage of living cells as measured by flow cytometry at Day 0 and Day 5 show no significant changes in cell death (n = 3).

Expression of pluripotent marker SOX2 (sex determining region Y)-box 2, a transcription factor critical for pluripotency and self-renewal of undifferentiated stem cells used as maker for pluripotency, did not significantly decrease across the experimental groups when compared to Day 0 undifferentiated cells (Figure 22) (one way ANOVA, $p > 0.05$). I found this result inconsistent with expectations, as RA release should decrease stem cell pluripotency. The large standard deviations from the sample groups suggest that biomarker measurement might not be accurate. Probably user error in the experimental replicates or labeling protocol.

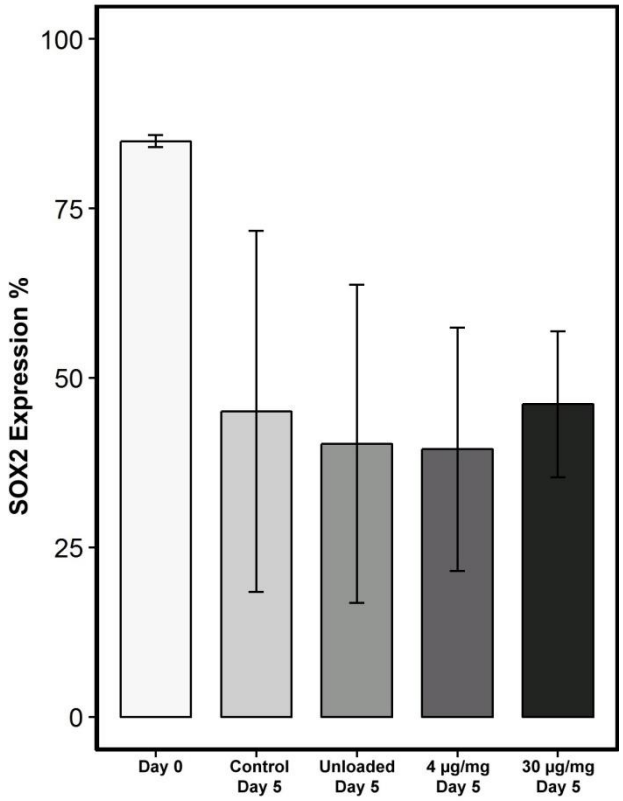

Figure 22 – SOX2 expression as measured by flow cytometry between hiPSC experimental groups. Pluripotency appears unchanged despite the presences of RA/PCL microspheres (n = 3).

Expression of pluripotent marker SSEA-4 (stage-specific embryonic antigen-4), a cell surface glycosphingolipid that is used as a maker for pluripotency in human pluripotent stem cells, changed in hiPSC-microsphere aggregates containing RA releasing microspheres when compared to Day 0 undifferentiated cells (Figure 23). SSEA-4 expression of the negative control and unloaded microspheres groups remained similar to Day 0 levels. However, SSEA-4 expression decreased in 4 and 30 µg/mg groups (Welch two-sample t-test[2], $p < 0.05$). The controlled release of RA is likely to be inducing differentiation as the cells were more differentiated than the untreated negative control and unloaded microsphere groups.

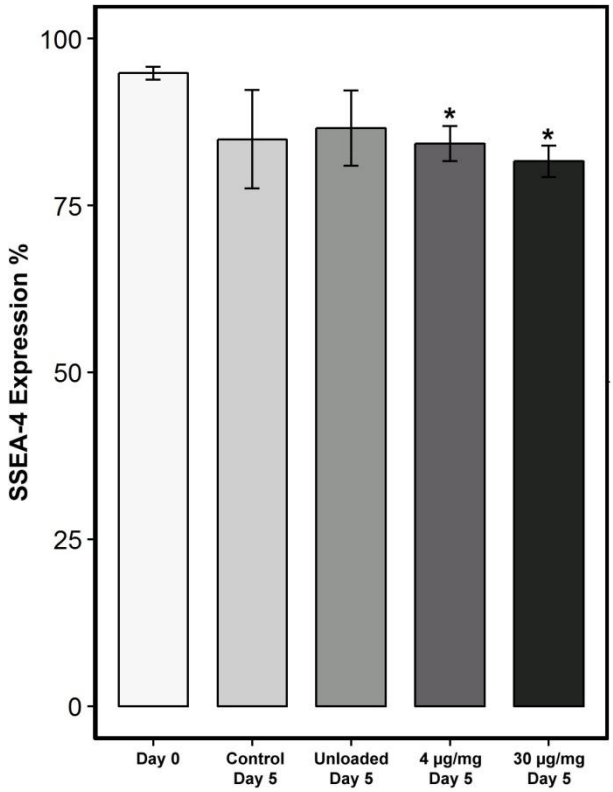

Figure 23 – SSEA-4 expression as measured by flow cytometry between hiPSC experimental groups. Pluripotency decreases in groups containing RA/PCL microspheres (n = 3).

Phase contrast microscopy observations revealed hiPSC-microsphere aggregates remained spherically uniform and maintained their integrity when transferred to PLO/laminin-coated plates on Day 5 (Figure 24A, E, I, M, and Q). This observation is encouraging as it implies that strong aggregate formation is sustainable with PCL microspheres and appears similar to both control groups without microspheres. By Day 9 of cell culture, phase contrast showed hiPSC-microsphere aggregates had readily adhered to PLO/laminin-coated surfaces, revealing the location of many microspheres as dark spheroids throughout the aggregates (Figure 24J, N, and R).

Day 12 phase contrast microscopy of cell culture confirmed that cell growth continued in all experimental groups and was not inhibited by the presence of PCL microspheres (Figure 24C, G, K, O, S). Immunocytochemistry and fluorescence microscopy performed at Day 12 showed TUJ1 positive neurite outgrowth in hiPSC and hiPSC-microsphere aggregates indicative of early neuron differentiation (Figure 24D, H, L, P, T). Both control groups and experimental cultures expressed the neuronal marker TUJ1 in green; cell bodies were visualized with DAPI (4′, 6-diamidino-2-phenylindole), a highly specific DNA fluorescence stain, in blue.

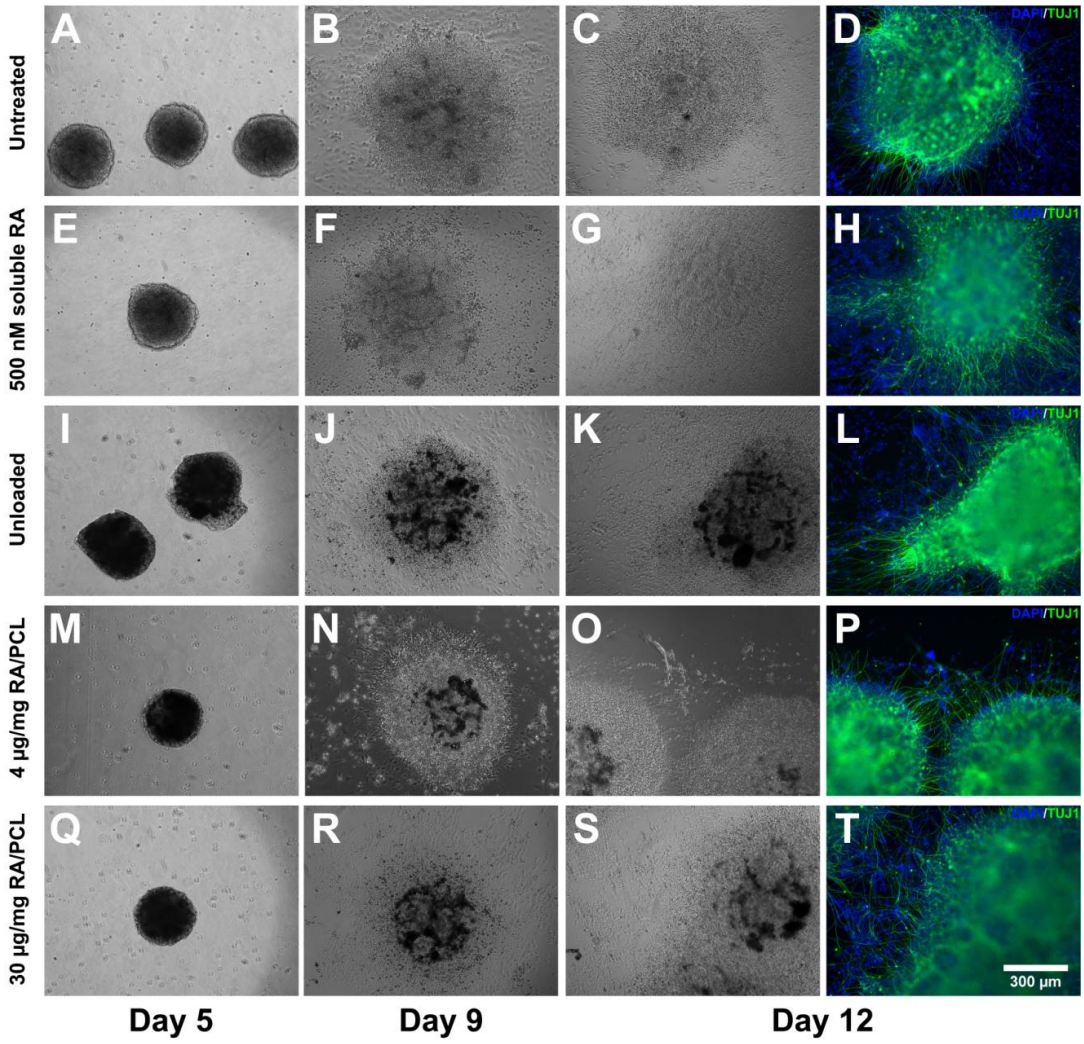

Figure 24 – Timeline of experimental hiPSC-microsphere groups subjected to a neural induction protocol. Day 5 micrographs show spherical aggregates for all experimental groups. Day 9 shows all groups have adhered to the PLO/Laminin coated plates, revealing microspheres as dark objects. Day 12 fluorescence microscopy shows neurite outgrowth in all experimental groups; positive control groups have a similar morphology as drug releasing groups. Leica DMI3000 B equipped with Qimaging Retiga-2000R camera and X-Cite 120Q fluorescent light source, Mag = 10X.

A quantitative analysis of TUJ1 positive images can be found in this reference [106]. Briefly, it was determined that relative aggregate surface area is higher with the 30 µg/mg group and lower with unloaded microspheres groups when compared to the untreated control. Relative neurite length and degree of branching is more pronounced in the hiPSC

aggregates treated with soluble RA and with unloaded microspheres when compared to the untreated controls. The 4 and 30 µg/mg hiPSC-microspheres groups showed less branching and shorter neurites when compared to the untreated controls. However, it is possible that hiPSC aggregate density per well had a negative effect, as various aggregates are so close that neurite extensions overlap or become blocked (Figure 25).

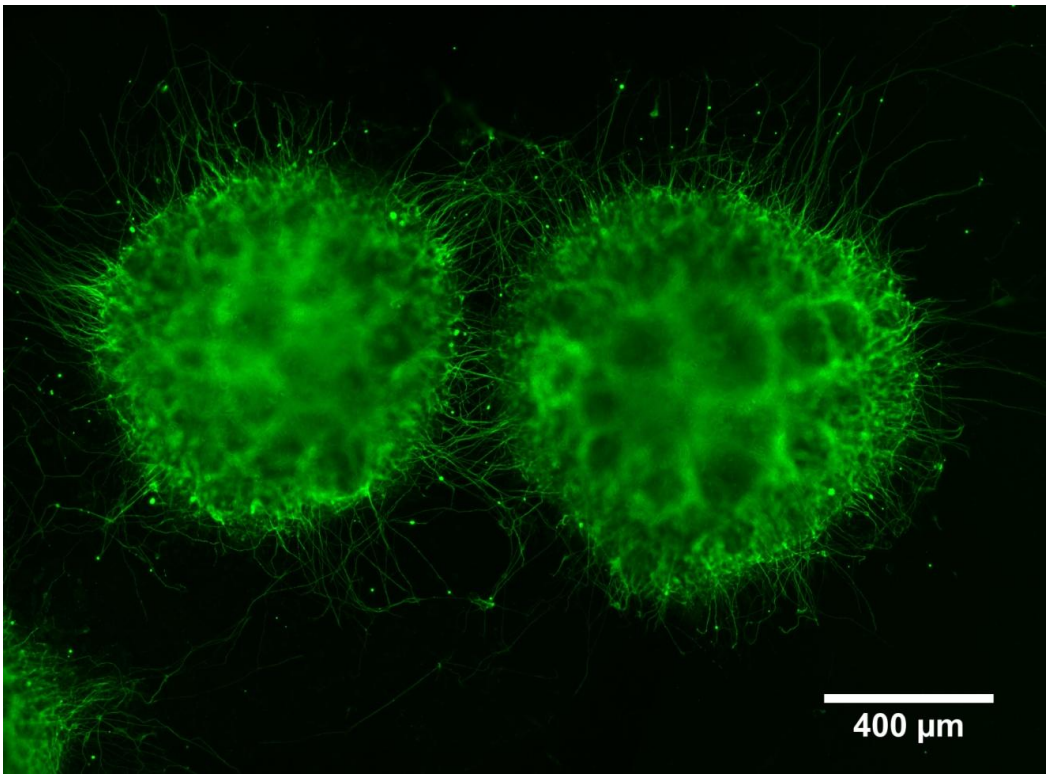

Figure 25 – Composite image of hiPSC-microspheres (4µg/mg) aggregates; various TUJ1 positive extensions are observed colliding. The aggregates are possibly too close together due to random settling on the plate. Reducing plating concentration may help isolate single aggregates. Leica DMI3000 B equipped with Qimaging Retiga-2000R camera and X-Cite 120Q fluorescent light source, Mag = 10X.

Inspired by the work of Carpenedo *et al.*, (2009), I successfully incorporated RA/PCL microspheres with hiPSC aggregates to overcome diffusion barriers and directly deliver drug to stem cell aggregates [74, 75]. Microsphere characterization techniques allowed me to test microsphere fabrication and confirm desired properties; size, morphology, and

drug loading/release. I tested PCL effects on hiPSCs and found PCL did not negatively impacted cell viability. After 12 days, hiPSC-microsphere aggregates following a neural induction protocol showed morphological features indicative of early neuron development, with RA/PCL groups showing morphological features that were distinct relative to control groups. However, these experiments did not explore the meaning of those differences. Collectively, this project serves as the foundation for further exploration of PCL microspheres as drug delivery vehicles to hiPSC aggregates. The application of microsphere drug delivery technology to human induced stem cells aggregates had not been shown before this project had been completed. The final work can now be found in the journal of Cellular and Molecular Bioengineering [106].

4.3 Variable Surface Morphology

I used SEM to characterize the size and surface morphology of poly (ε-caprolactone) (PCL) microspheres used in drug delivery. Surface morphology is suspected to affect drug release but most publications report surface features using qualitative terms only (i.e., smooth, rough, scarred). SEM is an established method to determine particle size and observe surface features. While the micrographs obtained are undeniably valuable, descriptive assessments fail to capitalize on the potential of SEM. Stereo-vision is an imaging technique capable of recovering 3-dimensional (3D) information by combining information from different perspectives. This multi-view approach requires a minimum of two SEM micrographs captured at different tilt-angles to recover height variations. Pixel matching of many stereo-images through computer algorithms can generate topographic maps for quantitative assessments.

Distinct fabrication conditions should yield different morphologies and sizes as reported in literature [11]. Therefore, the variable morphology experiments use six formulations of PCL microspheres fabricated via the oil-in-water (o/w) single emulsion/solvent evaporation technique. In this section, I carefully control the fabrication parameters of our microspheres and report final particles. I performed two electron microscopy sample preparations specifically aimed at automating particle diameter measurements and multi-view imaging. Insight gained from manual diameter analysis is combined with image processing techniques to automate measurements. I present stereo-pair micrographs of my microsphere formulations as anaglyphs to highlight surface detail and particle shape. Furthermore, several micrographs are recorded to obtain quantitative data via computer vision specialized software.

4.2.1 Microsphere Formulations

The previous work focused on fabricating reproducible RA/PCL microspheres for combination with hiPSCs aggregates; I observed morphology, measured size, and drug encapsulation/release as final products from the fabrication set up. Controlling morphology requires meticulous control over fabrication conditions and materials used. In theory, surface morphology can be altered by maintaining identical fabrication settings and: 1) increasing PCL concentration (w/w) in the oil phase (3, 5, or 10%), or 2) using different number average molecular weight concentrations (Mn) of PCL (45,000 or 80,000). Figure 26 refers to the ID system used with the microspheres in this section. Table 7 summarizes the initial conditions for my formulations.

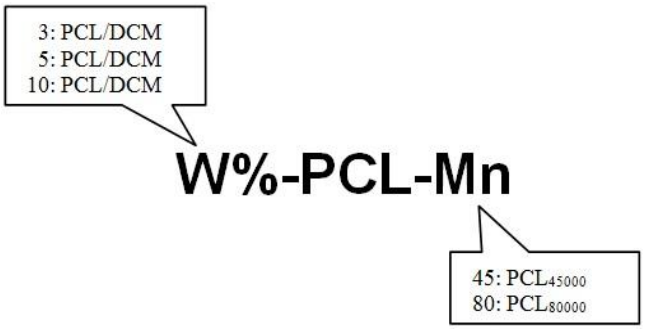

Figure 26 – An illustration of the Batch ID system used with the variable morphology microspheres.

Table 7 – Initial conditions for the variable morphology microspheres

Formulation	PCL Mass (mg)	DCM Mass/Volume (g:ml)	Temperature
3-PCL-45	411.2	13.2:10	RT
5-PCL-45	697.2	13.2:10	RT
10-PCL-45	661.6	6.6:5	RT
3-PCL-80	413.5	13.2:10	RT
5-PCL-80	695.4	13.3:10	RT
10-PCL-80	659.1	6.6:5	RT

4.2.2 Automated Microsphere Size

Previous diameter measurements were performed manually by identifying microspheres and using the ruler/measurement function in the Quartz PCI Software to obtain size. Two disadvantages became clear during this analysis: 1) manual measurement is time consuming, and 2) it can be susceptible to human error. To address this, I considered how microspheres can be indentified via image processing algorithms and prepared SEM aluminum stubs specifically for particle sizing. Furthermore, I

exploited the edge effect, a property of SEM that can be used to identify areas with higher secondary electron emission in a sample, to increase contrast around the microspheres and aid identification. Briefly, microspheres are reduced to 2-dimensional circles in a micrograph and the Circle Hough Transform (CHT) is an algorithm that allows circular objects to be extracted from edge pixels. Therefore, combining these two concepts should allow me to automatically detect objects that fit a circular parameter.

Figure 27A shows an unprepared aluminum SEM stub at a resolution range where I expect to find 10 µm sized microspheres. Distinct edges, holes, and groves are visible at this magnification, which pose a potential source of unnecessary information in image processing. Although a CHT would not detect these features, edge detectors would readily identify the changes in contrast and retain this information after transforming pixel data into a binary (black and white) image. However, smoothening of stub morphology can be achieved with some preparation.

Carbon paint (conductive graphite) is often used to provide conductivity and electron release to non-conductive samples, such as polymer microspheres. Furthermore, a carbon paint coating can be used to create a different surface morphology and a secondary electron emission profile, which will be perceived as a change in brightness relative to an aluminum surface. Figure 27B shows an air dried carbon painted SEM stub. Indeed, introducing a thin coat of carbon paint creates an amorphous surface throughout the SEM stub; peaks generate more favorable SE emission and are reported in the micrograph as bright regions, conversely valleys, areas of unfavorable emission, appear as dark regions. This amorphous surface can be further processed through gentle grinding. The final stub

morphology appears flattened at my target resolution; there is a change in grayscale when compared to an unprepared stub, no visible peaks or valleys, and bright areas are possibly the result of aluminum becoming exposed through carbon paint (Figure 27C).

A prepared SEM stub can serve as a distinct background to a single layer of dispersed microspheres. However, previous microsphere deposition relied on fast ethanol droplet evaporation, which often resulted in particle clustering (e.g., Figure 14). Furthermore, ethanol easily dissolves isopropanol based carbon paint effectively destroying surface preparation. Addressing this required a different deposition technique that would preserve carbon paint and would not induce particle clustering.

Water droplets can be carefully "wicked" through capillary action; this effect can remove water and deposit particles. A unidirectional wick resulted in particle clustering, however carefully placing two or more sources of capillary action around a droplet removed water without inducing large clusters. Indeed, Figure 28 shows various microspheres dispersed throughout a prepared stub in a single layer with minimal clustering. An increase in contrast can be observed at the edge of the microspheres. Others changes in brightness are possibly the result of electron charging, a phenomena that occurs when incident electrons are not able to dissipate throughout the sample, and are perhaps the reason for darker regions on the surface of the larger microspheres. Ultimately, the information desired has been achieved through this specimen preparation; no visible holes, groves, or edges are present in the background, and a single layer deposition of microspheres generates a clear increase in contrast in the foreground.

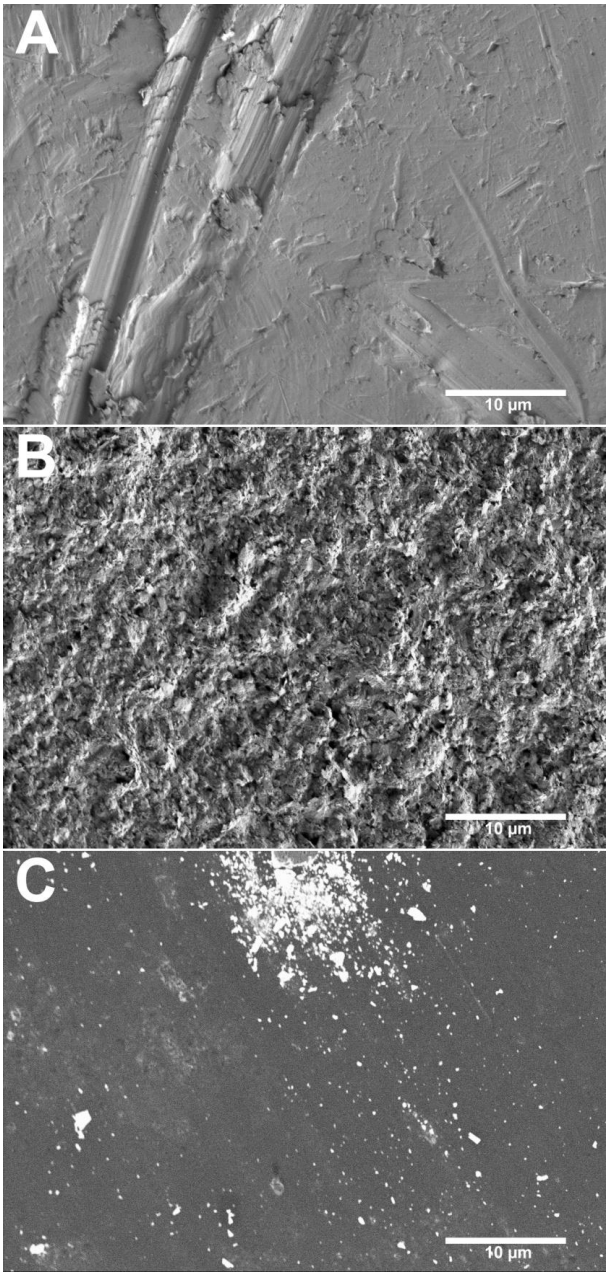

Figure 27 – Changes to SEM stub surface from our protocol (A) An unprepared standard aluminum stub shows various surface features. (B) A carbon paint layer creates an amorphous layer. (C) Gentle grinding of carbon paint creates a smooth surface. Hitachi FE-SEM 4800, WD = 8.0mm, Mag = 2000X, Vacc = 0.7 or 1kV, Current = 10µA, SlowScan(80).

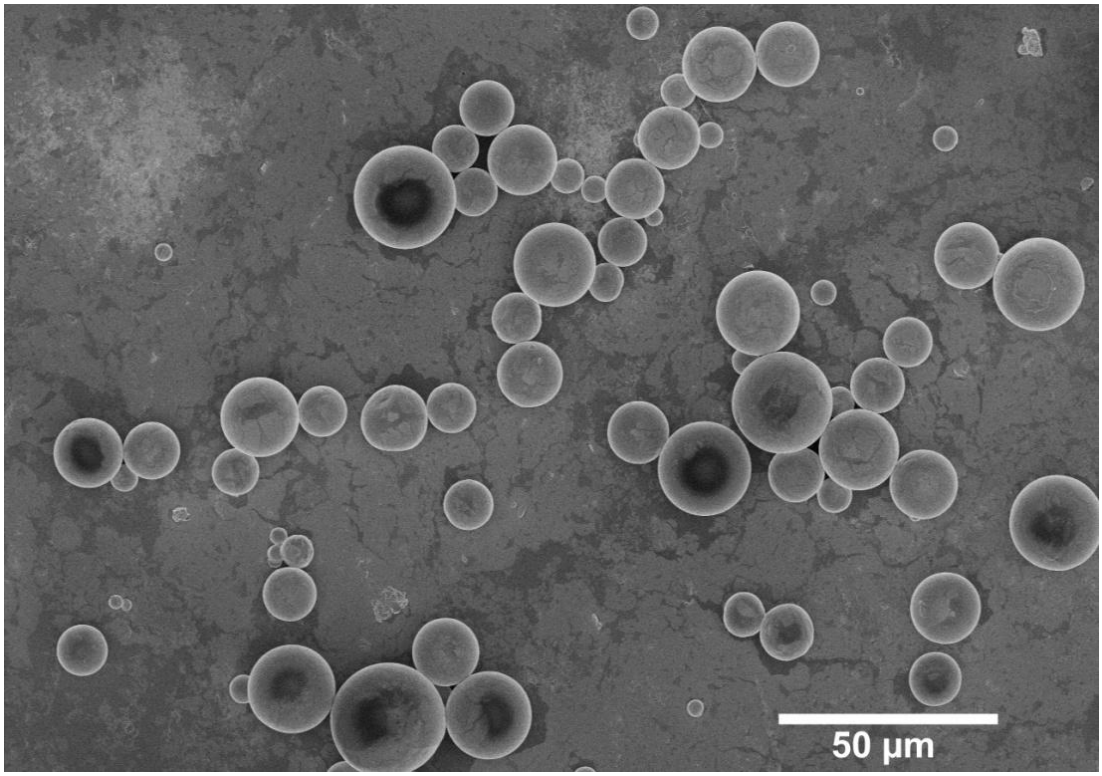

Figure 28 – Final preparation example of 5-PCL-45 shows successful dispersion of microspheres and an increasing in contrast at the edge of each particle. Hitachi FE-SEM 4800, WD = 12.0mm, Mag = 500X, Vacc = 2kV, Current = 10µA, FastScan(2).

Image processing through edge detectors, image thresholding, and CHT is perfectly suited to extract the desired information from a set of pixels. Figure 29A shows an image transformation of Figure 28 achieved through ImageJ 1.48v. Briefly, ImageJ's find edges function is applied to a SEM micrograph; the image is further transformed through thresholding, thereby reducing information to black and white pixels. Various black pixels are speckled throughout the imaged area and are possibly the result of contrast changes being preserved after image processing. Although the final transformation has lost detail, microsphere edges are preserved and clearly defined. Indeed, the micrograph has lost depth of field and its associated 3D effect. However, microspheres closely resemble 2D circles and are distinguishable from background or noise.

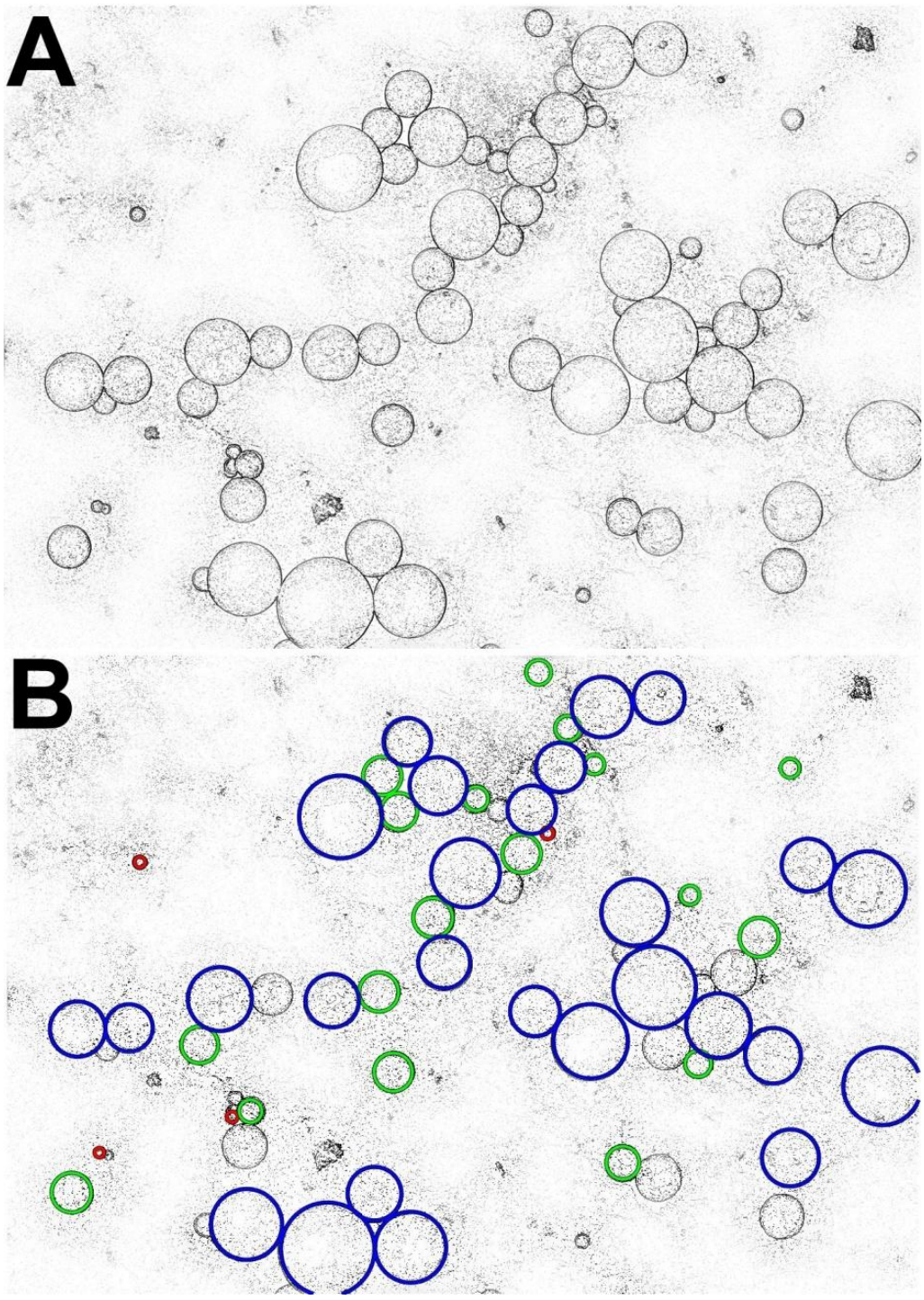

Figure 29 – Image processing example for automated microsphere detection. (A) ImageJ transformation highlights circumference of microspheres. (B) MATLAB® indentifies and labels detected circles.

The final transformation can be loaded into MATLAB® as a pixel array. The *imfindcircles* function from MATLAB® can detect and measure circles based on a CHT and a radius range guess. The function returns vectors with the location of each detected circle center and associated radii in pixels. Figure 29B shows outlines over microspheres with the *viscircle*s companion function. The blue, green, and red outlines represent different calls of the *imfindcircles* function as it is recommended to segment a large radii range guess into smaller ones. As a pixel to micrometer conversion is known, I can report detected radii as micrometer diameters. The example discussed here obtained 49 microsphere diameters in a just a few minutes. Although not all microspheres were detected, as seen by those without an outline, this process addresses the two disadvantages of manual measurement by improving collection time, and ensuring that only objects satisfying a circular parameter are reported.

Organic solvent evaporation rate and organic phase viscosity are perhaps the most important parameters influencing microsphere morphology. Slow evaporation permits the coalescence of smaller particles into larger ones, which is theorized to contribute to rough morphologies [11]. An increase in the viscosity of the oil phase will affect the diffusion rate of DCM, thereby affecting particle size and surface morphology.

To measure possible changes in particle size, I used my automated technique to detect a total of 1627 microspheres across six experimental groups. The automated approached enabled me to scan 43 micrographs in a relatively short period of time. Table 8 summarizes the measured diameters, standard deviations, and number of observations

obtained with this technique. These microspheres average ~ 13 μm in diameter and are consistent in size with previous fabrications explored in this thesis.

Table 8 – Measured microsphere diameter from variable morphology formulations

Formulation	Expected Diameter ± SD (μm)	Observations (n)
3-PCL-45	11.3 ± 5.6	249
3-PCL-80	17.7 ± 9	241
5-PCL-45	11.5 ± 7	213
5-PCL-80	14.2 ± 14.7	208
10-PCL-45	12.8 ± 5.4	371
10-PCL-80	10.9 ± 9.9	345

(mean ± SD)

Despite larger sample sizes than those obtained through manual measurement, all experimental groups continue to fail normality tests, indicating more data could be beneficial in further studies (Shapiro-Wilk test, $p < 0.05$). However, I find it important to note that my automated approach lowered the amount of time invested collecting data and improved confidence with the reported sizes. Indeed, between five and nine micrographs were used per sample group to detect microspheres; with an available SEM stub area of ~ 1.27 cm^2 there is plenty of available area left to be surveyed. Ultimately, the improved collection technique enabled me to conduct a thorough size analysis across six formulations. With this protocol, gathering data is only limited by time spent collecting micrographs from each sample.

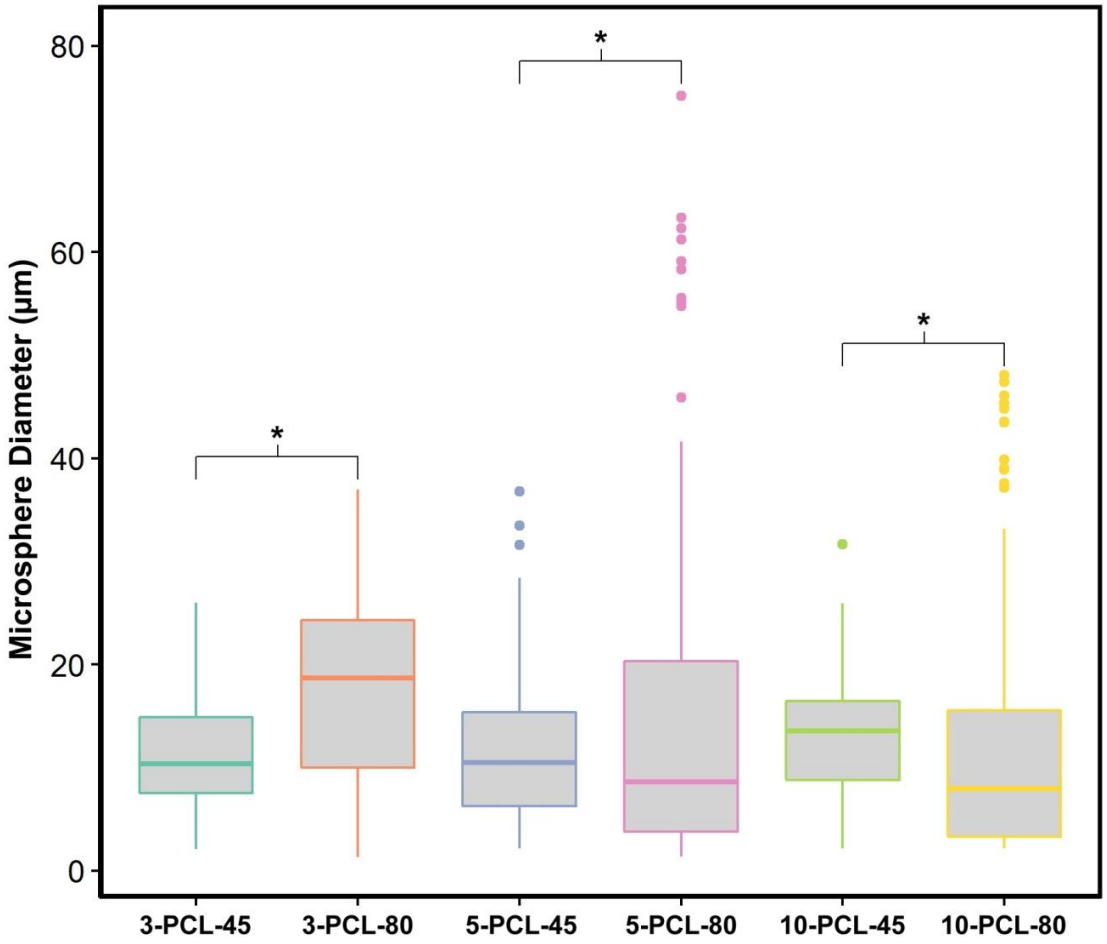

Figure 30 – Microsphere diameter analysis of molecular weight (Mn) pairs. There is a difference in size associated with changing Mn, however the 10% (w/w) pair counters my expectation that an increase of viscosity will yield larger, rough microspheres.

Figure 30 visually compares microsphere diameter based on an increase in polymer molecular weight. All paired groups are statistically different in size (pairwise Welch two-sample t-test[2], $p < 0.05$). 3 and 5% w/w (PCL/DCM) pairs showed an increase in particle size with an increase in molecular weight, which is congruent with the coalescence effect. Interestingly, the 10% w/w pair showed a decrease in size, counter to my expectation. Relative to the other two groups the 10% w/w pair had the smallest

difference between expected diameters suggesting, that although size has been affected by molecular weight, these microspheres are stabilizing around an 11-13 µm range.

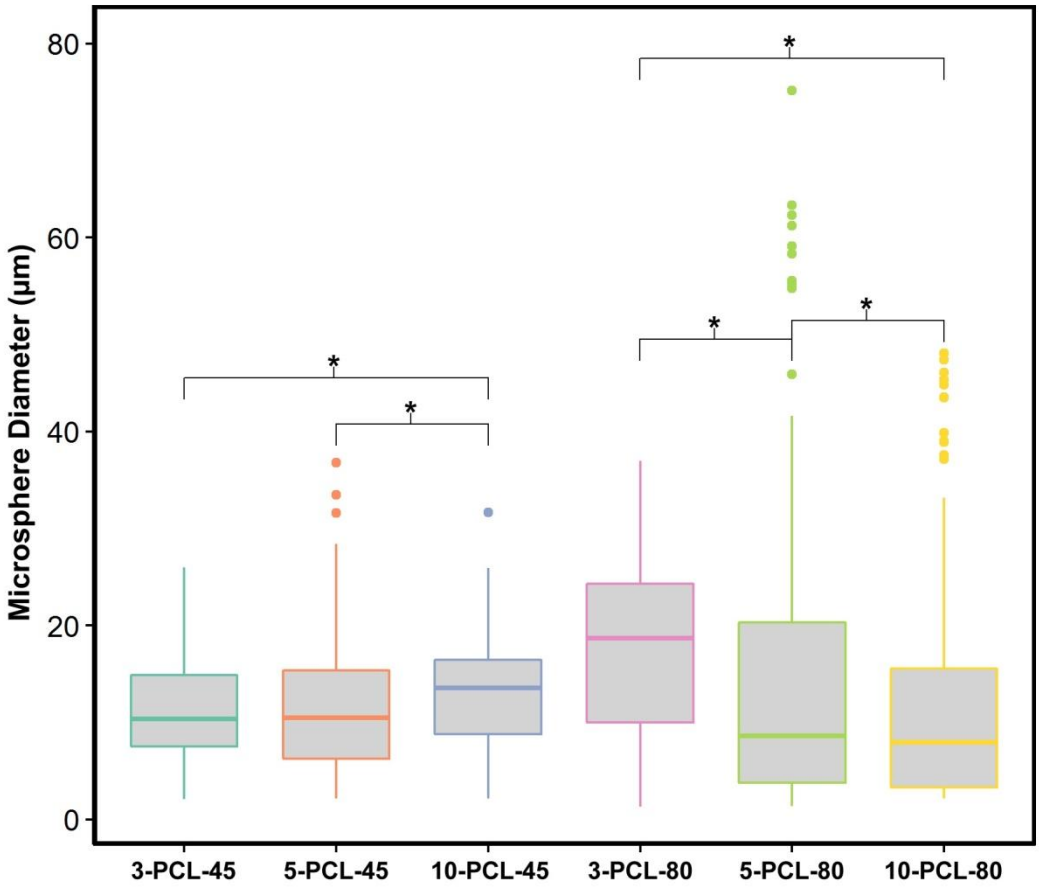

Figure 31 – Microsphere diameter analysis of increasing polymer concentration triplets PCL/DCM %(w/w). The $PCL_{80,000}$ triplet shows the most variation with a decrease in size between all formulations. The reduction in microsphere size is unexpected.

Figure 31 visually compares microsphere diameter based on increasing polymer concentration. This analysis shows a statistically significant difference in size between all $PCL_{80,000}$ formulations (pairwise Welch two-sample t-test[2], $p < 0.05$). However, there is a decrease in particle size with increasing concentration that is opposite to my expectation of the oil phase viscosity and evaporation rate effects. The opposite trend appears true within the $PCL_{45,000}$ triplet. 3-PCL-45 and 5-PCL-45 are not statistically different in size

suggesting the particles may possess a sufficiently similar viscosity and evaporation rate, thus generating similarly sized particles. However, 10-PCL-45 is statistically larger when compared to both and congruent with my expectation of increasing polymer concentration (pairwise Welch two-sample t-test[2], $p < 0.05$).

Motivated by a desire to see and automatically measure microsphere sizes, I successfully created a sample preparation procedure that isolates microsphere circumference from background and removes unwanted information. The edge effect creates an increase in contrast around the microspheres, making them readily identifiable through image processing techniques. A total of 43 micrographs were recorded with identical SEM settings across six samples enabling me to survey an area equal to 0.82 cm^2, thereby streamlining particle measurement. Collectively, the size analysis performed in this experiment captures a global parameter from my formulations that highlights dissimilarities from my particles. Indeed, based on this data I hypothesize that surface morphology differences are perhaps more pronounced in the $PCL_{80,000}$ triplet, as all particles report different sizes relative to each other.

4.2.3 Surface Morphology

Surface morphologies are expected to change by affecting the DCM evaporation rate and viscosity of the organic phase. Qualitatively, my variable morphology microspheres are mostly spherical, as confirmed by the large number of circles detected through image processing (1627 circles). Figure 32 shows variations in microsphere surface morphology obtained from these experiments; ranging from smooth, incomplete fusion (arrested coalescence), holes, ridges and other rough features. Size data suggested there are

differences among experimental groups which could be related to different surface morphologies. Indeed, a qualitative survey shows that the $PCL_{45,000}$ group falls into the smooth category, whereas the $PCL_{80,000}$ group exhibits a range of rough surface features.

Counter to my expectation, the $PCL_{45,000}$ group does not exhibit rough features with increasing polymer concentration. In fact, it is difficult to distinguish 3-PCL-45, 5-PCL-45 (theorized smooth) from 10-PCL-45 (theorized rough) using Figure 32. It is possible that the change in viscosity or evaporation rate is not enough to disrupt a smooth surface morphology in my $PCL_{45,000}$ microspheres. Indeed, Bile *et al.,* (2015) measured organic phase viscosity for $PCL_{45,000}$ at 3.3% and 10% PCL/DCM (w/w) and obtained 3.5 ± 0.1 and 30.8 ± 0.3 mPa·s respectively, indicating an increase in viscosity [11]. Moreover, Bile *et al.,* also estimated DCM evaporation rates for analogous 3-PCL-45 and 10-PCL-45 formulations to be 0.91 and 0.71 $\frac{g}{min}$ respectively, showing a mild decrease in evaporation [11]. My observations, combined with Bile's data, could explain the similarities between the surface morphology across my $PCL_{45,000}$ group.

Qualitatively, the $PCL_{80,000}$ group shows variability in surface morphology as hinted by my microsphere size analysis. Congruent with my expectations 3-PCL-80 has a smoother surface morphology, however some of these particles exhibit ridges and dimples that are not observed in the $PCL_{45,000}$ group at 500X, 12 mm WD. 5-PCL-80 microspheres show large ridges that span the particle surface; others have theorized that such features represent arrested coalescence, where complete fusion is prevented by the evaporation of organic solvent hardening particles [11]. My 10-PCL-80 microspheres fit the rough surface morphology description used in literature. Although the particles remain

spherical, various bumps, holes, and scars can be observed throughout surface, particularly in the larger microspheres. Based on Figure 32, the 10-PCL-80 microspheres are the most distinct relative to other fabrications. Indeed, Bile *et al.*, measured viscosity for $PCL_{80,000}$ at 3.3% and 10% and obtained 21.6 ± 0.2 and 528.4 ± 4 mPa·s respectively, showing a substantial increase in viscosity. Furthermore, DCM evaporation rates for analogous 3-PCL-80 and 10-PCL-80 formulations decreased by half from 0.80 to 0.41 $\frac{g}{min}$, thus providing physical characteristics that explain the rough features observed in my 10-PCL-80 formulation [11].

Stereo-micrographs can highlight variations in surface morphology and particle shape by presenting microspheres as 3D objects. To obtain a stereo micrograph, I collected two micrographs (stereo-pair) from the same object at different tilt angles, 8 º separations, and presented them within a single image via complementary color filters (red-cyan) to achieve stereopsis. For this analysis, I coated microsphere loaded SEM aluminum stubs with a layer of Au/Pd to obtain slow scanning rate micrographs with no charge-up. Samples created for the size analysis proved inadequate for obtaining quality stereo-pairs; as the size micrographs introduced streaking due to charge-up at a shorter working distance and slower scan rate.

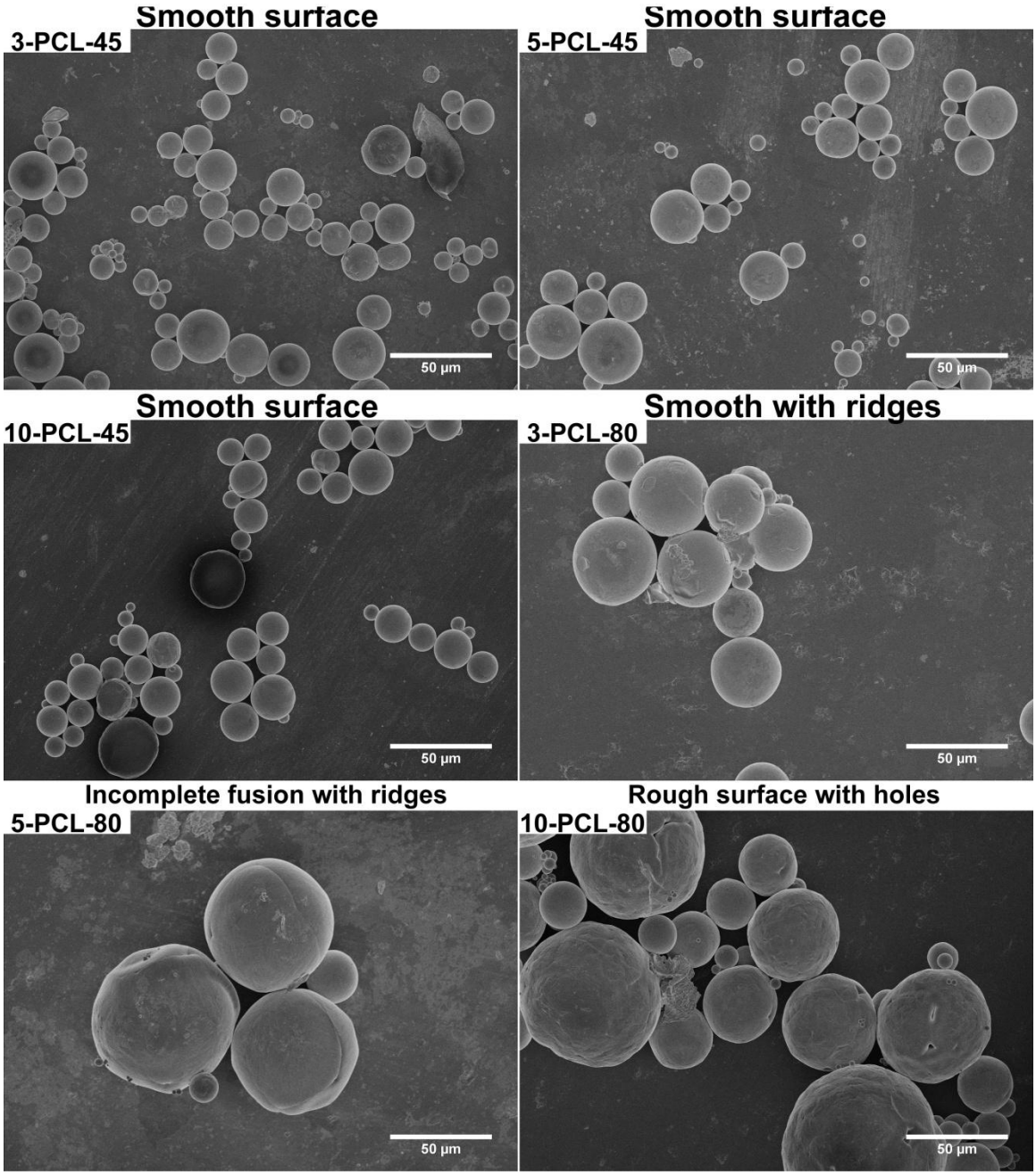

Figure 32 – SEM micrographs of variable morphology microspheres shows a range of surface features, from smooth surfaces, to rough surface morphologies with holes, ridges, and incomplete fusion. Hitachi FE-SEM 4800, WD = 12.0mm, Mag = 500X, Vacc = 2kV, Current = 10µA, FastScan(2).

Figure 33 shows a stereo-pair micrograph comparison of 3-PCL-45 vs. 3-PCL-80, and 10-PCL-45 vs. 10-PCL-80. At identical SEM settings, the surface morphology of 3-PCL-

45 is smooth with a few pits dispersed, whereas 3-PCL-80 has a few regions with rough features such as grooves, pits, ridges, and excess polymer. 10-PCL-45 remains predominantly smooth with a few rough features like excess polymer. At this magnification, however, even small 10-PCL-80 microspheres are covered in rough features such as a bump-like pattern throughout their surface. Indeed, larger 10-PCL-80 microspheres display rough features such as holes, ridges, and excess polymer (Figure 34). Furthermore, large particles appear to change circumference after tilting.

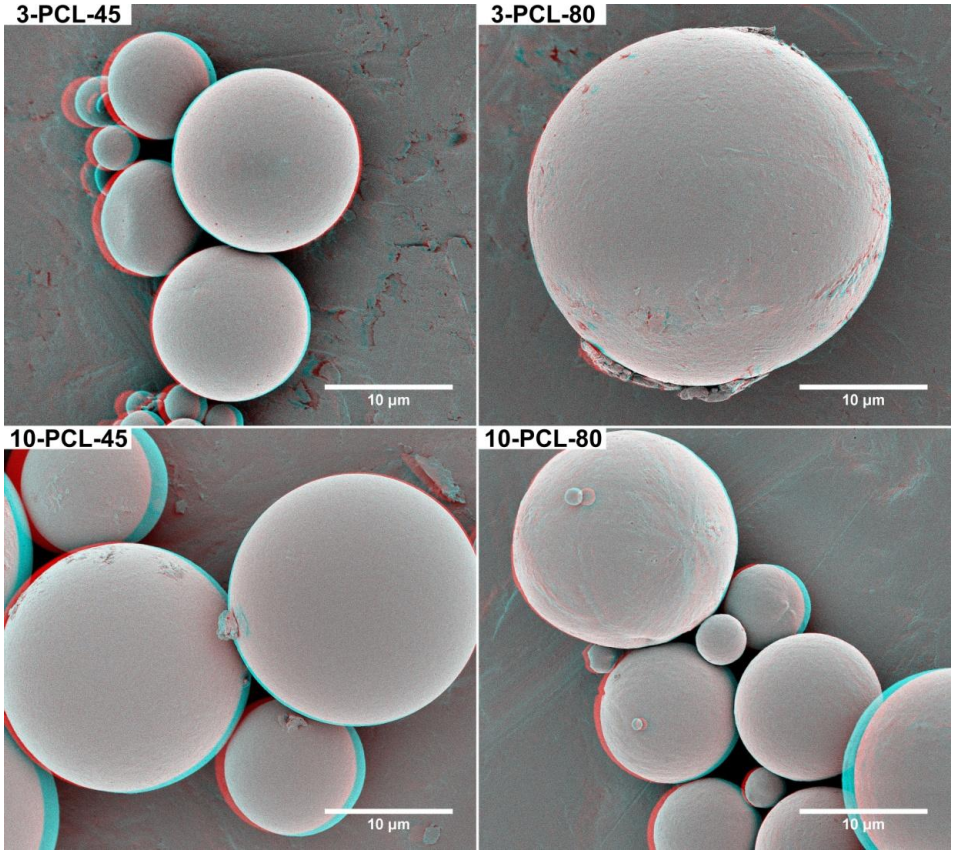

Figure 33 – Stereo-pair micrographs highlight minute surface features present in my formulations. Rough features can be observed throughout small particles from the 10-PCL-80 microsphere group. Hitachi FE-SEM 4800, WD = 7.0mm, Mag = 2500X, Vacc = 1kV, Current = 10µA, SlowScan(80).

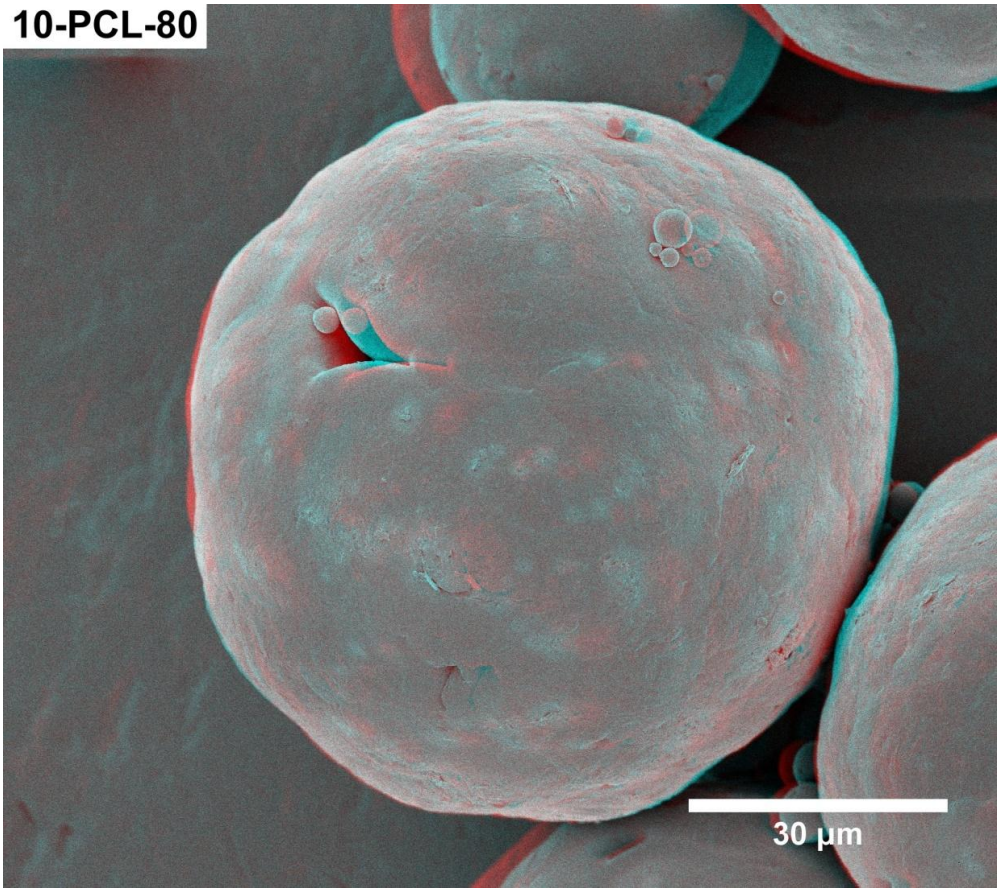

Figure 34 – Stereo-pair micrograph of larger 10-PCL-80 microspheres with various rough surface features. This image shows the effect of size on type of rough features, such as hole from incomplete fusion. Moreover, changes to particle circumference become apparent when tilting larger particles. Hitachi FE-SEM 4800, WD = 6.9mm, Mag = 800X, Vacc = 1kV, Current = 9.8µA, SlowScan(80).

Although stereo-microscopy undeniably enriches microsphere surface detail and highlights deviations from spherical shapes, the observations remain qualitative. A quantitative examination of surface features is not possible through stereo-vision alone. However, exploring surface features via pixel tracking could open the possibility of quantitatively studying microsphere surface via a structure from motion approach. As highlighted by my qualitative survey and 3D anaglyphs, 10-PCL-80 microspheres present the best group to analyze with various surface details that lend themselves to pixel

tracking for surface reconstruction. In theory, a selected 10-PCL-80 microsphere could help me present a 3D model of a microspheres' surface that captures its true 3D spherical nature.

A photogrammetric approach has been used by others to construct 3D models from SEM micrographs with some success [101]. A sequence of micrographs can be used to create a model that captures surface details from multiple perspectives (Figure 35, shows such a model obtained using 37 micrographs). Motion through rotation and tilt angle separation presents microspheres as true 3D objects. Indeed, an image sequence highlights pits and various crests located throughout a microsphere surface in a manner that a single micrograph cannot.

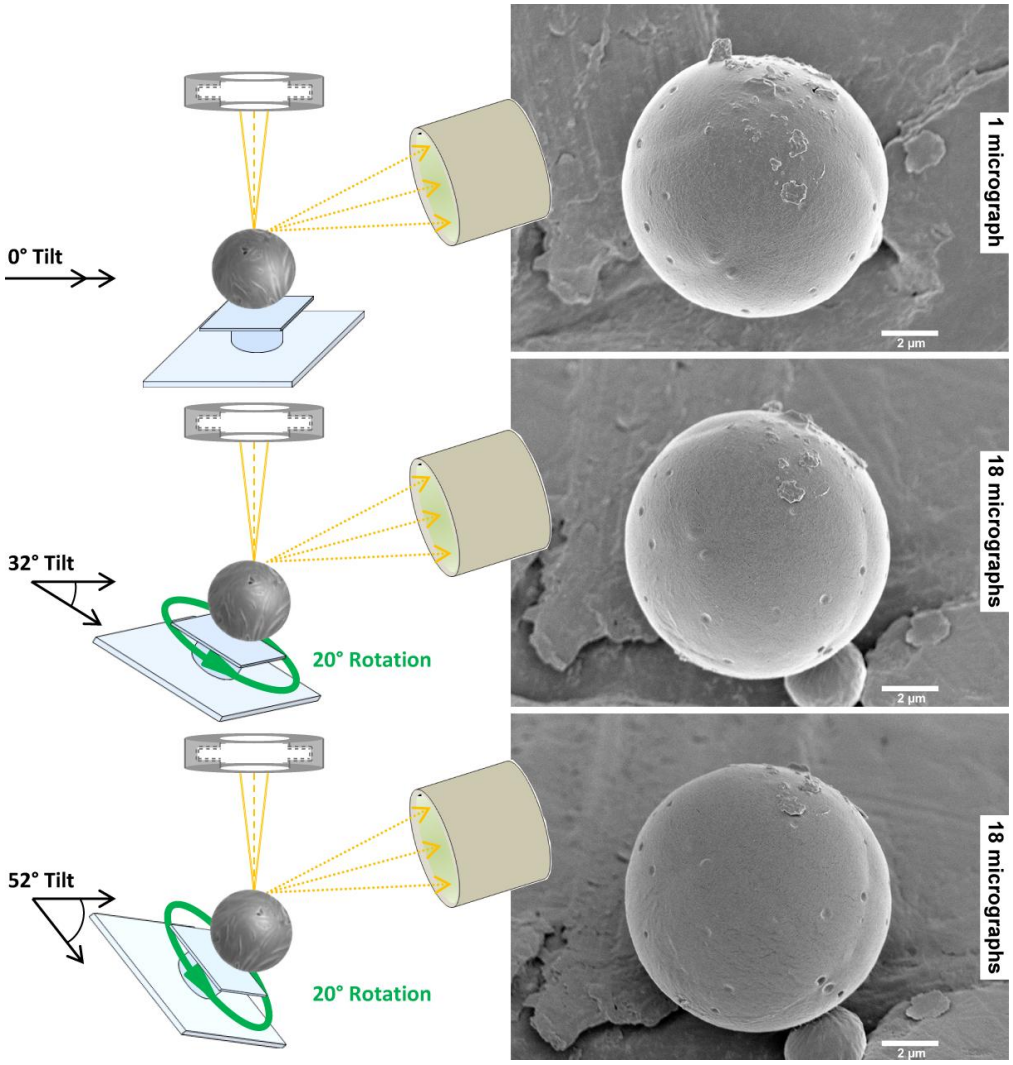

Figure 35 – Surface reconstruction diagram showing the process of gathering data for a 3D surface model. Inspired by Gontard *et al.,* (2016), I collected 37 micrographs from different perspectives. One with 0° tilt and 0° rotation, 18 with 32° tilt and 20° rotation intervals, and 18 with 52° tilt and 20° rotation intervals.

A bump-like pattern is more readily observed through motion than in a stereo-pair micrograph. These features can be indentified and tracked through specialized software, such as Autodesk Remake, to generate surface reconstructions. MATLAB®'s computer vision toolbox can be used to visualize how such software works. A pair of micrographs separated through some translation (rotation or tilt angle) is scanned through a Speeded

up Robust Features (SURF) algorithm, which stores areas that differ on brightness or color, relative to neighboring pixels. These areas can be tracked across an image pair to highlight translations incurred between images. Figure 36 for example, displays the strongest detected SURF regions between a 20° rotation pair.

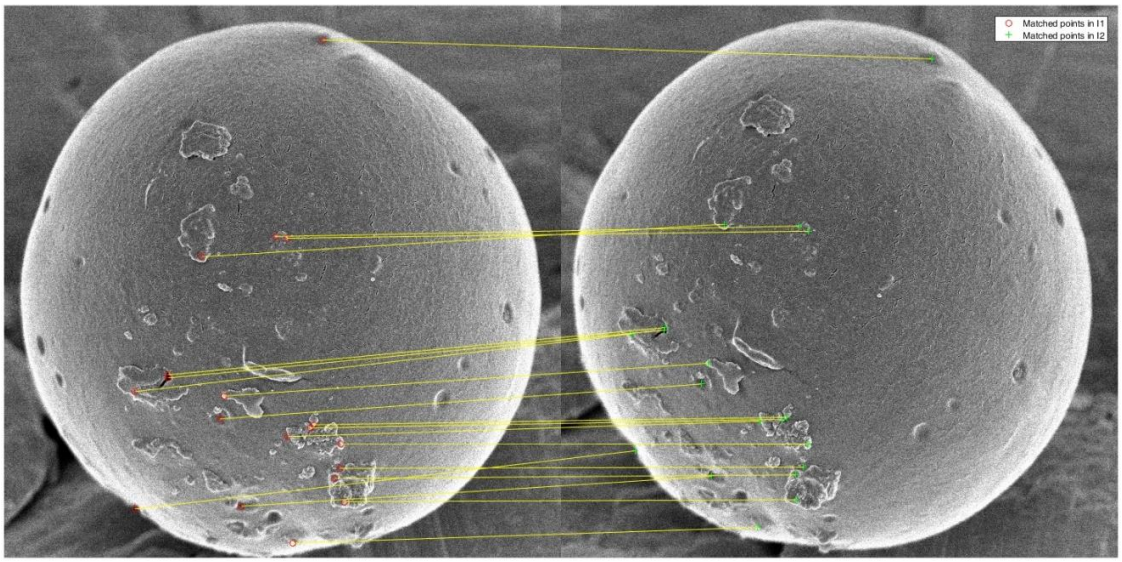

Figure 36 – A 10-PCL-80 microsphere image pair analyzed through MATLAB®'s SURF detector shows how surface tracking algorithms identify regions and tracks translations. Hitachi FE-SEM 4800, WD = 6.9mm, Mag = 7000X, Vacc = 2kV, Current = 9.4μA, SlowScan(80), 20°.

Figure 37 displays a reconstructed model of a selected 10-PCL-80 microsphere. This model enables me to perform new observations and measurements. The model highlights surface features by demonstrating deviations from an idealized smooth surface. For example, an excess polymer structure can be measured with SEM to be 308 nm. The same feature can be located in the X-Y plane of the model and measured again to be 308 nm. The X-Z plane of the model reveals that the same feature extends 205 nm above the microsphere surface. Indeed, the model quantifies surface features by enabling their measurement in any direction.

Manual particle measurement estimated my selected microsphere is 9.5 µm in diameter, whereas my automated circle detection approach obtained 9.6 µm. Assuming an idealized spherical particle, my model enables me to estimate diameter in two different ways: 1) by superimposing a circle over a X-Z plane and 2) by isolating a spherical cap and using cap height and radius to estimate a sphere radius. Both approaches estimate microsphere diameter to be 10.1 µm (Figure 38). It is possible that my 2D measurements underestimate diameter as it is well known that SEMs have excellent lateral resolution, but poor resolution in Z-height that plays a role in studying 3D objects.

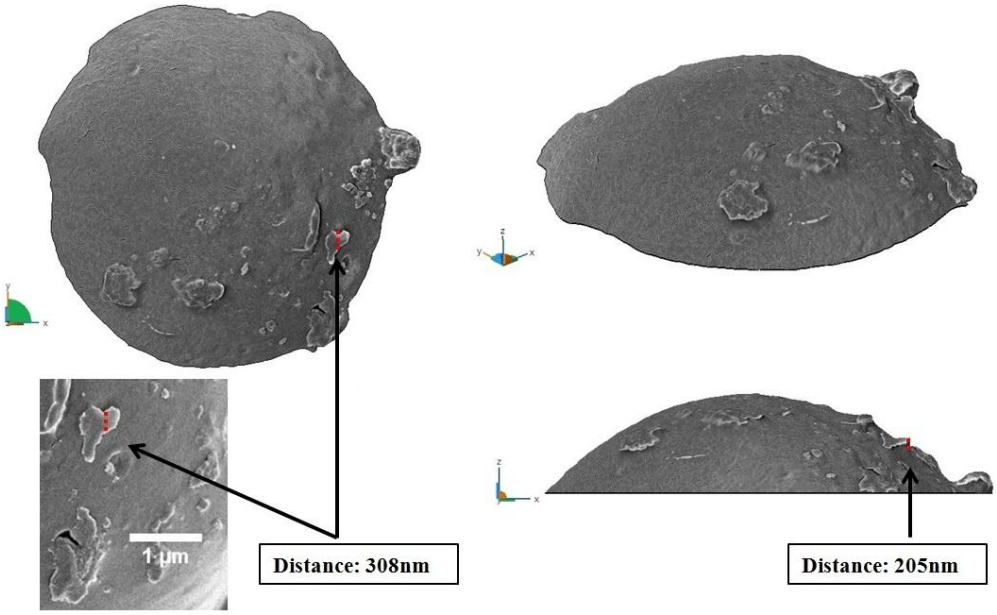

Figure 37 – 10-PCL-80 microsphere surface reconstruction from Autodesk Remake. A Z-plane slice isolates a region that captures the 3D spherical nature of microspheres. A 2D SEM insert and X-Y plane (top view) of the model measure the same rough feature at 308 nm. The model can be rotated to the X-Z plane to measure the Z-height of the same feature is 205 nm. The model enables measurement in any direction.

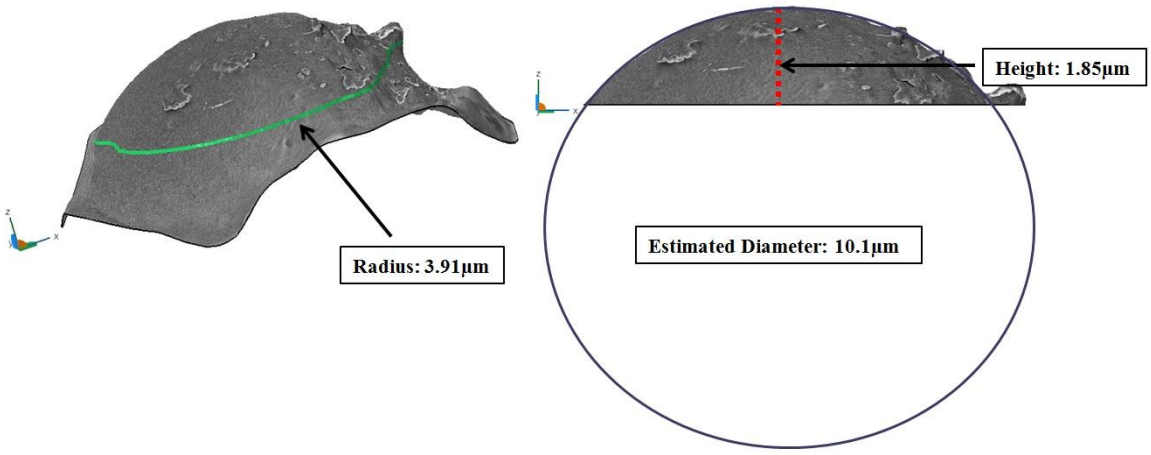

Figure 38 – Quantitative diameter through a 3D model of a 10-PCL-80 microsphere; both approaches estimate particle diameter to be 10.1 µm.

In summary, inspired by recent advances in 3D SEM, I sought to characterize variable morphology polymeric microspheres through traditional SEM micrographs, 3D anaglyphs, and multi-view reconstructions. The microsphere fabrication results confirmed qualitative observations made by Bile *et al.*, (2015), and confirmed that 10-PCL-80 microsphere possess rough features that have been associated with faster drug release. The 3D anaglyphs complemented 2D observations by showing how microspheres, particularly larger 10-PCL-80 particles, appear to change circumference after tilting; suggesting that particles with rough features not only deviate from a perfect sphere depending on my perspective but that 2D measurements may underestimate diameter. For further analysis, I successfully reconstructed a 3D model of a selected 10-PCL-80 microsphere through computer vision techniques and estimated particle size by digitally slicing sections of the model. Collectively, this project can serve as a foundation for reconstructing 3D models of microspheres with rough features and serves as a tool to obtain further measurements.

Chapter 5 Discussion and Future Work

5.1 Discussion

In this thesis, I demonstrated a mastery over the fabrication and characterization of PCL microspheres used in the drug delivery. My work focused on PCL as it is a low cost alternative to the polyester PLGA. Additionally, long term drug release has been identified by the community as a next step for smart delivery systems and PCL's long term degradation make it an ideal candidate for this application. Moreover, I choose to fabricate microspheres through a single emulsion solvent evaporation technique as it enabled the production a large number of particles in a short period of time, revision to my protocols to obtain the desired properties for drug delivery to stem cells aggregates, and control over fabrication conditions to vary surface morphology. In this chapter, I share the learning outcomes of my experiments, discuss avenues for improvements, potential significance of my work for drug delivery microspheres, and propose future experiments.

5.1.1 Microspheres

The first challenge was to learn to fabricate microspheres. To practice, I required a low-cost model drug to create microsphere particles I could characterize in terms of size, morphology, drug loading, and drug release. RA was chosen as a model drug several reasons. 1) RA is a lipophilic molecule easily dissolved in an organic solution, e.g., ethanol or DCM. 2) RA has been demonstrated to induce stem cell differentiation towards motor neurons, which is ideal for the objective of combining microspheres with stem cell aggregates [77, 78, 107]. 3) RA is relatively cheap. Indeed as of 2018, Sigma

Aldrich retails 50 mg of RA for $36.50 CAD whereas 25 mg of purmorphamine, another encapsulation target, retails for $478 CAD. 4) RA has been encapsulated in PLGA microspheres by Jeong *et al.,* (2003), thus providing a critical reference for the results I could expect [103]. The logic behind this approach was to replicate the work published by others, learn about microsphere fabrication in the process, and work towards creating RA-PCL microspheres for stem cell experiments; all to be completed with minimal expense of resources.

Two trial batches with identical fabrication conditions were created to test reproducibility. SEM micrographs confirmed that spherical particles were too large for combination with stem cell aggregates as suggested by Carpenedo *et al.,* (2010) [75]. Qualitatively, the particles possess similar surface morphology, but manual measurement of 100 particle diameters showed two distinct histograms. However, a statistical comparison did not reveal a difference between diameter data. Given this result, replacing histograms with box plots provided a better comparison between diameters and was applied to all following figures; the goal of this change was to decrease uncertainty about sample distributions that may rise through different shape histograms.

Trial batch drug encapsulation proved inconclusive. Drug release from the trial batches are statistically the same, but highlighted the need of more replicates and a different measurement protocol. Despite the lower quality drug encapsulation and release data, this experiment provided an opportunity to investigate any morphology or size changes the particles may experience in a release assay. Morphology changes are important to drug release, as deteriorated morphologies may result in faster release rate. Chen *et al.,* (2000)

reported no changes in morphology (qualitative) of unloaded PCL microspheres after 9-weeks of submersion in an aqueous solution; however no particle size comparison was included in their study [108]. I was unsure if RA-PCL microspheres would degrade differently and took this opportunity to report data on PCL microsphere degradation. My microspheres were submerged in aqueous solution for 4 weeks and it enabled the observation of morphology and potential size changes at various time points. The results showed that the microspheres did not change morphology or size at the selected time points. Given these results, it is suggested that observations be extended to 9 weeks and beyond. Moreover the inclusion of proteins, such as lipase, has been shown to accelerate degradation and could be used to observe morphology, size changes, and drug release in a shorter time span.

The goal of attaining consistency between fabrication batches was met, but changes to my particles became necessary to attain the desire size range of 2-5 μm diameter [75]. Particle size was addressed by increasing vortexing speed and time to reduce initial emulsion size. Similarly, increasing stabilizing bath speed promoted smaller particles. It is likely that the initial droplets coalesced during fabrication to create larger ones. Additionally, rough features were observed (e.g., Figure 4.1, 4.4, and 4.5), and may be the result of slow solvent evaporation hardening larger droplets on their top layer and cracking as the droplets shrink..

The refined microspheres were not only statistically smaller, but also featured a small standard deviation; suggesting that a majority of measured microspheres fit the average size and possibly did not coalesce to form larger particles. Smooth spherical surfaces

were also observed in my refined microspheres. The absence of rough features could be associated with organic solvent evenly exiting PCL droplets during fabrication. Drug encapsulation and drug release measurements were also improved by refining protocols. I measured success by obtaining encapsulation efficiencies reported in literature and reducing standard deviations in my drug release measurements.

Successfully fabricating PCL microspheres in a reproducible fashion serves as the foundation for the experiments performed throughout this thesis. Consistent results increased confidence in my fabrication and obtaining desired properties from the particles showed mastery over the single emulsion technique.

5.1.2 RA Delivery to hiPSC Aggregates via Microspheres[1]

These experiments demonstrated that PCL microsphere-mediated delivery of RA can overcome diffusion barriers of soluble morphogens into 3D hiPSC aggregates. PCL was chosen because it is an affordable alternative to PLGA, for its long-term biodegradation, and for its potential biocompatibility with cell culture. These features make PCL a suitable polymer for neural tissue engineering applications, where stem cell differentiation protocols can involve days to months of signaling for mature cells [109, 110]. A single emulsion technique was used to produce large quantities of microspheres in a relatively short period of time. I used a SEM to qualitatively report surface morphology of the microspheres and to manually measure particle size. I also characterized the particles for drug encapsulation efficiency and drug release. Finally, John Edgar and I conducted stem cell replicates experiments to quantitatively report percent cell viability, pluripotency marker expression, and immunocytochemistry to show

the effects of RA/PCL microspheres on hiPSC aggregates following a neural induction protocol.

Carpenedo *et al.*, (2010) showed that microsphere diameter affects incorporation efficiency within murine embryonic stem cell (mESC) aggregates, with smaller diameter microspheres (1 μm) being more readily incorporated within mESC aggregates than larger ones (3 μm) [75]. Additionally, Carpenedo's study revealed that incorporated microspheres ranged in size from 2 to 5 μm while larger diameter microspheres (11 μm) were excluded. The microspheres used by Carpenedo *et al.*, (2010) remained within the interstitial space of the aggregate as opposed to being internalized by ESCs, suggesting that an optimum microsphere size for interstitial incorporation exists.

The size of the RA-PCL microspheres reported here falls within the suggested range. Moreover, a statistical similarity between the two RA-PCL concentrations batches point towards a reproducible target size. Additionally, a qualitative morphology assessment of the three experimental groups (unloaded, 4 μg/mg, and 30 μg/mg) shows indistinguishable smooth surface features. The encapsulation efficiencies of the low-cost PCL microspheres reported here (~60%), are consistent with PLGA microspheres following a similar fabrication [103]. It is possible that during the 4 hour solvent evaporation a RA concentration equilibrium between the solvent and water phases may have been reached that prevented further diffusion of RA out of the PCL solution. The release studies show that RA cumulative release percent remained similar until day 24, at which point the higher concentration microspheres released more RA. Collectively, these

measurements indicate that my fabrication technique is indeed creating microspheres that possess desirable properties for incorporation with hiPSC aggregates.

My previous experiments with the trial microspheres showed no degradation in surface morphology or changes in particle size after drug release. Moreover, the complete published work included a SEM analysis at day 12 of incorporated microspheres that showed little bulk degradation from the particles, suggesting that RA release is mostly driven by diffusion [106]. However, it is not known at this time if a higher quantity of RA in microspheres increases the degradation rate of PCL or if, in a longer term release study, the microspheres will begin to break apart and result in a spike of RA released. Longer release studies would provide further insight into the mechanisms of RA release from PCL and whether the remaining RA would continue to be released gradually as the PCL degrades.

Quantitative viability studies confirmed that PCL is not cytotoxic to hiPSC aggregates and analysis of pluripotent marker expression confirmed that microsphere mediated RA delivery lowers pluripotency marker expression in hiPSCs. Specifically, viability analysis across the hiPSC experimental groups revealed that the relative percentage of viable cells following 5 days of culture with PCL microspheres remained similar to undifferentiated hiPSCs with and without RA delivery. Similarly, relative pluripotency marker percent expression of SSEA-4 in undifferentiated hiPSCs versus day 5 confirmed that RA enhanced the differentiation of hiPSC aggregates when compared to unloaded or no microsphere control groups. However, a parallel analysis for relative pluripotency marker percent expression of SOX2 was inconclusive. The high standard deviation for SOX2

measurements suggests a user error. It is possible I may have not followed the labeling protocol properly and it may be worthwhile to revisit this measurement in future experiments. Day 12 immunocytochemistry revealed that all hiPSC aggregate groups were positive for TUJ1 and all groups successfully acquired neuronal morphology indicative of neural progenitor cells with no negative effects associated with PCL microsphere incorporation. hiPSCs can be restricted to ectoderm lineages within 12 days but further studies are required to determine the extent of the differentiation reported here [109-111]. It is not known at this time if the hiPSCs will eventually express motor neuron markers, as the experiments did not extend past 12 days. While TUJ1 expression is an early neuronal marker, it cannot be used to determine what types of neurons are being produced, which would require further analysis.

The quantitative analysis of TUJ1 positive images highlighted differences in morphology between the experimental hiPSC aggregates groups of this study [106]. The aggregates that contained RA releasing microspheres extended less neurites with fewer branches than the negative control while the unloaded microsphere sample extended neurite lengths and branch points similar to the positive control. Although there may a chemical justification for this observed difference in aggregate morphology, i.e., elevated concentrations of RA may be toxic or that high concentration of RA within the aggregate may alter gene expression, it is my suggestion that hiPSC aggregate density per well be lowered to one to standardize TUJ1 images before drawing further conclusions. A direct apples to apples comparison between TUJ1 images would be a better foundation for a future quantitative analysis.

Taken together, the experiments discussed in this part of the thesis provide a foundation for further exploration of PCL microspheres for drug delivery to hiPSC aggregates. The results serve as a starting point for additional experiments incorporating microspheres into aggregates to direct neuronal differentiation of hiPSCs. The protocols for incorporating PCL microspheres within hiPSC aggregates reported here could be further refined to accommodate the fragile nature of hiPSC aggregates and to increase the incorporation rate of microspheres. Finally, other small molecules that influence stem cell differentiation into neural lineages, such as purmorphamine, are promising candidates for encapsulation into PCL to induce differentiation into motor neurons or other neuronal cell-types [109, 112, 113].

5.1.3 Variable Surface Morphology

Recently, Bile *et al.*, (2015) identified fabrication parameters that influence surface morphology of PCL microspheres in a single emulsion technique [11]. As part of my desire to quantify surface morphology, I adapted Bile's parameters to create rough features in PCL microspheres. My previous experiments relied on manual measurements or qualitative assessments to extract data from SEM. I used image processing and computer vision techniques to automate measurements and extract information from micrographs. An automated approach for size measurements can further increase confidence in the data by reducing human error. Moreover, a stereo-view or multi-view approach can be used to highlight surface details and create a 3D model for analysis. The goal of these experiments was to replicate the work performed by Bile *et al.,* (2015) and characterize the resulting microspheres via SEM in a quantitative manner.

Six microsphere formulations were created to capture a range of surface features, from smooth to rough. I maintained identical fabrication settings with the equipment while changing the viscosity of the oil phase through different PCL molecular weights (Mn) (45,000 vs. 80,000), and by increasing polymer concentration (3%, 5%, 10% w/w). Theory suggested rough PCL microspheres tend to be larger whereas smooth ones tend to be smaller, due to particle coalescence and slow solvent evaporation with increasing viscosity in the oil phase. Therefore, changes in microsphere surface morphology could also be present in particle size and quantified through a size comparison.

A size comparison across six experimental groups via the manual measurement protocol would prove time consuming. Fortunately, microspheres possess a distinct circular geometry that image processing algorithms can identify. Sample preparation is a step that can greatly impact the quality of the data obtained, but can also be used to enhance physical phenomena like the edge effect. The process of smoothening a SEM stub with carbon paint enabled me to distinguish dispersed microspheres with ease by increasing contrast around particle circumference via the edge effect. Detecting and measuring microspheres size was streamline with this approach. It is suggested that this sample preparation protocol be considered by others interested in creating distinct smooth backgrounds for their SEM samples.

The automated approach enabled me to detect 1627 objects that satisfied the circular parameter of microspheres in a short period of time. This sample pool captured size changes across my experimental groups. Specifically, polymer molecular weight pairs are shown to be statistically different in size at identical polymer concentrations. However,

the 10-PCL-45 vs. 10-PCL-80 pair defied theory by showing a reduction in particle size. It is possible that the current 10-PCL-80 dataset could benefit from further observations, as its large standard deviation signal a large range of microspheres in this group. Comparing microsphere size based on polymer concentration with identical polymer weight showed differences between all $PCL_{80,000}$ groups. Interestingly, a trend towards small average microspheres diameter was also present with increasing polymer concentration. Although the size comparison analysis succeeded in identifying the $PCL_{80,000}$ groups as the best place to look for variability in terms of surface morphology, the defying size trends, combined with large standard deviations of the groups, suggests that it may be worthwhile to investigate any possible bias against large microspheres in my approach. One possible explanation is that the automated size technique was programmed to use identical micrograph magnifications for all samples. Large microsphere could possibly occupy large sections of a scanned image and not be recognized in the image processing step.

A qualitative survey of selected micrographs from all experimental groups showed the range of surface features. Qualitatively, 10-PCL-80 was confirmed to be most distinct relative to other fabrications. I employed stereo-microscopy to show increased surface detail by presenting microspheres as 3D objects. Indeed, large microspheres from the 10-PCL-80 groups seem to change circumference in stereo-micrographs. It is possible that large particles are not completely spherical due to the presence of rough surface features. It is also possible that tilt angle changes affect the focus point in the SEM, thereby changing the perceived diameter of the particle. Both reasons are possible explanation for this qualitative change in circumference. Collectively, the qualitative SEM work

presented 10-PCL-80 microspheres as the best candidates with rich surface details for a multi-view reconstruction.

Quantitatively studying microsphere surface has only been performed a few times in literature via AFM [94, 95]. SEM, however, has recently been used to create 3D surface models that can provide a novel way of characterizing features [101, 114]. To create a model, I adapted a method by Gontard *et al.,* (2016) to study a selected rough 10-PLC-80 microsphere. A multi-view approach allowed me to reconstruct a partial surface from my selected microsphere; as reconstructions are only possible from the part of the microspheres that are exposed to the electron beam. The 3D structure was sliced to isolate a region that represents the idealized spherical nature of microspheres. A geometry based approached enabled me to estimate particle size with two independent measurements; one by superimposing a 2D circle in the X-Z plane and another by using a Z-section as a spherical cap to measure cap height and cap radius. Both approaches estimated 3D microsphere diameter to be 10.1 µm versus the 2D estimate of 9.5-9.6 µm. It is possible that the 3D measurement is more accurate as it not only accounts for X-Y dimensions but also the Z-height of the selected microsphere. This model presents microsphere surface as quantifiable structure.

Collectively, experiments discussed in this part of the thesis identify 10-PCL-80 microspheres as potential candidates with rough surface features to be further analysed through size studies and 3D models. The results show that it is possible to identify microspheres through image processing. The multi-view reconstruction illustrates that SEMs are suitable for novel analysis through modern computer vision techniques.

5.2 Conclusions and Future work

The work contained within this thesis was motivated by my desire to learn about drug delivering microspheres and their applications in tissue engineering. A literature review revealed that the delivery of RA via PCL microspheres to hiPSC aggregates had not been done before. My success in mastering the o/w single emulsion solvent evaporation technique allowed me to refine RA/PCL microspheres suitable for incorporation with hiPSC aggregates. The success of this project enabled its publication in the Journal of Cellular and Molecular Engineering, where it is currently serving as the foundation for future work delivering drugs to hiPSC aggregates; as noted by the works citing my project. In the course of characterizing PCL microspheres, I noticed the lack of quantitative works that study surface morphology, despite its known role in affecting drug delivering rates. Indeed, most works focus on drug delivering effects of microspheres, and AFM has only been used few times to measure surface morphology. I successfully fabricated variable surface morphology PCL microspheres and characterized them via particle size and through stereo-microscopy by using two SEM sample preparations. I identified a 10-PCL-80 microsphere suitable for 3D SEM surface reconstruction and constructed a 3D model using computer vision software. The model is suitable for dimensional measurement in any direction. Recovering the third dimension (height) with the 3D model opens possibility of new quantitative surface studies, and to the best of my knowledge, the existence of a 3D SEM microsphere surface model has not been done before.

Future work should include long-term (9 weeks+) drug release assays to observe the effects of PCL degradation on drug release. Since it is not known how PCL degradation may affect drug release, measuring drug in an extended assay and characterizing corresponding surface changes and particle size may serve as metric for PCL degradation effects on drug release. Recently, Agbay *et al.,* (2018) built upon the microsphere incorporation work I showed here by delivering guggulsterone to hiPSC aggregates via PCL microspheres [115]. Their work included a 5 week drug release assay that paralleled the timescale at which their microspheres released drug to stem cell aggregates. However, microsphere surface quality after drug release, which would provide information on PCL microsphere degradation, was not discussed. Similarly, recovering microspheres after incorporation with stem cell aggregates would provide insight into how surface degrades or if particle size changes with stem cell contact.

In future experiments, the image processing technique I showed in this thesis could be used to reduce the amount of time spent manually measuring particles and reduce human error. The smoothening of SEM stubs greatly enhances size studies of PCL microspheres, as it also creates a dark, mostly uniform background. This sample preparation is not overly complex and it is recommended for other particle size studies. Another future source of improvement could be the automated particle measurement protocol. Microsphere identification could be refined by performing a search for circular objects at lower magnifications and determining sections in a sample that should be analyzed at higher magnification. Although the current script is hardcoded to process micrographs of identical resolution and magnification, changes to the script can incorporate extracting

information from text files that accompany every micrograph created in the FE-SEM 4800.

Perhaps the area with the most potential is that of 3D model analysis. Although preliminary, my model is a proof of concept that multi-view reconstructions can capture the 3D spherical nature of microspheres and facilitate the study of particles through a geometry-based approach. While this method proved to be exhaustive, as it required several hours to track a microsphere through many translations, it brings the potential to measure rough features, such as excess polymer dimensions in Z-height and deviations from an idealized sphere. A practical 3D microsphere model that quantitatively represent microsphere surface could be created by replicating the process outlined in my thesis. Virtual slices of the model could then be used to measure particle dimensions, test spherical symmetry, and study surface roughness by measuring peaks and valleys along the particle surface. 3D models of microspheres before and after drug release could then be compared to quantify surface degradation. Although it was time consuming to obtain the 37 micrographs with the FE-SEM 4800 to create the discussed model, optimization experiments could be performed to find the minimum number of micrographs necessary for a successful reconstruction. Alternatively, creation of 3D microsphere surface models could be streamlined by access to specialized tools for 3D SEM reconstruction currently offered or under development by SEM manufactures and programmers (e.g., Digital Surf Mountains® software and nanoScience instruments PhenomSEM). Places such as the National Institute of Standards and Technology are confirming the accuracy of 3D SEM models [116]. Therefore, it can be expected that 3D SEM reconstructions will become routine analysis in near future. Ultimately, it is the hope of this author that the reflections

contained here be applied and considered in future drug release studies and characterization of PCL microspheres.

Bibliography

1. Langer, R., *New methods of drug delivery.* Science, 1990. **249**(4976): p. 1527-1533.
2. Park, K., *Controlled drug delivery systems: Past forward and future back.* Journal of Controlled Release, 2014. **190**: p. 3-8.
3. Uhrich, K.E., et al., *Polymeric Systems for Controlled Drug Release.* Chemical Reviews, 1999. **99**(11): p. 3181-3198.
4. Mao, S., et al., *Recent advances in polymeric microspheres for parenteral drug delivery – part 1.* Expert Opinion on Drug Delivery, 2012. **9**(9): p. 1161-1176.
5. Yang, W.-W. and E. Pierstorff, *Reservoir-Based Polymer Drug Delivery Systems.* Journal of Laboratory Automation, 2012. **17**(1): p. 50-58.
6. Ulery, B.D., L.S. Nair, and C.T. Laurencin, *Biomedical applications of biodegradable polymers.* Journal of Polymer Science Part B: Polymer Physics, 2011. **49**(12): p. 832-864.
7. Benita, S., et al., *Characterization of drug-loaded poly(d,l-lactide) microspheres.* Journal of Pharmaceutical Sciences, 1984. **73**(12): p. 1721-1724.
8. Ogawa, Y., et al., *A New Technique to Efficiently Entrap Leuprolide Acetate into Microcapsules of Polylactic Acid or Copoly(Lactic/Glycolic) Acid.* Chemical & Pharmaceutical Bulletin, 1988. **36**(3): p. 1095-1103.
9. Wischke, C. and S.P. Schwendeman, *Principles of encapsulating hydrophobic drugs in PLA/PLGA microparticles.* International Journal of Pharmaceutics, 2008. **364**(2): p. 298-327.
10. Dash, T.K. and V.B. Konkimalla, *Poly-ϵ-caprolactone based formulations for drug delivery and tissue engineering: A review.* Journal of Controlled Release, 2012. **158**(1): p. 15-33.
11. Bile, J., et al., *The parameters influencing the morphology of poly(ε-caprolactone) microspheres and the resulting release of encapsulated drugs.* International Journal of Pharmaceutics, 2015. **494**(1): p. 152-166.
12. Mitragotri, S., P.A. Burke, and R. Langer, *Overcoming the challenges in administering biopharmaceuticals: formulation and delivery strategies.* Nature Reviews Drug Discovery, 2014. **13**(9): p. 655-672.
13. Tafti, A.P., et al., *Recent advances in 3D SEM surface reconstruction.* Micron, 2015. **78**: p. 54-66.
14. Hall, C.E., *Introduction to electron microscopy*. 1983, Malabar, Florida: Krieger.
15. Saka, S.K., *Light Microscopy and Resolution*, in *Super-Resolution Microscopy Techniques in the Neurosciences*, F.E. Fornasiero and O.S. Rizzoli, Editors. 2014, Humana Press: Totowa, NJ. p. 1-11.
16. Isobel, F., *J J Thomson and the discovery of the electron.* Physics Education, 1997. **32**(4): p. 226.

17. Weinberger, P., *Revisiting Louis de Broglie's famous 1924 paper in the Philosophical Magazine.* Philosophical Magazine Letters, 2006. **86**(7): p. 405-410.
18. Freundlich, M.M., *Origin of the Electron Microscope.* Science, 1963. **142**(3589): p. 185-188.
19. McMullan, D., *Scanning electron microscopy 1928–1965.* Scanning, 1995. **17**(3): p. 175-185.
20. Wells, O.C. and D.C. Joy, *The early history and future of the SEM.* Surface and Interface Analysis, 2006. **38**(12-13): p. 1738-1742.
21. Wischnitzer, S., *Introduction to electron microscopy*. 3rd Edition ed. 1980: Pergamon Press Inc.
22. Rose, H., *Aberration correction in electron microscopy*. International Journal of Materials Research, 2006. **97**(7): p. 885-889.
23. Spence, J.C., *Aberrations*, in *High-resolution electron microscopy*. 2013, Oxford Univ. Press. p. 31-36.
24. Hawkes, P.W., *Aberration correction past and present.* Philosophical Transactions of the Royal Society A: Mathematical, Physical and Engineering Sciences, 2009. **367**(1903): p. 3637-3664.
25. Hawkes, P.W., *The correction of electron lens aberrations.* Ultramicroscopy, 2015. **156**: p. A1-A64.
26. Spence, J.C., *Instabilities and the microscope environment*, in *High-resolution electron microscopy*. 2013, Oxford Univ. Press. p. 315-323.
27. Spence, J.C., *Experimental methods*, in *High-resolution electron microscopy*. 2013, Oxford Univ. Press. p. 324-346.
28. Spence, J.C., *Elementary principles of phase-contrast TEM imaging*, in *High-resolution electron microscopy*. 2013, Oxford Univ. Press. p. 2-8.
29. Hayat, M.A., *Principles and Techniques of Scanning Electron Microscopy*. Vol. 6. 1978: New York: Van Nostrand Reinhold.
30. Bruining, H., *The depth at which secondary electrons are liberated.* Physica, 1936. **3**(9): p. 1046-1052.
31. Dekker, A.J., *Secondary Electron Emission*, in *Solid State Physics*. 1981, Macmillan Education UK: London. p. 418-445.
32. Bruining, D.H., *1 - INTRODUCTION*, in *Physics and Applications of Secondary Electron Emission*. 1962, Pergamon. p. 1-7.
33. Finch, J., *The ancient origins of prosthetic medicine.* The Lancet, 2011. **377**(9765): p. 548-549.
34. Kulinets, I., *1 - Biomaterials and their applications in medicine*, in *Regulatory Affairs for Biomaterials and Medical Devices*. 2015, Woodhead Publishing. p. 1-10.
35. Rezaie, H.R., L. Bakhtiari, and A. Öchsner, *Biomaterials and Their Applications*. 2015: Springer.
36. Ratner, B.D., *A History of Biomaterials*, in *Biomaterials Science (Third Edition)*, A.S. Hoffman, F.J. Schoen, and J.E. Lemons, Editors. 2013, Academic Press. p. xli-liii.
37. Williams, D.F., *On the nature of biomaterials.* Biomaterials, 2009. **30**(30): p. 5897-5909.

38. Holzapfel, B.M., et al., *How smart do biomaterials need to be? A translational science and clinical point of view.* Advanced Drug Delivery Reviews, 2013. **65**(4): p. 581-603.
39. Vert, M., et al., *Bioresorbability and biocompatibility of aliphatic polyesters.* Journal of Materials Science: Materials in Medicine, 1992. **3**(6): p. 432-446.
40. Levitt, S.R., et al., *Forming method for apatite prostheses.* Journal of Biomedical Materials Research, 1969. **3**(4): p. 683-684.
41. Shepherd, J.H., R.J. Friederichs, and S.M. Best, *Synthetic hydroxyapatite for tissue engineering applications*, in *Hydroxyapatite (Hap) for Biomedical Applications*. 2015, Woodhead Publishing. p. 235-267.
42. *The Discovery of Stainless Steel*. 2017; Available from: http://www.bssa.org.uk/about_stainless_steel.php?id=31.
43. Sumita, M., T. Hanawa, and S.H. Teoh, *Development of nitrogen-containing nickel-free austenitic stainless steels for metallic biomaterials—review.* Materials Science and Engineering: C, 2004. **24**(6–8): p. 753-760.
44. Navarro, M., et al., *Biomaterials in orthopaedics.* Journal of The Royal Society Interface, 2008. **5**(27): p. 1137-1158.
45. Bhatia, S., *Natural Polymers vs Synthetic Polymer*, in *Natural Polymer Drug Delivery Systems: Nanoparticles, Plants, and Algae*. 2016, Springer International Publishing: Cham. p. 95-118.
46. *Glycolic acid (HMDB00115)*. 2017; Available from: http://www.hmdb.ca/metabolites/HMDB00115.
47. Vert, M., S. Li, and H. Garreau, *New insights on the degradation of bioresorbable polymeric devices based on lactic and glycolic acids.* Clinical Materials, 1992. **10**(1): p. 3-8.
48. Alters, S., in *Biology: Understanding Life*, T.C.o. Life, Editor. 2000, Jones & Bartlett Learning. p. 42-43.
49. Cooper, G.M. *The Molecular Composition of Cells*. The Cell: A Molecular Approach 2000; 2nd:[Available from: http://www.ncbi.nlm.nih.gov/books/NBK9879/.
50. Alberts, B., A. Johnson, and J. Lewis. *The Chemical Components of a Cell*. Molecular Biology of the Cell 2002; 4th:[Available from: http://www.ncbi.nlm.nih.gov/books/NBK26883/.
51. Bray, A., et al., *Chemical Components of Cells; Molecules in Cells*, in *Essential Cell Biology*. 2009, Gardland Science. p. 50-56.
52. *Small and large molecules*. 2016; Available from: http://pharma.bayer.com/en/innovation-partnering/technologies-and-trends/small-and-large-molecules/.
53. Cohen, Y. *Small Molecules: The Silent Majority of Pharmaceutical Pipelines*. 2015 [cited 2017 March 23rd]; Available from: http://www.xconomy.com/boston/2015/11/23/small-molecules-the-silent-majority-of-pharmaceutical-pipelines/#.
54. Hedman, C.A., T. Lindström, and H.J. Arnqvist, *Direct Comparison of Insulin Lispro and Aspart Shows Small Differences in Plasma Insulin Profiles After Subcutaneous Injection in Type 1 Diabetes.* Diabetes Care, 2001. **24**(6): p. 1120-1121.

55. Helfand, W.H. and D.L. Cowen, *Evolution of Pharmaceutical Oral Dosage Forms.* Pharmacy in History, 1983. **25**(1): p. 3-18.
56. Langer, R., *Biomaterials and biotechnology: From the discovery of the first angiogenesis inhibitors to the development of controlled drug delivery systems and the foundation of tissue engineering.* Journal of Biomedical Materials Research Part A, 2013. **101A**(9): p. 2449-2455.
57. Beck, L.R., et al., *A New Long-Acting Injectable Microcapsule System for the Administration of Progesterone*.* Fertility and Sterility, 1979. **31**(5): p. 545-551.
58. Beck, L.R., et al., *New long-acting injectable microcapsule contraceptive system.* American Journal of Obstetrics and Gynecology, 1979. **135**(3): p. 419-426.
59. Langer, R. and J. Folkman, *Polymers for the sustained release of proteins and other macromolecules.* Nature, 1976. **263**(5580): p. 797-800.
60. Wurster, D.E., *Method of applying coatings to edible tablets or the like*. 1953, Google Patents.
61. Guignon, B., A. Duquenoy, and E.D. Dumoulin, *FLUID BED ENCAPSULATION OF PARTICLES: PRINCIPLES AND PRACTICE.* Drying Technology, 2002. **20**(2): p. 419-447.
62. Christensen, F.N. and P. Bertelsen, *Qualitative Description of the Wurster-Based Fluid-Bed Coating Process.* Drug Development and Industrial Pharmacy, 1997. **23**(5): p. 451-463.
63. Langer, R., et al., *Isolation of a Cartilage Factor That Inhibits Tumor Neovascularization.* Science, 1976. **193**(4247): p. 70-72.
64. Langer, R., *The Struggles And Dreams Of A Young Chemical Engineer*. Chemical & Engineering News Archive, 2012. **90**(13): p. 20-24.
65. Langer, R., *Interview: Leading the way in biomedical engineering: an interview with Robert Langer.* Nanomedicine, 2012. **7**(10): p. 1483-1484.
66. *FDA Approved Producs: New Drug Application (NDA): 019732*. 2016 [cited 2017 January 24th]; Available from: http://www.accessdata.fda.gov/scripts/cder/daf/index.cfm?event=overview.process&ApplNo=019732.
67. Barua, A. and H. Furr, *Properties of retinoids.* Molecular Biotechnology, 1998. **10**(2): p. 167-182.
68. Sharow, K.A., B. Temkin, and M.A. Asson-Batres, *Retinoic acid stability in stem cell cultures.* Int J Dev Biol, 2012. **56**(4): p. 273-8.
69. Bray, A., et al., *Protein Structure and Function; The Shape and Structure of Proteins*, in *Essential Cell Biology*. 2009, Gardland Science. p. 119-138.
70. Langer, R. and J. Vacanti, *Advances in tissue engineering.* Journal of Pediatric Surgery, 2016. **51**(1): p. 8-12.
71. Langer, R. and J. Vacanti, *Tissue engineering.* Science, 1993. **260**(5110): p. 920-926.
72. Subramanian, A., U.M. Krishnan, and S. Sethuraman, *Development of biomaterial scaffold for nerve tissue engineering: Biomaterial mediated neural regeneration.* Journal of Biomedical Science, 2009. **16**(1): p. 108-108.
73. Khorshidi, S., et al., *A review of key challenges of electrospun scaffolds for tissue-engineering applications.* Journal of Tissue Engineering and Regenerative Medicine, 2015: p. n/a-n/a.

74. Carpenedo, R.L., et al., *Homogeneous and organized differentiation within embryoid bodies induced by microsphere-mediated delivery of small molecules.* Biomaterials, 2009. **30**(13): p. 2507-2515.
75. Carpenedo, R.L., S.A. Seaman, and T.C. McDevitt, *Microsphere size effects on embryoid body incorporation and embryonic stem cell differentiation.* Journal of Biomedical Materials Research Part A, 2010. **94A**(2): p. 466-475.
76. Freiberg, S. and X.X. Zhu, *Polymer microspheres for controlled drug release.* International Journal of Pharmaceutics, 2004. **282**(1–2): p. 1-18.
77. Bain, G. and D.I. Gottlieb, *Expression of Retinoid-X Receptors in P19 Embryonal Carcinoma-Cells and Embryonic Stem-Cells.* Biochemical and Biophysical Research Communications, 1994. **200**(3): p. 1252-1256.
78. Rhinn, M. and P. Dolle, *Retinoic acid signalling during development.* Development, 2012. **139**(5): p. 843-858.
79. Toyooka, Y., et al., *Embryonic stem cells can form germ cells in vitro.* Proceedings of the National Academy of Sciences of the United States of America, 2003. **100**(20): p. 11457-11462.
80. Bain, G., et al., *Embryonic Stem Cells Express Neuronal Properties in Vitro.* Developmental Biology, 1995. **168**(2): p. 342-357.
81. Van Winkle, A.P., I.D. Gates, and M.S. Kallos, *Mass Transfer Limitations in Embryoid Bodies during Human Embryonic Stem Cell Differentiation.* Cells Tissues Organs, 2012. **196**(1): p. 34-47.
82. Bratt-Leal, A.M., R.L. Carpenedo, and T.C. McDevitt, *Engineering the embryoid body microenvironment to direct embryonic stem cell differentiation.* Biotechnology Progress, 2009. **25**(1): p. 43-51.
83. Tokiwa, Y., et al., *Biodegradability of Plastics.* International Journal of Molecular Sciences, 2009. **10**(9): p. 3722-3742.
84. Woodruff, M.A. and D.W. Hutmacher, *The return of a forgotten polymer—Polycaprolactone in the 21st century.* Progress in Polymer Science, 2010. **35**(10): p. 1217-1256.
85. Tice, T.R., J.K. Staas, and T.M. Ferrell, *Injectable naltrexone microsphere compositions and their use in reducing consumption of heroin and alcohol*. 2001, Google Patents.
86. Ehrich, E., *Naltrexone long acting formulations and methods of use*. 2011, Google Patents.
87. Rosilio, V., et al., *A physicochemical study of the morphology of progesterone-loaded microspheres fabricated from poly(D,L-lactide-co-glycolide).* Journal of Biomedical Materials Research, 1991. **25**(5): p. 667-682.
88. Courteille, F., J.P. Benoit, and C. Thies, *The morphology of progesterone-loaded polystyrene microspheres.* Journal of Controlled Release, 1994. **30**(1): p. 17-26.
89. Vehring, R., *Pharmaceutical Particle Engineering via Spray Drying.* Pharmaceutical Research, 2008. **25**(5): p. 999-1022.
90. Lamprecht, A., U. Schäfer, and C.-M. Lehr, *Structural analysis of microparticles by confocal laser scanning microscopy.* AAPS PharmSciTech, 2000. **1**(3): p. 10-19.

91. Zhao, A. and V.G.J. Rodgers, *Using TEM to couple transient protein distribution and release for PLGA microparticles for potential use as vaccine delivery vehicles.* Journal of Controlled Release, 2006. **113**(1): p. 15-22.
92. Huang, X., et al., *Quantitative three-dimensional analysis of poly (lactic-co-glycolic acid) microsphere using hard X-ray nano-tomography revealed correlation between structural parameters and drug burst release.* Journal of Pharmaceutical and Biomedical Analysis, 2015. **112**: p. 43-49.
93. Hartmann, U., T. Göddenhenrich, and C. Heiden, *Magnetic force microscopy: Current status and future trends.* Journal of Magnetism and Magnetic Materials, 1991. **101**(1): p. 263-270.
94. Montanari, L., et al., *Poly(lactide-co-glycolide) microspheres containing bupivacaine: comparison between gamma and beta irradiation effects.* Journal of Controlled Release, 2003. **90**(3): p. 281-290.
95. Dorati, R., et al., *Surface characterization by atomic force microscopy of sterilized PLGA microspheres.* Journal of Microencapsulation, 2006. **23**(2): p. 123-133.
96. Lungan, M.-A., et al., *Surface characterization and drug release from porous microparticles based on methacrylic monomers and xanthan.* Carbohydrate Polymers, 2015. **125**: p. 323-333.
97. Lungan, M.-A., et al., *Complex microparticulate systems based on glycidyl methacrylate and xanthan.* Carbohydrate Polymers, 2014. **104**: p. 213-222.
98. Kayaalp, A., A. Ravishankar Rao, and R. Jain, *Scanning electron microscope-based stereo analysis.* Machine Vision and Applications, 1990. **3**(4): p. 231-246.
99. Tafti, A.P., et al., *3D Microscopy Vision Using Multiple View Geometry and Differential Evolutionary Approaches*, in *Advances in Visual Computing: 10th International Symposium, ISVC 2014, Las Vegas, NV, USA, December 8-10, 2014, Proceedings, Part II*, G. Bebis, et al., Editors. 2014, Springer International Publishing: Cham. p. 141-152.
100. Amish, T., B.T. Hansen, and E.R. Fischer, *Generation of 3D Surface Models from Scanning Electron Microscope Images.* Microscopy and Microanalysis, 2016. **22**(S3): p. 1144-1145.
101. Gontard, L.C., et al., *Photogrammetry of the three-dimensional shape and texture of a nanoscale particle using scanning electron microscopy and free software.* Ultramicroscopy, 2016. **169**: p. 80-88.
102. Limandri, S., et al., *3D scanning electron microscopy applied to surface characterization of fluorosed dental enamel.* Micron, 2016. **84**: p. 54-60.
103. Jeong, Y.-I., et al., *Preparation of poly(DL-lactide-co-glycolide) microspheres encapsulating all-trans retinoic acid.* International Journal of Pharmaceutics (Kidlington), 2003. **259**(1-2): p. 79-91.
104. Mohtaram, N.K., et al., *Electrospun biomaterial scaffolds with varied topographies for neuronal differentiation of human-induced pluripotent stem cells.* Journal of Biomedical Materials Research Part A, 2015. **103**(8): p. 2591-2601.
105. Montgomery, A., et al., *Engineering personalized neural tissue by combining induced pluripotent stem cells with fibrin scaffolds.* Biomaterials Science, 2015.

106. Gomez, J., et al., *Incorporation of Retinoic Acid Releasing Microspheres into Pluripotent Stem Cell Aggregates for Inducing Neuronal Differentiation.* Cellular and Molecular Bioengineering, 2015: p. 1-13.
107. Novitch, B.G., et al., *A requirement for retinoic acid-mediated transcriptional activation in ventral neural patterning and motor neuron specification.* Neuron, 2003. **40**(1): p. 81-95.
108. Chen, D.R., J.Z. Bei, and S.G. Wang, *Polycaprolactone microparticles and their biodegradation.* Polymer Degradation and Stability, 2000. **67**(3): p. 455-459.
109. Hu, B.Y. and C. Zhang, *Differentiation of spinal motor neurons from pluripotent human stem cells.* Nature Protocols, 2009. **4**(9): p. 1295-1304.
110. Hu, B.-Y., Z.-W. Du, and S.-C. Zhang, *Differentiation of human oligodendrocytes from pluripotent stem cells.* Nature Protocols, 2009. **4**: p. 1614.
111. Haile, Y., et al., *Reprogramming of HUVECs into Induced Pluripotent Stem Cells (HiPSCs), Generation and Characterization of HiPSC-Derived Neurons and Astrocytes.* Plos One, 2015. **10**(3).
112. Karumbayaram, S., et al., *Directed Differentiation of Human-Induced Pluripotent Stem Cells Generates Active Motor Neurons.* Stem Cells, 2009. **27**(4): p. 806-811.
113. Li, X.J., et al., *Directed differentiation of ventral spinal progenitors and motor neurons from human embryonic stem cells by small molecules.* Stem Cells, 2008. **26**(4): p. 886-893.
114. Mills, O.P. and W.I. Rose, *Shape and surface area measurements using scanning electron microscope stereo-pair images of volcanic ash particles.* Geosphere, 2010. **6**(6): p. 805-811.
115. Agbay, A., et al., *Guggulsterone-releasing microspheres direct the differentiation of human induced pluripotent stem cells into neural phenotypes.* Biomedical Materials, 2018. **13**(3).
116. Tondare, V.N., J.S. Villarrubia, and A.E. Vladár, *Three-Dimensional (3D) Nanometrology Based on Scanning Electron Microscope (SEM) Stereophotogrammetry.* Microscopy and Microanalysis, 2017. **23**(5): p. 967-977.

Appendix 1[14]

Electrostatic lenses suffer from the following errors:

1) Spherical aberration
2) Distortion
3) Curvature of the field
4) Astigmatism
5) Coma

Electromagnetic lenses, due to the rotational nature of the magnetic field, suffer from additional errors:

6) Anisotropic Distortion
7) Anisotropic Astigmatism
8) Anisotropic Coma

Other significant aberrations that do not depend on geometry include:

9) Chromatic Aberration
10) Rotational Chromatic Aberration
11) Space-charge Distortion